ETH Dissertation Number 25487

Biophysics and Biomimetics of Hagfish Slime

A thesis submitted to attain the degree of
DOCTOR OF SCIENCES of ETH ZURICH
(Dr. sc. ETH Zurich)

presented by
LUKAS JOHANNES BÖNI

MSc in Food Science ETH Zurich

born 14.06.1989

citizen of Möhlin, AG

accepted on the recommendation of
Prof. Dr.-Ing. Erich Josef Windhab, Examiner
Prof. Dr. Dimitris Vlassopoulos, Co-Examiner
Dr. Patrick Alberto Rühs, Co-Examiner

2018

Biophysics and Biomimetics of Hagfish Slime

ISBN: 978-3-905609-83-7

Published and distributed by:
Laboratory of Food Process Engineering
Institute of Food, Nutrition and Health
ETH Zurich
8092 Zurich
Switzerland

Printed in Switzerland by:
ETH Print & Publish
HG D 34.1
Rämistrasse 101
8092 Zürich

In dubio pro rheo

Acknowledgements

This might take longer.
Either skim for your name or relax and be awed by how many hands helped reeling in this fish.

My first thanks goes to **Prof. Windhab** for making me a member of the exclusive VT family, for genuinely supporting creative work, for the many inspirational talks where not only fish-fibers were spun, and your constant endeavors to bring out the best of each of your students. I highly value that you put the person in the center and then you help tailoring ‘a science’ that fits the character. I am also grateful for the opportunity to spend an exceptional semester in Australia and New Zealand for your help in building a bridge from slime to tofu 2.0.

Next I want to thank the initial **hagfish team**, who got this work started and running.
A big thanks goes to **Pefi** for all the good times we had on land, at sea, and in the air - space is yet to come. I will never forget yet struggle to exactly recall all the places we’ve been, all the fish we ate and all the gin we drank. Thanks for being the mind-easing and soul-warming shadow covering my back. As a photographer, you somehow always saw the bigger picture and knew that only a combination of both, light and shadow makes a truly great shot.
A big thank goes to **Patrick** for lighting the fire. You have accompanied me on my scientific track from the very beginning. You showed me how to write, argue, and think in a scientific manner, and how to structure my scattered thoughts. We shared tiny rooms, icy garages, smelly labs, bumpy boats, and unforgettable views. Thanks for being a great mentor and becoming a true friend.
I further thank **Simon** for starting to unravel the mysteries of the hagfish. Without your efforts, hagfish slime would have remained merely some softly spoken words by David Attenborough. You taught me that - also in science - money gets things done and that there are people on this planet that use even more butter to cook than I do. Thanks for all your crazy ideas, for being a facilitator for my creativity, for your truly hands-on chemistry lessons and all the overly smokey whiskeys.
As the last member of the hagfish team I thank **Lukas**, for taking the interim slime management and keeping haggy in the loop while I was enjoying life. I will keep it short here as my thanks reach far beyond our time and work here at ETH: thanks for being the most truthful friend one can have. Once you took my name tag by mistake, now you are part of my family.

I now head towards the cold west coast of Norway, where a big thanks goes to the Aquarium in Ålesund and in particular to **Rune and Trond**. Over the last almost five years you guys had been providing hagfish and asking for nothing in return. You are true supporters of science and a real proof for Norwegian kindness. It has been amazing to work with you, going fishing and getting a hint of the lives nordic fishermen live. I also want to thank **Snorre and Trygg** from Møreforsking for always helping us organize the room, supervising the sampling of the hagfish and the possibility to use their facilities at NTNU.

With slime in my baggage I now take towards the south-east of Europe to beautiful Crete, where I want to thank **Dimitris** for supporting us on the slime journey and for making me feel so welcome in Greece. You contributed a great deal of work and thought to the project. My research profited from your good listening skills, your patience, and your broad knowledge and curiosity. Above all, however I am inspired by your seemingly endless hospitality and friendliness, which you live on Crete and all places you travel to. Combined with your scientific skills, your kind personality, and

your strive for a good spirit within your group makes you a role model scientist. I finally understood why Peter keeps coming to Crete. It's not only because of the delicious olive oil.

An even bigger leap takes me to the other side of the globe, where I thank **Ray** for welcoming me in his group in Melbourne as if I was his own student. You made my probably best semester possible. Not many people can say they had unlimited access to an AR Cypher in the year 2017 - for those not being from the field: it's like being given a Ferrari on Nürnburgring. I spent an amazing time with you and your group in Australia, had a steep learning curve on the AFM and could profit from your vast experience. I greatly appreciate your attitude towards scientific exchange and how you intensely and closely guide and work with your students. I never felt lost. Also a big thanks to you **Matt**, for taking all those hours to bring me from a contact-mode rookie to a tapping-in-liquid expert. One shall say we'd been tapping in the dark. Your close company, your open mouth and your even more open heart played an integral part in our stay.

My furthest thanks go to **Bill**, where I was given a warm welcome to the grassy slopes, the stoney cliffs and the cloudy skies of Aotearoa. Thanks for the opportunity to hop over, the support and the creative talks regarding hagfish and tweezers and the heavy metal we enjoyed together. Thanks also to **Susav and Rob** for going hands-on on the tweezers with me and giving me a profound introduction.

I come back from the other side of the world and enter the ever open door of **Tony**. From my fist knock onwards you openly and extensively shared your broad scientific knowledge with me and my students. You always made sure who ever leaves the room learnt something. You spent many hours shooting and fitting X-ray data for me and your scientific inputs were influential on the outcomes of the slime project. Thanks a lot for your patience, your time, your great teaching and eventual fascination for hagfish slime.

Another thanks goes to **Tom** for the great collaboration we had on the cystic fibrosis project. This project was as smooth as collaborations can be. Both parts were pulling equally, which I highly enjoyed. I hope this is to be continued in some way.

A very big thanks goes to all my students - **Ruben, Madeleine, Mirjam, Patrizia, Peter, Keita and Aikaterina**. A great part of the success of this thesis is based on your sweat and creativity. I learned incredibly a lot from you all, scientifically as well as personally. Also, my PhD would not have been half as fun without you. You were all truly excellent and you are my personal proof that ETH really forms sharp and creative minds.

I also thank my office mates - **Steph**, **Damien**, **Jotam 1 and 2 (good- and bad mood)**, and **Pascal**. I think I have been sitting in the coolest office ever. Our office had many faces, ranging from a temporary tropical basil forest in summer, to a seemingly open-meeting space for all kinds of complaints to a whiskey and beer-tasting room. I had great fun spending my time with you all here.

I thank **Dani, Jan and Bruno** for always helping me out with small gadgets I needed as well as **Bernie** for the latest origin versions and supporting the best of all computer brands

My last thanks go to my families, namely the **VT family** and to my own **family**.
My time here in the **VT group** was unique. I do not know many people who liked working as much as I did. And I am certain that my joy in work is mainly due to all of you and the free and creative workspace we all share. The plentiful social activities - ranging from running dinners, to sola, to ski weekends, to conferences, to science week, etc. - were always absolute highlights.

At last I want to thank my family and my partner. I am very grateful for all the support and freedom **Hadi and Maria** gave me during my whole education. I could always count on you from the very beginning. This is true stability. Also, since recently the term family was extended for me and I am truly happy to have you, **Jasmin**. You are simply the best partner in crime, soulmate and mother.

So long, and thanks for all the fish.

Table of Contents

Summary

Hagfish defend themselves with vast amounts of slime when provoked or attacked. The slime forms when so-called exudate, which consists of coiled-up threads (‘skeins’) and mucin vesicles is released into the surrounding seawater. Skeins resemble a ‘ball-of-wool’ as they are made of a single coiled-up intermediate filament (IF) protein thread that is up to 30 cm long and 1 - 3 µm in diameter. Skeins unravel and create an underwater fiber network. Simultaneously, the mucin vesicles swell and burst and release mucin-like glycoproteins, which interact with the threads and together form hagfish slime. The secreted slime is a unique biomaterial as it is the most dilute and fastest forming hydrogel known to date. Furthermore, the fibers provide high elasticity and cohesiveness to the otherwise soft gel and were found to have similar properties to spider’s silk. Intrigued by its fast, efficient, and cold gelation, hagfish slime was used as a model to characterize and mimic high-performance marine soft-materials. By pursuing a holistic ‘from fish to fiber’ approach, we investigated how slime can be harvested, stabilized, regenerated, and eventually transformed into novel biomimetic materials.

In a first part, harvesting and stabilization of hagfish exudate is investigated, whereby two stabilization methods - immersion in MCT (medium chain triglycerides) oil and dispersion in a high osmolarity citrate/PIPES (CP) buffer - were compared. Using water retention measurements to assess the functionality of hagfish slime, it was shown that for short storage times (< five hours) both stabilization methods produced slime networks equal to fresh exudate. Longer storage times caused the exudate samples to degrade, whereby MCT samples formed clumps after about seven days, probably due to osmotic and temperature driven rupture of mucin vesicles. CP buffer stabilized samples, in contrast showed a gradual loss of functionality due to reduced skein unraveling. Long buffer exposure times caused less skeins to unravel and therefore less water was retained. It is likely that a seawater soluble glue, which holds the threads together and mediates unraveling denatures during storage in the buffer and becomes insoluble and thus decreases slime functionality.

Having stabilization guidelines at hand, we dealt with the dynamics of slime formation. Motivated by the fact that this fibrous polyelectrolyte hydrogel efficiently and rapidly forms in a high ionic strength environment, we demonstrate the crucial role of ionic strength and seawater cations - especially Ca^{2+} - for the formation dynamics and functionality of hagfish slime. We suggest that sufficient ionic strength controls the dynamics of skein unraveling and slime network formation. A low ionic strength caused a confined and narrow thread network in contrast to the widespread and expanded network formed in seawater. In Milli-Q thread skeins swelled and unraveled uncontrolled from both sides, causing tangling of the threads and thus preventing a widespread network. The fast unraveling in ion-free water seems to originate in an excessive swelling of the intermediate filament slime thread, which would possess increased stored strain energy. Only in the presence of Ca^{2+} and Mg^{2+} a functional slime network is realized at seawater strength osmolarity. The presence of calcium allowed the formation of a functional slime network up to 3 M NaCl, corresponding to 4-5 times the ionic strength of seawater. These results show that a functional defensive slime that entraps and retains water can only be formed in the presence of divalent seawater cations Ca^{2+} or Mg^{2+} at a high ionic strength.

With the boundaries of slime formation outlined, we tackled the question whether slime flow properties have implications on hagfish defense behavior. Oscillatory rheological measurements revealed that hagfish slime forms viscoelastic networks and that mucins alone do not contribute viscoelasticity at their natural concentration. However, in shear flow viscosity was observed. We propose that the threads provide extensibility and cohesiveness, prevent mucin wash-out, and

allow the mucin to contribute to viscoelasticity by supplying anchoring points. When mucins were exposed to elongational stresses - experienced by hagfish slime during suction feeding by predators - mucin viscosity strongly increased. This increased resistance to flow could support clogging of an attacker's gills. Shear flow, in contrast decreased the slime's viscosity by mucin aggregation and lead to a collapse of the slime network. Hagfish may benefit from this collapse by tying a sliding knot with their body to shear off the slime when trapped in their own defensive weapon and facing suffocation. This removal could be facilitated by the apparent shear thinning behavior of the slime. Therefore hagfish slime, thickening in elongation and thinning in shear, possesses flow properties that seem beneficial for both, defense and escape.

In a final step, we explored the potential to transform intermediate filaments (IFs) obtained from hagfish slime fibers into biomimetic films and fibers. Formic-acid solubilized hagfish IFs were used to produce films by drop-casting and coagulation on a $MgCl_2$ buffer. Drop-casting yielded self-supporting, smooth, and dense films rich in β-sheets (61%) whereas coagulation formed thin, porous films with a nano-rough surface and a lower β-sheet content (51%). When immersed in water the films immediately swelled. X-ray scattering revealed that the β-crystallites remained stable upon hydration and that swelling presumably happens in the amorphous C-terminal tail-domains of the IFs. X-ray measurements further suggested a polyelectrolyte behavior of hagfish IFs as the average mesh-size of the IF network as well as the inter β-sheet distance decreased upon increase of salt concentration. Using AFM nanoindentation it was observed that hydration caused a roughly thousand-fold decrease in apparent elastic modulus from roughly 10^9 to 10^6 Pa and that the hydrated films displayed distinct viscoelastic behavior, characteristic for soft-solid and tough hydrogels. Fitting a power-law rheology model directly to the force-distance curves yielded a power-law relaxation exponent α of roughly < 0.2 for both films, suggesting 80% of elastic storage and 20% of viscous loss in force measurements. We propose that hagfish IF films possess β-sheet clusters from an α→β transformed central part of the IFs embedded in an amorphous matrix constituted by the physically entangled C-terminal tail-domains, which determines cohesion and viscoelasticity in hydrated films. We further suggest that viscoelasticity and strong hydrogen bonding interactions of the coagulation film with the buffer surface are crucial for a successful fiber making process, in which a coagulation film is pulled from the buffer interface into a fiber. The combination of relaxing stresses within the film and strong hydrogen bonding of the film with the water interface allow for a continuous stretching yet prevent early removal of the film from the interface, thus creating long biomimetic fibers with high IF alignment similar to natural hagfish fibers. This last part shows that functional IF materials that immediately swell and soften in water without dissolving can be produced from hagfish slime fibers, which could be used in applications such as tissue implants, scaffolds for cell cultures, or contact lenses.

Zusammenfassung

Schleimaale verteidigen sich mit riesigen Schleimmengen. Der Schleim bildet sich, wenn sogenanntes Exsudat, welches aus aufgewickelten Fäden ("Knäuel") und Muzinvesikeln besteht, in das umgebende Meerwasser abgegeben wird. Die Knäuel bestehen aus einem einzelnen aufgerollten Intermediärfilament (IF)-Proteinfaden, der bis zu 30 cm lang und 1-3 µm im Durchmesser ist und sich im Wasser abwickelt und zusammen mit anderen Fäden ein Netzwerk schafft. Gleichzeitig quellen die Muzinvesikel auf und geben Muzin-ähnliche Glykoproteine ab, die mit den Fäden interagieren und zusammen den Schleim bilden. Der abgesonderte Schleim ist ein einzigartiges Biomaterial, da es bis anhin das am stärksten verdünnte und am schnellsten entstehende Hydrogel ist. Darüber hinaus verleihen die Fasern dem ansonsten weichen Gel eine hohe Elastizität und Kohäsion. Faszinierd von der schnellen, effizienten und kalten Gelierung wurde der Schleim als Modell zur Charakterisierung und Nachahmung leistungsstarker mariner Materialien verwendet. Mit einem ganzheitlichen "Vom Fisch zur Faser"-Ansatz untersuchten wir, wie Schleim geerntet, stabilisiert, regeneriert und schließlich in neuartige biomimetische Materialien umgewandelt werden kann.

In einem ersten Teil wird die Gewinnung und Stabilisierung von Exsudat untersucht, wobei zwei Stabilisierungsmethoden - Stabilisierung unter MCT (mittelkettige Triglyceride) Öl und in einem hochosmolaren Citrat / PIPES (CP) Puffer - verglichen wurden. Mit Hilfe von Wasserretentionsmessungen zur Beurteilung der Funktionalität des Schleims wurde gezeigt, dass beide Stabilisierungsmethoden bei kurzen Lagerzeiten (< fünf Stunden) Netzwerke ausbilden, welche denjenigen von frischem Exsudat entsprachen. Längere Lagerzeiten verursachten eine Degradation des Exsudats, wobei MCT-Proben nach etwa sieben Tagen Klumpen bildeten, wahrscheinlich aufgrund osmotisch- und temperaturbedingten Platzens der Muzinvesikeln. CP Puffer stabilisierte Proben zeigten dagegen einen allmählichen Funktionsverlust aufgrund einer verringerten Abwicklung der Knäuel. Lange Pufferexposition führte dazu, dass sich weniger Knäuel abwickeln und so ein geringeres Netzwerk vorhanden war, um Wasser zurückzuhalten. Ein meerwasser-löslicher Kleber, der die Fäden des Knäuels zusammenhält und sich auflöst wenn Exsudat ins Meerwasser abgegeben wird, scheint während der Lagerung im Puffer unlöslich zu werden, was die Funktionalität verringert.

Motiviert durch die Tatsache, dass sich dieses faserige Polyelektrolyt-Hydrogel effizient und schnell in einer Umgebung mit hoher Ionenstärke bildet, demonstrierten wir weiter die entscheidende Rolle von Ionenstärke und Kationen - insbesondere Ca^{2+} - für die Funktionalität des Schleims. Es scheint, dass eine ausreichend hohe Ionenstärke die Dynamik der Knäuelentwirrung reguliert. Eine zu geringe Ionenstärke verursachte ein enges statt eines ausgedehnten Fadennetzwerks, wie es im Meerwasser gebildet wird. In deionisiertem Wasser schwollen die Knäuel auf und der Faden löste sich von beiden Seiten des Knäuels statt nur von einer, was ein Verheddern verursachte und somit ein weitmaschiges Netz verhinderte. Das schnelle Abwickeln in ionenfreiem Wasser scheint auf ein übermäßiges Aufquellen des Fadens zurückführbar zu sein. Ein prallerer Faden besitzt eine höhere Spannungsenergie, welche das Abwickeln bei zu starkem Aufquellen übermäßig beschleunigen kann. Bei Osmolaritäten im Bereich von Meerwasser bildet sich ein funktionelles Schleimnetzwerk nur in Gegenwart von Ca^{2+} und Mg^{2+}-Ionen aus. Die Anwesenheit von Ca^{2+} ermöglicht die Bildung eines funktionellen Schleimnetzwerkes in Lösungen bis zu 3 M NaCl, was dem 4-5-fachen der Ionenstärke von Meerwasser entspricht. Diese Ergebnisse zeigen, dass ein funktioneller Schleim in einem Umfeld hoher Ionenstärke nur in Gegenwart von Ca^{2+} und Mg^{2+}-Ionen gebildet werden kann.

Wir haben uns weiter die Frage gestellt, ob die Fließeigenschaften des Schleims Auswirkungen auf das Abwehrverhalten des Schleimaals haben. Oszillations-Rheologische Messungen zeigten,

dass der Schleim viskoelastische Netzwerke bildet und dass Muzine in natürlicher Konzentration alleine keine Viskoelastizität beisteuern. Wir schlagen vor, dass die Fäden Dehnbarkeit und Kohäsivität beisteuern, das Auswaschen von Muzin verhindern und es dem Muzin ermöglichen, über Verankerungspunkte zur Viskoelastizität beizutragen. Wenn Muzine Dehnströmungen ausgesetzt wurden, nahm deren Viskosität stark zu. Ein erhöhter Strömungswiderstand könnte das Verstopfen der Kiemen von Angreifern unterstützen, welche ein dehnströmungs-dominiertes Saugschnappen für Angriffe nutzen. Scherströmung hingegen verringerte die Schleimviskosität durch Muzinaggregation und führte zu einem Kollaps des Netzwerks. Schleimaale könnten von diesem Kollaps und dem Scherverdünnungsverhalten profitieren, da sie einen Knoten mit ihrem Körper formen können, mit welchem sie den Schleim abstreifen wenn sie selbst darin gefangen sind und zu ersticken drohen. Ein Schleim, der sich bei Dehnung verdickt und unter Scherung verdünnt hat Fließeigenschaften, die sowohl für die Verteidigung als auch für die Flucht nützlich erscheinen.

In einem letzten Schritt untersuchten wir, wie aus Schleimfasern IFs biomimetische Filme und Fasern hergestellt werden können. IFs wurden in Ameisensäure aufgelöst und Filme wurden durch Gießen und Koagulieren in einem $MgCl_2$-Puffer hergestellt. Gießen ergab selbsttragende, glatte und dichte Filme, die reich an β-Faltblättern (61%) waren, während Koagulation dünne, poröse Filme mit einer nano-rauhen Oberfläche und einem niedrigeren β-Faltblatt-Gehalt (51%) bildete. Beim Eintauchen in Wasser quollen die Filme sofort auf und Röntgenstreuung zeigte, dass die β-Kristalle stabil blieben. Das Quellen findet vermutlich in den amorphen C-terminalen Enden der IFs statt. Ferner wird ein Polyelektrolyt-Verhalten der IFs vermutet, da die durchschnittliche Maschenweite des IF-Netzwerks bei Erhöhung der Salzkonzentration abnahm. Nanoindentation zeigte, dass Hydratation eine tausendfache Abnahme der Elastizität von 10^9 auf 10^6 Pa verursachte und dass hydratisierte Filme ein ausgeprägtes viskoelastisches Verhalten besaßen. Anwendung eines Potenz-Rheologiemodels an Indentationskurven ergab einen Relaxationsexponenten α von ungefähr < 0,2 für beide Filme. Das legt nahe, dass ca. 80% der Energie elastisch gespeichert wird und 20% in viskoser Reibung verloren geht. Wir schlagen vor, dass Viskoelastizität und starke Wasserstoffbrückenbindung mit der Pufferoberfläche entscheidend sind für einen erfolgreichen Faserherstellungsprozess, bei welchem ein Koagulationsfilm von der Puffergrenzfläche zu einer Faser gezogen wird. Die Kombination von relaxierenden Spannungen innerhalb des Films und starker Interaktion mit der Wassergrenzfläche ermöglicht ein kontinuierliches Langziehen, verhindert jedoch ein frühzeitiges Entfernen des Films von der Grenzfläche. Dadurch entstehen lange biomimetische Fasern mit starker IF-Ausrichtung, ähnlich der natürlichen Fasern. Dieser letzte Teil zeigt, dass aus Schleimfasern funktionelle IF-Materialien hergestellt werden können, die sofort im Wasser quellen ohne sich aufzulösen. Solche neuen biomimetischen Produkte könnten für Gewebeimplantate, Zellkulturen oder Kontaktlinsen verwendet werden.

Prelude

Ode to Gel

Dear ladies and gents, allow me to tell
Of studies we do with an uncommon gel.

Unlike gelatin in a gummy bear
This natural gel's a slimy affair.

It can be found in the depth of the sea.
Much deeper than jellyfish, kelp or algae.

On the bottom there lives the ancient slime eel
And as the name says, it does not appeal.

For hundreds of millions of years it survived
And whilst mother nature a defense contrived.

Upon attack these hagfish secrete
Plenty of slime, which helps to defeat

The attacking fish, by clogging their gills.
Thus no one chokes, and neither one kills.

The myth of the slime's been intriguing for long
It's ultra dilute, cohesive and strong!

It's made of long threads and mucins alike
Alone they are weak, together they strike.

The threads are like silk, elastic and tough.
Promising stuff, too good to rebuff.

While in the fish, the threads are found twined
Like balls of wool, most greatly designed.

Big vesicles are their neighbouring part
The mucins inside, viscos'ty impart.

Once in the water, the vesicles swell
The threads then uncoil and well, there's gel!

A network is formed and water entrained.
But quick as it's in, as quick it has drained.

Unlike other gels, that chemically bind
Most water in there, is only confined.

And here comes our part, the researcher's task
We start to look, explore and to ask

Why this all works, so perfectly fine,
Utterly quick, in the cold and in brine?

So one of our goal's to mimic these traits
To make such a gel and to save all the baits.

Demand for new gels, as prime as this slime
Is certainly there, just give it some time.

2nd Prize
Action Award
Materials and Processes (MaP) Graduate Symposium 2015

Chapter 1 - Introduction

Hagfish are notorious for the vast amounts of slime they produce when provoked or attacked[1]. The slime serves as an immediate defense mechanism against potential predators[2] by clogging their mouth and gills[3]. The slime forms when a glandular secretion, so-called exudate, is released into the surrounding seawater from a battery of ventrolateral pores. The whitish exudate consist of two major functional components: coiled-up threads (called skeins) and mucin vesicles. The thread skeins resemble a 'ball-of-wool' as they are made of a single coiled-up protein thread that is up to 30 cm long and 1 - 3 µm in diameter. When the skeins are ejected from the slime gland via holocrine secretion into the seawater they unravel and release their long intermediate filament bundle fiber, creating a fiber network[4,5]. Simultaneously, the mucin vesicles swell and burst and release mucin-like glycoproteins[6,7], which interact with the threads and together form hagfish slime. The secreted slime is a unique biomaterial in many ways as it is the most dilute and fastest forming hydrogel known to date[8]. The fibers provide high elasticity and coherence to the otherwise soft gel[9] and were found to have similar properties to spider's silk[10]

The fast, efficient, cold, and salt-tolerant gelation makes hagfish slime an intriguing candidate for the design of biomimetic hydrogels with possible applications in food and pharma. Also, its flexible and tough slime threads are a promising source for novel fibers in clothing and biomedical applications and the abundant mucin constitutes a functional and relatively easily accessible source for mucins, which could be of particular interest for mucin replacers for people suffering from a depleted gastrointestinal mucosa. Despite its vast potential for applications and biomimicry, the biophysical properties of hagfish slime remain largely unexplored compared to other biomaterials such as spider's silk, nacre, or marine hydrogels such as alginate and chitosan.

Therefore, in this thesis a vertically integrated 'from fish to fiber' approach was pursued. I investigated how hagfish slime can be harvested, stabilized, functionally regenerated in the lab, and eventually transformed into novel biomimetic materials such as reconstituted fibers. This approach comprised many steps critical for functionality, starting from exudate ('pre-slime') harvest to the final material transformation and allowed to gain a holistic insight in biological and physical properties along the slime value chain, which are essential for mimicry or a *de novo* material design.

This thesis is structured in eight chapters. After this brief introduction being **Chapter 1**, a detailed description of the current knowledge about hagfish, their slime, and the components of the slime - mucus and intermediate filaments - follows in **Chapter 2**. This theoretical background together with the materials and methods covered in **Chapter 3** provides a solid fundament to the reader to tackle the four main chapters 4-7 in this thesis. **Chapter 4** focuses on the stabilization and functionality of harvested hagfish exudate as the basis for *in vitro* reconstitution and characterization of hagfish slime. Building on that knowledge, **Chapter 5** deals with the dynamics of hagfish slime formation and effects of ionic strength on the slime formation process. These two chapters outline the boundaries of slime formation with respect to its physico-chemical environment and pave the way for an investigation of slime flow properties in **Chapter 6**. This chapter aims to link animal behavior to slime flow properties from functionally reconstituted hagfish slime and derives implications from rheology for defense situations. In **Chapter 7**, hagfish slime fiber protein is extracted and used to produce biomimetic films and fibers, which are then hydrated and characterized for their viscoelastic properties and compared to natural hagfish fibers. In a final **Chapter 8** concluding remarks and an outlook for further hagfish slime research are discussed.

Chapter 2 - Background

The hagfish and its slime

Hagfishes are considered the most ancient of the jawless fishes and inhabit all oceans, except the Polar Seas[11]. They are a group of craniate chordates that belong to an ancient lineage, which evolved more than 500 million years ago and they are regarded to be a sister group to vertebrates as they do not have vertebrae but possess cranial bones. Hagfish are almost blind, but have excellent senses of touch and smell given the four pairs of sensing tentacles that are arranged around their mouth (Fig. 2.1). The mouth lacks jaws, but is equipped with two pairs of tooth-like rasps[11–14]. Hagfishes are exclusively marine, bottom-dwelling, cold water animals that occur in depths from 2500 m to 30 m and are primarily scavengers, playing important ecological roles. Their burrowing and feeding activities are considered to have a significant impact on substrate turnover and generally on the cleanup and recycling of carrion-falls and fishery by-catch[11]. There are approximately 67 described species of hagfishes but only a few of those have been used in research. The Pacific hagfish (Eptatretus stoutii) and the Atlantic hagfish (Myxine glutinosa) (Fig. 2.1) are probably the two most studied species. To the public, hagfish are generally known for their leather (“eel-skin”)[15], their use in culinary dishes predominantly in Korea and the slime they secrete[11].

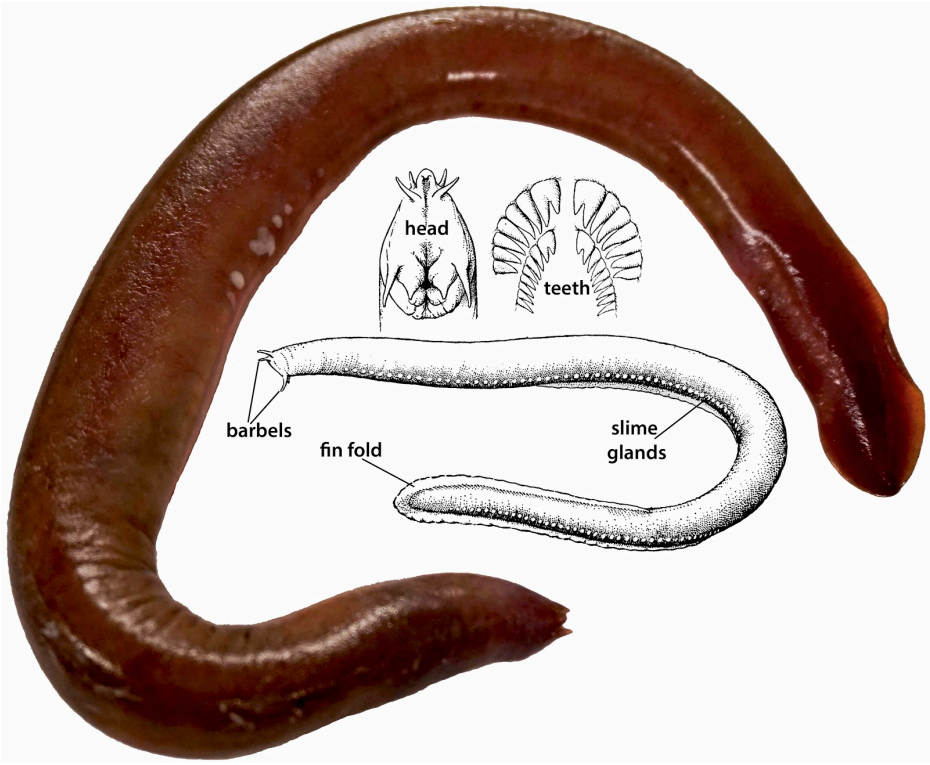

Figure 2.1: Photograph of an Atlantic hagfish *(M. glutinosa*) with schematic inlet depicting major anatomical features. The schematic inlet figures were modified from Bigelow and Schroeder[16]

Carl Linnaeus described the ability of hagfish to produce slime in his Systema Naturae (1758) and gave the Atlantic hagfish the short description "Intrat et devorat pisces; aquam in gluten mutat" - it

enters into fish and eats them; it turns water into slime[17]. Since then, hagfish have been notorious for the vast amounts of slime they produce when provoked or attacked[1].
The slime serves as an immediate defense mechanism against potential predators[2] by clogging their mouth and gills[3,4]. The slime can comprise 3 - 4% of the total body weight, representing a major energetic commitment[8]. The slime forms when a glandular secretion, so-called exudate, is released into the surrounding seawater from a battery of ventrolateral pores. The exudate is produced by approximately 150 slime glands that line the entire length of the body in two rows (Fig. 2.2). The glands are covered in connective tissue and a striated muscle layer, which can contract and expel the gland contents[8,18–20].

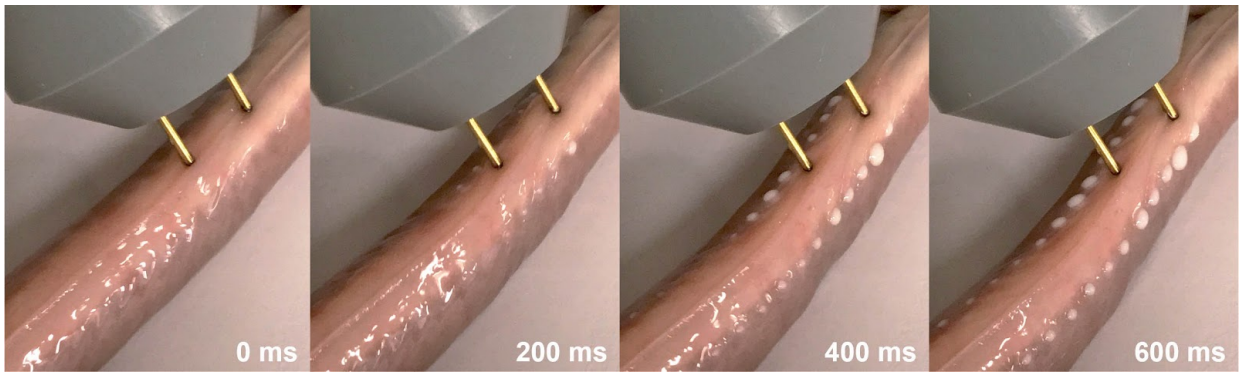

Figure 2.2: **Release of slime exudate from ventro-lateral pores upon mild electrostimulation.** Exudate release happens within milliseconds.

The whitish exudate consist of two major functional components - coiled-up threads (named skeins[21]) and mucin vesicles - that are secreted together with a 'residual fluid' (Fig. 2.3 a). The residual fluid is high in organic osmolytes and has a somewhat but not fully stabilizing effect on the mucin vesicles[6] but its functions are still elusive[22]. The thread skeins resemble a 'ball-of-wool' as they are made of a single coiled-up protein thread that is up to 15 cm long and 1 - 3 µm in diameter. When the skeins are ejected from the slime gland via holocrine secretion into the seawater they unravel and release their long fiber, creating a network[4]. The mucin vesicles contain sulfonated mucin-like glycoproteins[7]. Upon ejection, the vesicles swell, rupture and release their mucus[6]. Swelling vesicles are considered to adhere to the uncoiling thread and together with agitation of the surrounding water aid skein unraveling[23]. The hydrated mucus and the network of unraveled threads together form hagfish slime (Fig. 2.3 b). The slime is an astonishing natural hydrogel in many ways as it is fast forming (< 100 ms)[3,8], cold gelling, salt tolerant, coherent, highly elastic yet soft[9]. Furthermore, its complex network structure allows to physically confine up to 26'000 times its own weight in water, making it roughly three orders of magnitude more dilute than other mucous secretions[8] and thus the most dilute hydrogel known to date.

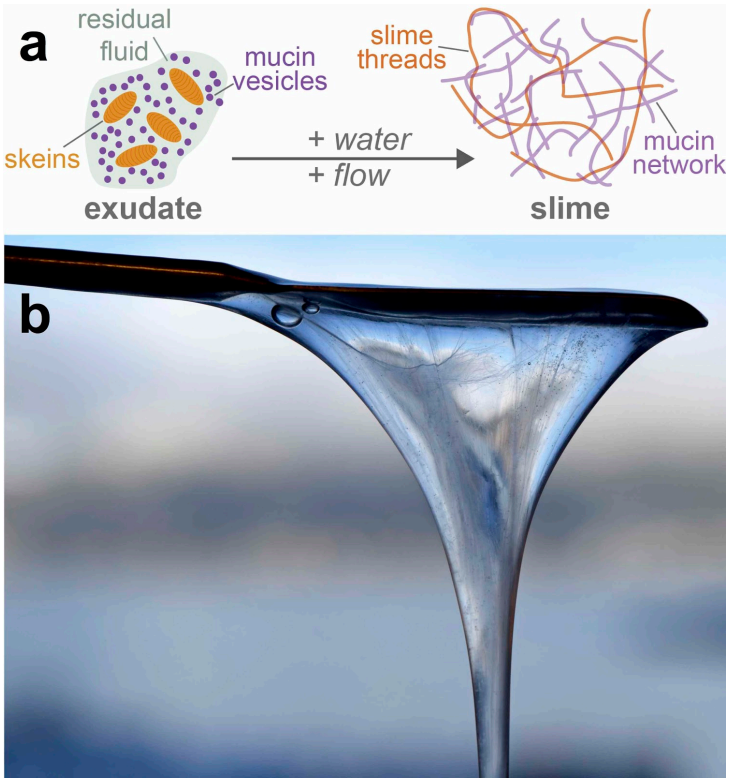

Figure 2.3: Hagfish exudate and slime formation. (a) Schematic illustration of the slime formation mechanism. **(b)** Hagfish slime hanging on a spatula.

Intermediate filaments and hagfish slime fibers

Intermediate filaments (IFs)

Hagfish slime fibers - commonly referred to as hagfish fibers or hagfish threads - mainly consist of proteins belonging to the intermediate filament (IF) family[22]. IFs are a major structural element of animal cells, playing an important role in cell mechanics by acting as stress absorbers, imparting integrity, and by mediating mechanotransduction processes[24–29]. IFs have a diameter of approximately 10 nm, and all share a common architecture characterized by of a central α-helical coiled-coil 'rod' domain, flanked by a largely amorphous N-terminal 'head' and C-terminal 'tail' domain of variable length and sequence[30]. Given their open molecular architecture and their unique assembly plan[27], IFs possess extraordinary mechanical properties[31–33] by combining extreme extensibility[34–36], flexibility[37], and toughness, making them much more flexible and resistant to large deformations than other cytoskeletal polymers such as F-actin and microtubules[36,38,39]. Keratin-like IFs are the building blocks of hagfish slime threads[40–44]. Hagfish IFs comprise three thread keratin (TK) proteins (TKα, TKβ, and TKγ)[43], whereby TKβ is likely a post-translationally modified version of TKγ[41]. They are classified as IFs because they contain a central rod domain with heptad repeat motifs of apolar residues, rod subdomains shared with other IF proteins, a 'stutter' of the heptad repeat in subdomain 2B, conserved sequences at each end of the rod domain, and non-helical N- and C-terminal domains that connect to the central rod domain[22,42,44]. Hagfish IFs were termed 'keratin-like' due features in the head and tail domains that are similar to keratin[42,44]. TKα was found to be a type II keratin homolog and TKγ possesses features of type I keratins, but also contains structural similarities to type III IFs, which include desmin and vimentin[22,45]. Furthermore, TKα and TKγ were found to self-assemble into hetero-dimeric IF like nanofibrils in vitro[43,46,47]. Hagfish fibers still comprise the only known example of extracellularly secreted IFs as in all other known cases IFs occur strictly intracellularly[5,48].

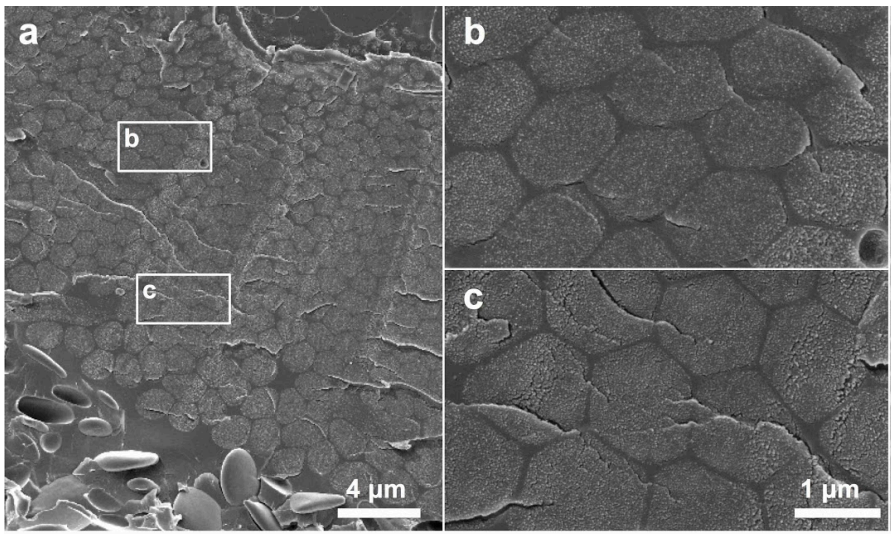

Figure 2.4: Ultrastructure of hagfish thread skein. (a) Cryo-SEM image of skein cross-section from secreted exudate. On the bottom of the image mucin vesicles are visible. **(b)**,**(c)** Magnification of two selected areas from (a) depicting different shapes of the slime thread, ranging from round to hexagonal.

Thread maturation and skein unraveling

Hagfish threads consist of axially aligned IFs, which mature and condense to a solid 1 - 3 µm diameter fiber[4,5,10,49]. The fiber is produced within gland thread cells (GTCs), which are found in the slime glands[5,18,40,50]. Thread production and maturation in the young GTCs starts with bundle of only a handful of IFs that form the initial immature thread. By the addition of more IFs as well as microtubules (MTs) - probably involved in the delivery of IFs and/or IF subunits[51,52] - the thread diameter then increases. The next development stage comprises the condensation of discrete IFs to a single IF 'superstructure'[40,49,50] (Fig. 2.4 a,b,c). The MTs remain visible in threads after the IF condensation stage. In the final stages of maturation, the spaces occupied by MTs are filled in as in fully mature threads MTs are absent[22,40,49,50]. In the early stages of GTC development thread diameter and length appear to increase simultaneously but after the condensation it seems likely that thread length remains constant, and further growth only increases diameter[22]. During holocrine secretion, the GTCs lose their plasma membrane[4] and are henceforth called skeins (Fig. 2.5 a), as they can now release their fiber and form a fiber network (Fig. 2.5 b) to immobilize water. The mechanism of skein unraveling and network formation are still somewhat elusive. It is believed that skein unraveling is driven on the one hand by a swelling of the slime thread once in contact with seawater and on the other hand by a stored strain energy, which is released when a protein adhesive between the threads is dissolved by seawater[22,53]. However, for skeins from the Atlantic hagfish it was shown that unraveling is not spontaneous in seawater but requires turbulent mixing combined with the presence of elongated mucin strands that attach to the skeins and pull them apart[23]. In contrast, it was found that skeins of the Pacific hagfish unravel spontaneously in seawater even in the absence of mucins and mixing, which was attributed to a possibly higher stored strain energy in Pacific hagfish skeins[53].

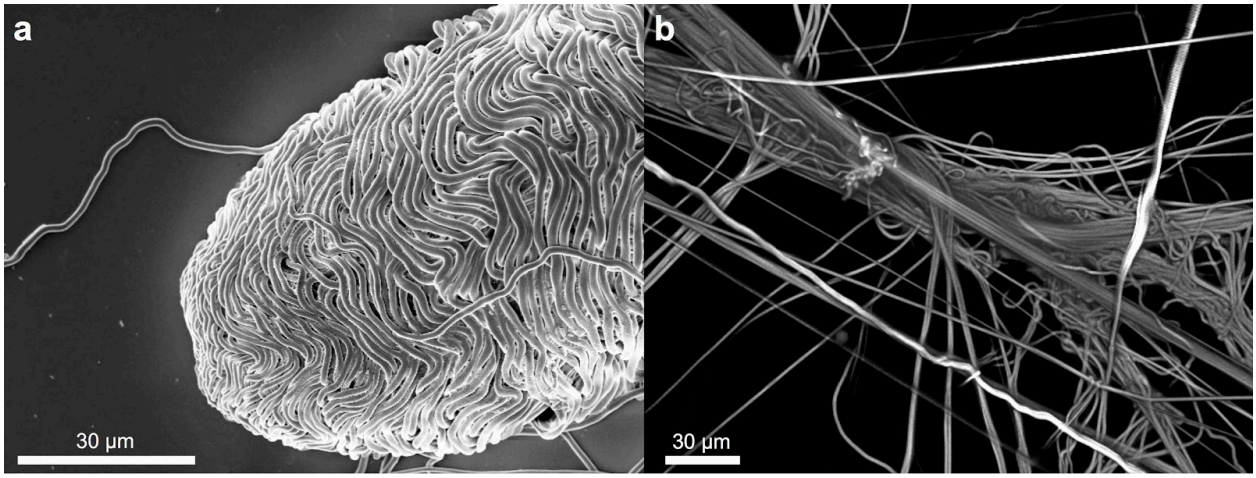

Figure 2.5: Hagfish slime thread skein and fiber network. (a) SEM image of thread skein from hagfish exudate that was partly unraveled using Milli-Q water. **(b)** Confocal laser scanning microscopy (CLSM) image of a hagfish slime fiber network dyed with nile blue. The image also depicts a so-called 'cable' - many fibers twisted to a massive fiber aggregate.

Physical properties of hagfish fibers

Slime threads mainly consist of keratin-like IFs but their material properties are very distinct from mammalian α-keratin, which is also an IF-based material and is found in hair, wool, and nail. Whereas α-keratins are stiff (2 GPa[54]) - even when immersed in water - slime threads are flexible (6.4 MPa) and rubberlike up to strains of 35% when hydrated and possess a high breaking strain of 220%[10]. The differences between slime threads and α-keratin seem to originate in the presence of matrix proteins that surround the IFs in keratins. The matrix is a highly cross-linked network and seems to prevent the IFs in keratins from fully hydrating when immersed in water[22,54,55]. Slime threads are plastically deformed when stretched more than 35% in water, resulting in the formation of extensive amounts of β-sheets in the thread. This increase in β-sheets is considered to originate from an α-to-β transition, whereby α-helices within thread IFs are disrupted and reannealed to β-sheets[10]. These stable β-sheet structures combined with the flexible linker domains of the IFs that string them together impart to slime threads impressively high breaking stress, strength and toughness (draw-processed slime threads)[10,22,55,56], rivaling tensile properties of spider dragline silk[57].

Hagfish mucin vesicles and mucin

Hagfish mucin vesicle production, release, and stabilization

Apart from thread skeins, hagfish exudate contains disc shaped mucin vesicles (Fig. 2.6 a-c), which are enclosed by a single phospholipid membrane and are produced by the Golgi apparatus in gland mucous cells (GMCs)[58]. Upon stimulation the striated muscle layer surrounding the slime gland contracts, which causes an expulsion of the GMCs (together with the GTCs) through the narrow slime gland pore. Forcing both cells through the pore sheares off their plasma membrane, releasing the skein from the GTC and the plentiful mucin vesicles from the GMC[20]. This holocrine secretion results in the rapid and extensive release of mucin vesicles and stands in contrast to the common exocytotic mucin release, where vesicles fuse with the apical plasma membrane inside a mucous cell and release the mucin molecules on the membrane of the cells[59]. Once in seawater, the vesicles rapidly swell, burst, and release the mucins that then interact with the threads and the seawater to produce slime[58].

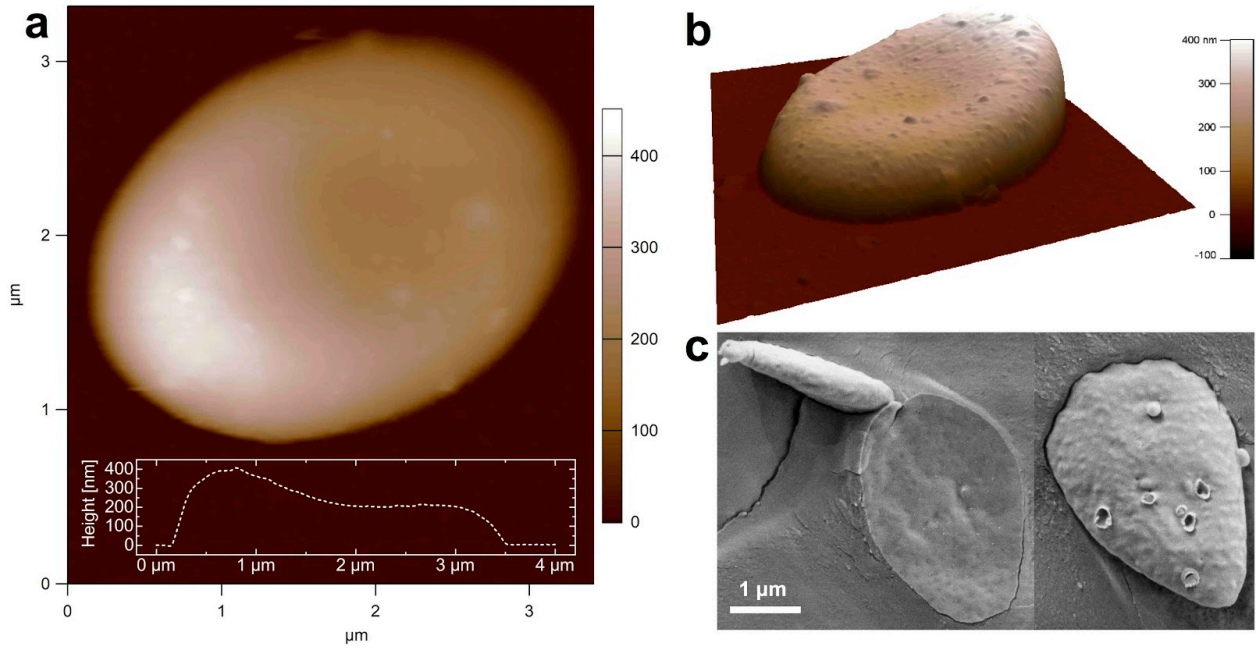

Figure 2.6: Hagfish mucin vesicle shape and size. (a) AFM height image of a hagfish mucin vesicle in Citrate/PIPES (CP) buffer. The height profile of the vesicle along its major axis is shown below. **(b)** 3D representation of the vesicle in (a). **(c)** Cryo-SEM images of mucin vesicles in CP buffer.

Exuded vesicles can be stabilized in concentrated buffer solutions containing polyvalent anions such as citrate, phosphate or sulfate at concentrations of 1 mol/l and higher. In contrast, solutions containing monovalent anions do not stabilize the vesicles, regardless of the valency of the associated cations[5–7,58]. Because these salts are able to keep the vesicles in a condensed state, they also inhibit slime formation as vesicle decondensation and skein unraveling seem intimately linked for the Atlantic hagfish[22]. A study by Herr *et al*.[6] revealed that the vesicle population consists of slow and fast swellers and that disruption of the vesicle membrane with a surfactant homogenizes the swelling kinetics, implying that swelling differences are mediated by the membrane. The authors suggested that aquaporins - channel proteins in membranes of cells that facilitate water flux across the membrane - appear to mediate this process, which was supported by genetic analyses, which showed that two aquaporin-like genes expressed in hagfish slime gland tissue. Furthermore, it was found that in a hypoosmotic environment (distilled water) all vesicles swelled and ruptured by only about 40% of the vesicles ruptured in hyperosmotic sodium chloride solutions. The authors found that Ca^{2+} ions must be present at concentrations of roughly 3 mM or higher in order to rupture all vesicles in high ionic strength environments**,** suggesting the presence of Ca^{2+}-activated channels[60].

Mucin structure and biophysics

The chemical composition of hagfish mucus was analyzed by Salo *et al*.[7], who found that it consists of 77% protein, 12% carbohydrate, 5% lipid, and 6% sulfate by dry weight. Their findings suggested that hagfish mucins are sulfated mucin-like glycoproteins. The term ‘mucin-like’ was used, because a carbohydrate content of 12% is unusually low for mucins, which typically contain around 75% of carbohydrate and about 25% of amino acids[61,62]. Furthermore, the sequence of hagfish mucin is unknown, making it difficult to say whether they are closely related to mucin proteins of the MUC family[22,63]. It would be interesting to know if hagfish mucins are related to the MUC-familiy, which cover all luminal epithelial surfaces in the human body. These mucus layers

predominantly consist of water, mucins, salts, small secreted proteins. Human mucins are either membrane-bound or secreted high-molecular weight (10^6 - 10^7 Da) polymeric glycoproteins that have important protective and lubricative functions. Secretory mucin monomers - as possibly the case for hagfish mucin - possess a central linear protein core with attached sugar moieties, displaying a bottle brush configuration (Fig. 2.7 a).

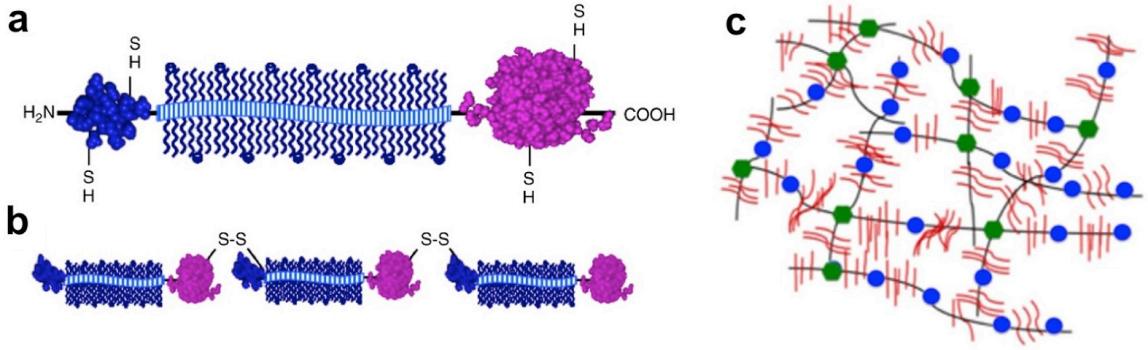

Figure 2.7: Mucin structure and mucin networks. (a) Schematic dumbbell structure of a typical mucin subunit. The central linear glycosylated domain is flanked by globular non-polar domains. **(b)** A mucin molecule composed of subunits that are linked linearly by disulfide bonds (adapted from Coles *et al*.[64]). **(c)** Mucin multimer network with alternating glycosylated (black with red brush) and non-glycosylated (blue) domains forming a mucin gel via hydrophobic associations (blue) and non-covalent cross-linking (green) (adapted from Bansil *et al*.[65])

The carbohydrates, mainly N-acetylgalactosamine, N-acetylglucosamine, fucose, galactose, sialic acid, mannose and sulfate are linked by O-glycosidic bonds to serines and threonines[6162]. At the amino and carboxy terminals of the linear central core there are globular domains with relatively little O-glycosylation and N-glycosylation sites[66–68], giving the mucin monomer a dumbbell appearance. The globular domains are typically high in cysteine, which is involved in dimerization and subsequent polymerization of mucin monomers via disulfide bond formation (Fig. 2.7 b)[62,65,69]. The linear addition of these single dumbbells gives mucins a ball-and-chain structure[70,71]. Mucin networks (Fig. 2.7 c) possess complex non-Newtonian flow behaviors, ranging from viscous liquids to elastic solids. The flow behavior is considered highly important in fulfilling their physiological functions. Rheology offers a valuable tool for the characterization of material properties of mucins such as aggregation behaviour, sol-gel transition, and viscosity[68]. Altered rheological properties may reflect changes in the ability to exert physiological function such as acting as a lubricant, as selective barrier, and as defense against infection[72–76].

Viscoelasticity of liquids and soft-solids

Viscoelasticity is the main physical material property investigated in this thesis. Information about viscoelasticity helps to elucidate structure-property relationships and helps to gain insight into interactions between different material components of the system. The linearized theory of viscoelasticity is governed by the same fundamental equations as is the linearized theory of elasticity, with the exception that Hooke's law of elasticity is replaced by a constitutive description that is sensitive to the material's history of loading and deformation[77]. Characterising time-dependent material properties helps to better understand the fast forming yet short lived structure of hagfish slime, whose nature itself is strongly governed by time.

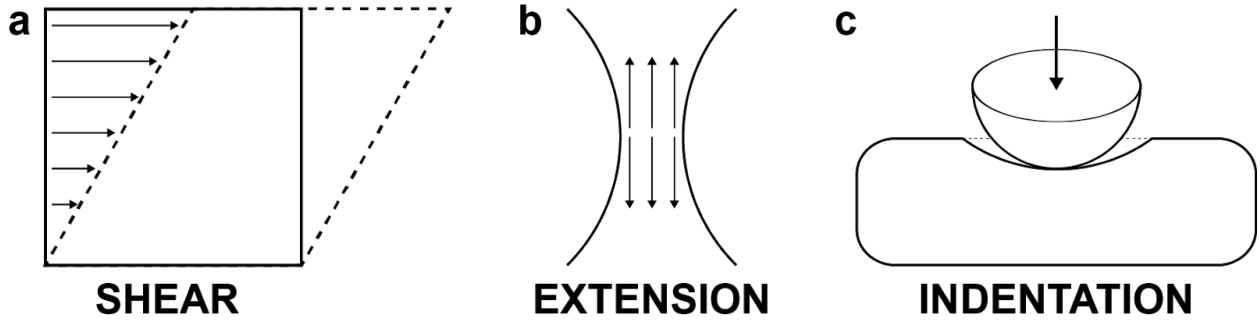

Figure 2.8: Overview of different material deformation modes used in this thesis. (a) Shearing flow field, characterized by a gradient in velocity perpendicular to the direction of travel. **(b)** An extensional flow field, characterized by a gradient in velocity in the direction of travel. **(c)** Indentation a flat (soft-)solid surface by a hard sphere.

Two different approaches were used to study viscoelasticity, namely shear and extensional rheology (Fig. 2.8 a,b) and AFM (atomic force microscopy) nanoindentation (Fig. 2.8 c) based rheology, which will be briefly explained in the following section.
Rheology is the study of the flow and deformation of matter, whereby ideally a well-defined force or deformation is applied to a material and the corresponding force or deformation response is measured. Generally, two different types of flow are defined - extension and shear flow. In shear rheology, a material is sheared by a defined rotation or oscillation of a cylindrical device. In extensional rheology a material is stretched in opposite directions ideally in the absence of shear. In contrast to the closed streamlines achieved by cylindrical devices in shear rheology, extensional rheology typically suffers from open streamlines. This obliges the rheologist to use methods that are designed to indirectly measure material properties, such as optically evaluating the thinning of capillaries, which corresponds to an extensional flow phenomenon. However, rheological models can also be applied to stress-relaxation or creep tests performed in indentation measurements. Also, force-distance (FD) curves obtained in indentation measurements can be analyzed for their viscoelastic behavior as explained further below.

Shear rheology

In simple shear tests, a force is applied by a rotating device, which either operates shear rate $\dot{\gamma}$ controlled or shear stress τ controlled to calculate the viscosity η according to the generalized Newton's law:

$$\eta(\dot{\gamma}) = \frac{\tau}{\dot{\gamma}(t)} \qquad \text{Equation 1}$$

If viscosity is independent of the shear rate, the fluid behaves Newtonian. For Non-Newtonian fluids viscosity depends on the shear rate $\eta(\dot{\gamma})$, which can result in shear thickening, shear thinning or yielding behavior. In contrast to fluids, the stress for purely elastic materials is proportional to the imposed strain $\gamma(t)$. The elastic modulus G is thus defined using Hooke's law[78]:

$$G = \frac{\tau}{\gamma(t)} \qquad \text{Equation 2}$$

Viscoelastic materials comprise both strain and strain rate dependence and their properties can be measured by oscillatory experiments. In oscillatory shear a sinusoidal shear strain $\gamma(t) = \gamma_0 sin(\omega t)$ is applied at a specific angular frequency ω and amplitude γ_0 and the periodic

material stress response $\tau(t) = \tau_0 sin(\omega t) + \delta$ with a phase shift δ is measured. The obtained stress or strain waves can then be converted into the resulting material function $G^*(\omega)$, being the dynamic complex shear modulus[78]:

$$G^*(\omega) = \frac{\tau_0 e^{i\delta}}{\gamma_0} = \frac{\tau_0}{\gamma_0} cos(\delta) + i\frac{\tau_0}{\gamma_0} sin(\delta) = G'(\omega) + iG''(\omega) \qquad \text{Equation 3}$$

$G^*(\omega)$is composed of the storage modulus $G'(\omega)$, representing the elastic material contribution and the loss modulus, $G''(\omega)$, quantifying the viscous loss. A purely elastic material is in phase with the applied strain, resulting in $G' = G$ and $G'' = 0$. In contrast, a purely Newtonian fluid shows a stress response that is 90° out of phase with the strain rate, resulting in $G' = 0$ and $G'' = \eta'\omega$. Consequently, a viscoelastic material exhibits contributions of both, G' and G''[78].

Extensional Rheology - CABER

Extensional flows are of high relevance in many processing operations such as engine technology, ink-jet printing, irrigation, mold blowing[79] as well as in biological processes such as thrombosis[80] or spider silk spinning[81]. Complex fluids often exhibit dramatically different extensional flow characteristics from Newtonian fluids and therefore an integral material characterization should include extensional flow measurements[79,82]. Although the importance of extensional flows is well known, homogenous uniaxial extensional flows are difficult to realize[83]. Extensional flows can be generated in devices such as cross-slots[84], rotational clamps[85], four roll mills[86], opposed jets[87], or by a constriction in a pipe[83]. Low viscosity liquids additionally pose difficulties in their measurability as they cannot be gripped between rotating clamps and their force signal received by the rheometer is too low, which makes techniques used for solid-like materials (approximately 10^3 Pas) not suitable for these fluids. Filament stretching, fiber spinning, and capillary breakup rheology are suitable techniques to generate extensional flows and measure the flow properties of intermediate-to-low viscoelastic liquids[88–92].

In this thesis capillary breakup extensional rheometry (CABER) is used to measure the transient extensional viscosity evolution of low viscosity hagfish mucin solutions. In CaBER a liquid bridge is formed between two cylindrical test fixtures, followed by an axial step-strain to generate a fluid thread between the two fixtures (Fig. 2.9). What follows is a self-driven uniaxial extensional flow, which preferably leads to a break-up of the filament[92]. The reader should note that also in CaBER the range of applicable fluids can be limited by free-surface phenomena such as 'beads-on-a-string' formation and possible end-plate instabilities[93].

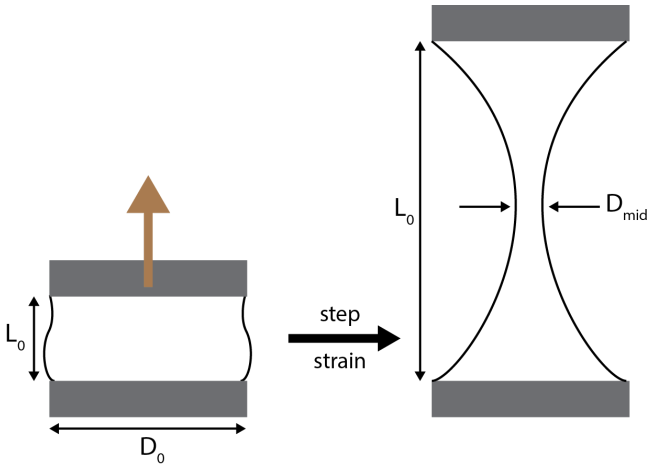

Figure 2.9: Schematic diagram of a capillary thinning experiment in a capillary breakup extensional rheometry (CaBER) measurement. Figure partly based on drawings by Anna and McKinley[92]).

The process of break-up is driven by surface tension and resisted by the extensional stresses that result from the capillary thinning of the liquid bridge. While capillarity tries to minimize the interfacial energy of the created free surface of a fluid thread by formation of spherical droplets, extensional stresses resulting from viscous, elastic, and inertial contributions resist the necking of the thread[94,95] The response of a fluid following an axial step strain is encoded in an apparent transient elongational viscosity function $\eta_{app}(\epsilon)$, which can be determined by measuring the change of the filament diameter D_{mid} (or filament radius R_{mid}) and strain rate $\dot{\epsilon}$ as a function of time:

$$\eta_{app}(\epsilon) = \frac{\sigma / R_{mid}(t)}{\dot{\epsilon}(t)} = \frac{-\sigma}{dD_{mid}/dt} \qquad \text{Equation 4}$$

, where σ is the surface tension. The resulting system Hencky strain ϵ is defined as $\epsilon = 2\ln(D_0/D_{mid}(t))$, where D_0 is the initial diameter of the fluid thread before stretching [92,94]. In the case of the HAAKE CaBER rheometer, the diameter is measured with a laser. The 'true' extensional viscosity can then be calculated by fitting the diameter measurements with the functional form[92]:

$$D_{mid}(t) = Ae^{-Bt} - Ct + E \qquad \text{Equation 5}$$

, which is then differentiated with respect to time. The choice of fitting parameters must have its physical relevance. However, the equation above is not true in all cases as for suspensions a spline is fit and then differentiated numerically. Also, the decay of the fluid filament diameter at intermediate times can be related to the extensional relaxation time of polymers and the fitting parameter B (such that B = 1/3λ_z, which is explained in the next section). Furthermore, C can be related to steady-state value of the extensional viscosity as explained below ($C = \sigma/\eta_{E,\infty}$)[92,95].
Newtonian and viscoelastic fluid filaments neck and break differently. Whereas the axial profile of a Newtonian filament is inhomogeneous and the minimum diameter is always close to the mid-plane, the axial profile of a viscoelastic filament is initially similar to the Newtonian profile but evolves rapidly into an axially uniform cylindrical filament that connects the two almost hemispherical fluid reservoirs near the endplates[92,94]. For Newtonian fluids, the linearly decreasing filament diameter is described by the form:

$$D_{mid}(t) = \alpha \left(\frac{2\sigma}{\eta_s}\right)(t_b - t) \qquad \text{Equation 6}$$

where t_b is the time to breakup and α is the numerical prefactor (α = 0.0709 according the similarity solution to the Stokes equations given by Papageorgiou for viscous Newtonian liquids)[92]. Equation 6 represents the analytical solution to the term $-Ct$ in equation 5.

Elongational viscoelasticity and relaxation times
If the test fluid is viscoelastic, large elastic stresses grow during the transient elongational stretching process. If corresponding viscous stresses are negligible during thinning and thus only elastic and capillary stresses balance each other, then an elasto-capillary force balance predicts that the mid-filament diameter $D_{mid}(t)$ (normalized by the midpoint diameter D_1 following cessation of stretching) decays exponentially in time as follows:

$$\frac{D_{mid}(t)}{D_1} = \left(\sum_i \left(\frac{G_i D_1}{2\sigma} \right) \exp(-t/\lambda_i) \right)^{1/3} \qquad \text{Equation 7}$$

Where $G_i = \eta/\tau$ is the elastic modulus of the material. As dilute polymer solutions have a spectrum of relaxation times, it remains to determine which moment of this spectrum is actually measured in capillary thinning. The same equation can be obtained from the Rouse-Zimm model for an N-bead-spring chain except that G_i and the relaxation time λ_i are related in each mode by $G_i = nk_BT$, where k_B is the Boltzmann constant and $\lambda_i = \lambda_Z / i^{2+\widetilde{\sigma}}$, where λ_z is the Zimm relaxation time $\widetilde{\sigma}$ is a measure of the hydrodynamic interaction and for dilute polymer solutions around 0.4 and n is the number of beads.

In the elasto-capillary regime, a thin uniform thread with a radius that decreases exponentially in time is obtained, resulting in a constant strain rate $\dot{\epsilon}_{mid}$. Using the Rouse-Zimm relationship and the assumption of a constant strain rate, the thinning rate of the capillary can be approximated to:

$$\frac{D_{mid}(t)}{D_1} = \exp(-t/3\lambda_Z) \qquad \text{Equation 8}$$

, with $\dot{\epsilon}_{mid} = 2/3\lambda_Z$. Regression of experimental data to this equation for dilute viscoelastic solutions undergoing elasto-capillary thinning thus yields estimates of the Zimm relaxation time λ_Z [92,96]. Although this time constant is referred to as relaxation time - being the same time constant that is associated with stress relaxation following cessation of steady shear in a capillary-thinning experiment - the stress is not relaxing *per se* but in fact the tensile stress diverges as the radius decays to zero. The 'CABER relaxation time' is thus rather a characteristic time scale for the viscoelastic stress growth in a uniaxial elongational flow[94].

Nanoindentation

Indentation consists of touching a material of interest with unknown mechanical properties such as hardness, elastic modulus (Young's modulus), fracture toughness, or viscoelasticity with an indenter made of another material whose properties are known. Indentation has its origins in Mohs' hardness scale of 1822, in which materials that could leave a permanent scratch in another material were ranked harder, with diamond holding the maximum value of 10. Nanoindentation refers to indentation testing with penetration depths in the range of nanometres (10^{-9} m) rather than microns (10^{-6} m) or millimetres (10^{-3} m)[97]. Nanoindentation is often used to determine mechanical properties when only small or thin samples are available[77], as is the case for hagfish films and fibers tested in this thesis. Probably the most distinguishing feature of nanoindentation to conventional indentation is the indirect measurement of the contact area, being the area between the indenter and the specimen when in direct contact. In indentation tests the area of contact is typically measured directly from the residual impression left in the sample surface when the load is removed whereas in nanoindentation the size of these impressions is too small to be conveniently measured directly. Thus, the area of contact is obtained indirectly by measuring the depth of penetration of the indenter into the sample, which - combined with the known geometry of the indenter, provides the contact area at maximum load[97].

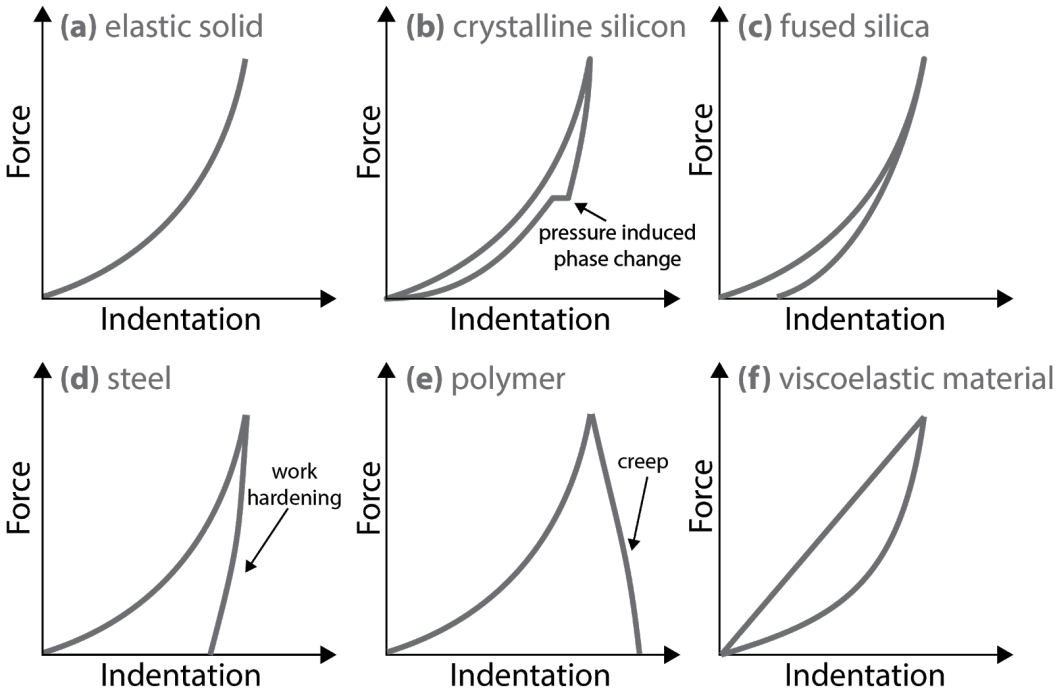

Figure 2.10: Schematic examples of force-distance (FD) curves for different materials. Image created based on data from Fischer-Cripps[97]).

Atomic force microscopy (AFM) can be used to perform nanoindentation measurements. Load-displacement or force-distance (FD) curves are most commonly used in AFM to measure the local elastic properties of soft materials. FD show distinct forms, depending on the indented material (Fig. 2.10 a-f). The Hertz model can then be applied to the approach part of the FD curve to extract Young's modulus E_{Hertz}. The Hertz's model describing the indentation with a spherical indenter has the following form:

$$F(\delta) = \frac{4\sqrt{R}}{3(1-\nu^2)} E_{Hertz} \delta^{\frac{3}{2}} \qquad \text{Equation 9}$$

,where δ is the indentation depth, ν is the Poisson's ratio of the sample (the indenter is assumed to be infinitely rigid compared to the indented sample), and R is the effective radius of curvature of the probe-sample system ($1/R = 1/R_{probe} + 1/R_{sample}$) - or when the sample surface is flat it can be assumed that R is is simply the radius of the spherical probe[98,99]. The Hertz theory assumes that the sample is a purely elastic half-space, that the stress-strain response is linear, and that the elasticity is constant. However, in biology many samples are viscoelastic, which is revealed by a hysteresis between the approach and retraction parts of the FD curves[100] indicating viscous loss, by an indentation speed dependence of the elasticity[101], and by the observations of force relaxation and creep[102]. Therefore, the Hertz model provides a valuable guess but is not sufficient to describe the time-dependent mechanical properties of biological materials[98].

Viscoelasticity in AFM nanoindentation

In general, viscoelastic properties can be obtained by three approaches in AFM based nanoindentation: (1) in the frequency domain, where the cantilever is sinusoidally oscillated with a fixed small amplitude at changing frequencies during indentation[103–105] - representing a nano-DMA test, (2) in the time domain by creep and stress relaxation experiments, where a Heaviside step-loading function is assumed (step-hold experiments) to simplify the analysis[106–108], (3) or directly from FD curves by analysis of the hysteresis between the approach and retraction curve[109].

In this thesis, viscoelastic properties of thin hydrated films produced from hagfish fiber protein was calculated from stress-relaxation measurements and directly from FD measurements.
The major challenge in viscoelastic analysis of FD curves in AFM nanoindentation testing is a moving boundary condition. Pushing a hard indenter into a soft viscoelastic material results in a changing contact area with time between the indenter and the sample half-space, making the elastic-viscoelastic correspondence principle not applicable[97]. Lee and Radok[110] showed that if the solution of the elastic problem is known, then the time-dependent stresses and deformations for an axisymmetric indenter (i.e. the solution to the corresponding viscoelastic problem) may be found by replacing the elastic modulus after introduction of an appropriate hereditary integral operator:

$$F(t,\delta(t)) = \frac{4\sqrt{R}}{3(1-\nu^2)} \int_0^t \Psi(t-\xi)\frac{\partial \delta^{3/2}}{\partial \xi}\partial\xi \qquad \text{Equation 10}$$

,where ψ(t) is a sample relaxation function and ξ is the dummy time variable required for the integration[97,98]. This method provides a time-dependent indentation depth for any load history that does not produce a decrease in contact area, i.e. the function is only valid for the approach curve[97].
A more general approach to solving the linear viscoelastic contact problem for an approach-retraction indentation cycle with a spherical rigid indenter was presented by Ting[111]. Ting's solution can can be applied to any arbitrary history of contact area and is described by following equations:

$$F(t,\delta(t)) = \begin{cases} \frac{4\sqrt{R}}{3(1-\nu^2)} \int_0^t E(t-\xi)\frac{\partial \delta^{3/2}}{\partial \xi}\partial\xi, & 0 \leqslant t \leqslant t_m \\ \frac{4\sqrt{R}}{3(1-\nu^2)} \int_0^{t_1(t)} E(t-\xi)\frac{\partial \delta^{3/2}}{\partial \xi}\partial\xi, & t_m \leqslant t \leqslant t_{ind} \end{cases} \qquad \text{Equation 11}$$

$$\int_{t_1(t)}^{t} E(t-\xi)\frac{\partial \delta}{\partial \xi}\partial\xi = 0 \qquad \text{Equation 12}$$

,where E(t) is the Young's relaxation modulus (analogous to the sample relaxation function ψ(t) of Lee and Radok), t is the time of initial contact between sample and indeter, t_m is the duration of the approach phase, t_{ind} is the duration of the complete indentation cycle) and t_1 is the auxiliary function (Equation 12). The first part of Equation 11 is valid for the indentation approach curve, during which the contact area increases ($0 \leq t \leq t_m$, t_m is the end of the approach phase). This solution is equal to the solution presented by Lee and Radok (Equation 10). The second part of Equation 11 is valid for the retraction curve ($t > t_m$). Here, an auxiliary function t_1 is introduced and defined by $a(t_1) = a(t)$, $t_1(t) < t_m$, which means that the contact area a at time t during the retraction phase is equal to the contact area at time t_1 during the approach phase. The t_1 values found must satisfy the formula in the Equation 11. Using the auxiliary $t_1(t)$ function, the contact area $a(t_1(t))$ and the effective indentation $\delta_1(t_1(t))$ during the retraction phase - best imagined as the indentation relative to the relaxing sample surface - can then be calculated[98]. A time-dependent relaxation modulus E(t) then allows for the use of linear viscoelastic constitutive equations with Ting's model. As the relaxation modulus is a decaying function, it can be well described by rheological models like the standard linear solid (SLS) model or a power-law rheology (PLR) model[98], which was used in this thesis.

Chapter 3 - Materials and Methods

Exudate sampling and stabilization

Atlantic hagfish (M. glutinosa) were fished by the staff of the Atlanterhavsparken in Ålesund, Norway. Hagfish were captured in the Fjords of Ålesund in a depth of about 80 m, using custom built traps from old gasoline canisters, in which holes were drilled and which were then filled with fish scraps. The traps were lowered to the sandy bottom and remained there for about 2 h before they were reeled in. The captured hagfish were transferred to a seawater fed basin. Slime exudate sampling was performed according to the approved ethical application by the Forsøksdyrutvalget (FOTS ID 6912) and followed a modified protocol of Herr *et al*.[6]. In brief, hagfish were anaesthetized using a 1:9 mixture of clove bud oil (Sigma, Switzerland) to ethanol, which was added to seawater in a 10 l bucket at a concentration of 1 ml of anesthetic per liter of seawater. The sedated hagfish were quickly rinsed with tap water, transferred to a dissection tray, blotted dry, and slime exudate was obtained by mild electric stimulation (80 Hz, 18 V, HPG1, Velleman Instruments) on the ventral side. The released exudate was collected and stabilized in MCT oil (medium chain triglycerides, Delios GmbH, Germany), heptane (VWR), or in a high osmolarity citrate/PIPES (CP) buffer (0.9 M sodium citrate and 0.1 M PIPES at pH 6.7, 0.02% sodium azide and protease inhibitor, Sigmafast, Sigma) and immediately stored at 4 °C. After sampling the fish were transferred to a recovery bath and released back to the sea after 1-2 days. Import of the samples was approved by the Swiss Federal Food Safety and Veterinary Office (FSVO) and export was approved by Norwegian Seafood Council.

Water retention measurements

The cohesiveness of hagfish slime mediated by its long fibers allows to lift up the slime mass. The slime network formation efficiency can therefore be directly evaluated by lifting up the entire slime, as the network formation is based on the ability of the threads and mucins to form a cohesive slime. Slime for water retention measurements was prepared by placing MCT or CP stabilized exudate on the bottom of a 20 ml glass flask with a micropipette. Subsequently, 20 ml liquid were poured in, the lid was closed, and the flask was gently turned upside-down eight times. The deployed slime was transferred from the glass flask to a small beaker and placed on a laboratory scale, which had an in-house built mixing device attached on top and a video camera (Sony alpha 5100) placed in front to optically monitor the weight change over time (Figure 3.1).

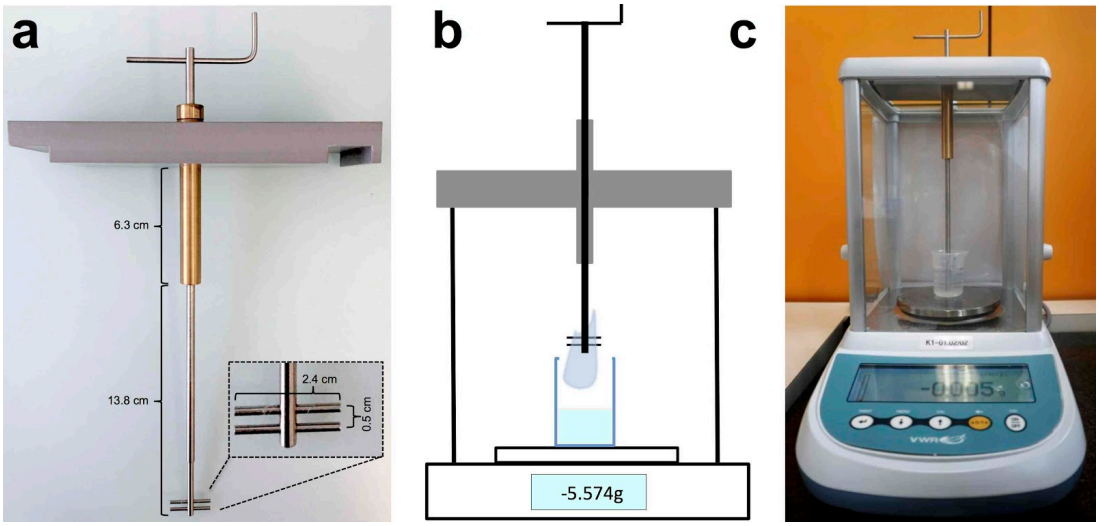

Figure 3.1: Design of the water retention measurement device. (a) Picture of the water retention measurement device with dimensions. **(b)** Schematic drawing of the water retention device with slime. **(c)** Water retention device placed on top of an analytical scale.

The mixing device was then slowly lowered into the slime and rotated ten times to wrap up the slime mass. The wrapped slime was lifted up, the device arrested in the upper position, and the water egress recorded gravimetrically for five minutes The exudate concentration of the measurements was determined according to the assumption of Ewoldt *et al.*[9] (density of the exudate is close to 1 g ml^{-1}, as about 66% of the exudate mass is water). MCT samples could be accurately pipetted with a micropipette as the exudate sunk to the bottom of the Eppendorf tube. To ensure an accurate concentration of exudate in CP buffer, exudate from MCT oil was pipetted into a defined volume of CP buffer for stability and pH tests. For pH experiments the pH of seawater was adjusted with HCl and NaOH, respectively. Seawater for all experiments was obtained in the Fjords of Ålesund and was sterile filtered (0.45 µm, cellulose acetate sterile syringe filter, VWR, USA) prior to measurements. Artificial seawater (ASW) was prepared according to a recipe of Kester *et al.*[112]. All salts were obtained from Sigma. The ionic strength I of all solutions was calculated using following equation:

$$I = \frac{1}{2}\sum_{1}^{n} c_i z_i^2 \qquad \text{Equation 1}$$

,where c is the concentration of the dissolved salt ion in mol l^{-1} and z is the valency of the ion. For the dissolved salts a complete dissociation was assumed. All experiments were performed in triplicates and at room temperature.

Optical microscopy

Light microscopy

Light microscopy was performed on a Nikon Diaphot (Nikon, Japan) in transmission illumination mode using 10x, 20x and 40x magnification objectives. Images and videos were captured and analyzed with the NIS elements D3.0 software. High speed image sequences of skein unraveling were captured with a high speed camera (Memrecam fx RX6, nac Image Technology, USA)

connected to the light microscope. Movies were recorded at a framerate of 1000 frames per second and a shutter speed of 20 kHz.
Rupture of mucin vesicles at different temperatures was investigated by mounting a heating plate onto the microscope. The heating plate was preheated to the corresponding temperature for 5 min. A microscopy slide with 1 µl exudate from MCT oil and covered with a coverslip was mounted on the heating plate. The time needed for the vesicle halo to burst was used as rupture time. All experiments were performed in triplicates. The value for rupture at 4°C was determined by measuring the time needed for MCT samples to clump in the fridge. Skein unraveling assays under the microscope with trypsin (trypsin from porcine pancreas, Sigma, 30000 units ml^{-1} in 5 mM potassium phosphate buffer pH 6.5) were performed on old skeins (8 months) that were stabilized in CP buffer and that did not unravel anymore. The skeins were washed with 100 mM DTT to remove mucins and then dialyzed against milliQ water (24 h, 3 x) and freeze dried. Also non freeze dried skeins were investigated and showed the same unraveling behaviour.

Scanning Electron Microscopy

For Scanning Electron Microscopy (SEM) fresh unstabilized exudate was placed on SEM plates and a few drops of Milli-Q water were added onto the sample without stirring. The samples were air dried for 48 h and subsequently sputter coated (SCD 050 sputter coater, Bal-Tec) with a 3 nm thick platinum layer. SEM was performed on a LEO 1530 (Carl-Zeiss SMT AG). For cryo-SEM, heptane and CP stabilized exudate samples were snap frozen with a high pressure freezer (Bal-Tec HPM100) and subsequently freeze-fractured (Bal-Tec BAF060). Cryo-SEM was conducted on a Zeiss LEO 1530.

Confocal Laser Scanning Microscopy

Confocal Laser Scanning Microscopy (CLSM) was performed on a Zeiss LSM 780 (Carl Zeiss AG, Germany). Slime fibers were stained with Nile Blue (Sigma Aldrich, USA) and imaged in reflection made. Freeze dried mucin was not stained and imaged in transmission made. Image stacks were acquired and collapsed to a yield 2D image.

High Pressure Liquid Chromatography

Lipid analysis was performed using High Pressure Liquid Chromatography (HPLC). Vesicles for lipid analysis were obtained similar to the protocol of Salo *et al.*[7]. Exudate stabilized in CP buffer was filtered through a series (60 and 20 µm) of nylon mesh filters (Merck) to separate the mucin vesicles from the skeins. The vesicle suspension was washed with CP buffer three times and subsequently concentrated by repeated centrifugation (2960 g for 30 min). The concentrated vesicles were then decomposed according to the protocol of Bligh and Dyer[113]. A mixture of chloroform methanol, chloroform, and nanopure water at a ratio of 2 : 2 : 1 were added to the sample while homogenizing with a colloidal mill (Ultra Turrax, IKA). The homogenized sample was centrifuged (2960 g for 10 min), the chloroform phase was collected and the contained lipids were concentrated by bubbling N_2 through the sample. Lipid classes were qualitatively analysed by a Nexera/Prominence HPLC system (Shimadzu, Japan) coupled to a LTII evaporative light scattering detector (Shimadzu, Japan) according to Olsson *et al.*[114] with the following modifications. The sample was dissolved in a mixture of eluents (eluent A : eluent B = 1:1 by vol.) to a concentration 0.05 – 0.10 mg ml^{-1} and separated on Reprosil-Pur 120 CN column (250 x 4.6 mm, 5 µm) equipped with a guard column (ReproSil-Pur 120 CN, 10 x 4.6 mm, 5 µm) (Dr. Maisch GmbH, Ammerbuch, Germany) kept at a constant temperature (26.0°C). A binary gradient elution

at a constant flow rate of 1.0 ml min^{-1} and consisting of eluents A = n-Hexane and B = Toluene : Methanol : Acetic acid : Triethylamine = 60 : 40 : 0.2 : 0.1 (by wt.) was used with the following timetable: at 0.0 – 3.0 min 95 : 5 (%A : %B), at 8.0 min 60 : 40, at 14.0 min 50 : 50, at 15.0 min 5 : 95. The ELSD evaporation temperature was 30°C and the gas pressure (N_2) was kept at 3.20 bar. The injection volume was 10 µl. All solvents were of LC-grade (Merck and VWR chemicals). The lipid classes were identified by comparison with retention times of commercial analytical standards (Avanti, NuCheck and Sigma).

Vesicle concentration (UV-VIS)

Turbidity scales with the amount of condensed vesicles in a solution (e.g. CP buffer) as found by Salo *et al.*[7]. In brief, vesicle suspensions were prepared by filtering exudate in CP buffer through a series (60 and 20 µm) of nylon mesh filters (Merck, Germany) to separate the vesicles from the skeins. The vesicles were then concentrated by centrifugation at 3000 g for 10 min and the supernatant was discarded. The mucin content of the vesicle stock suspension was determined in triplicates by dialysis (25 kDa MWCO, SpectraPor, USA), dialyzing 0.5 ml of the vesicle stock against Milli-Q (three batches à 2 l, 12 h each) and subsequent freeze drying to obtain the mucin dry weight[7]. The mucin dry weight was then correlated to UV-VIS turbidity measurements (Fig. 3.2), whereby the absorption of dilutions (dilution with CP buffer) of the same vesicle stock suspension was measured at 350 nm in the linear range (0.1 < absorption < 0.8) using a UV-VIS spectrophotometer (Cary 300, Agilent Technologies, USA). This correlation then allows for a quick determination of the vesicle content in CP buffer of a stock solution of unknown mucin content without the need to dialyse and freeze dry. It is important to disaggregate (vortex in Eppendorf) the vesicles in the stock suspension when they are diluted before UV-VIS measurements in order to obtain a linear relationship.

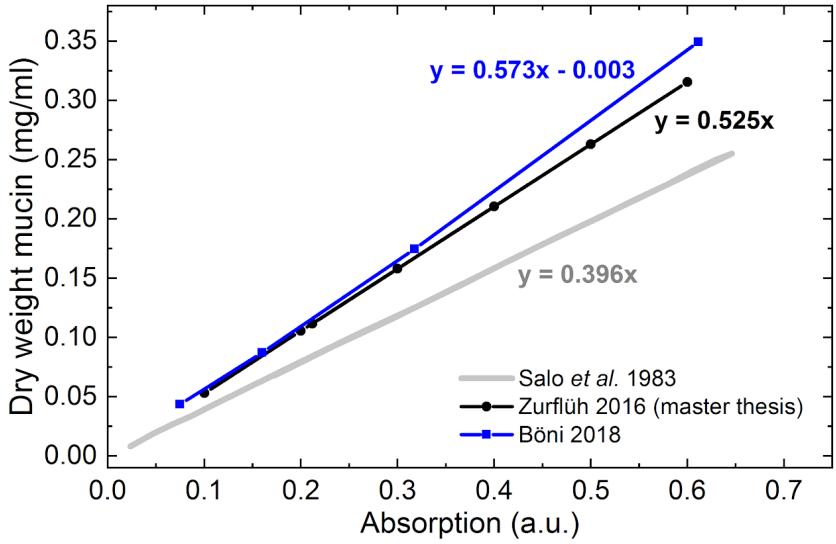

Figure 3.2: UV-VIS absorption vs mucin dry weight relationships of three different hagfish mucin vesicles stock suspensions, measured at a wavelength of 350 nm.

Similarly, UV-VIS can be used to monitor the presence of unopened / condensed vesicles in solutions other than CP buffer, such as high molarity NaCl solution, which also have a stabilizing effect on the vesicles. NaCl solutions of different molarities were poured over fresh MCT-oil stabilized exudate without mixing. Because no mixing was applied many skeins did not open, especially at higher NaCl concentrations. The solutions were let to rest for 1 hour, allowing for unopened skeins to sediment. The condensed vesicles will not sediment within this time frame

because of their smaller size. 1 ml liquid was then taken from the top and filled into cuvettes for turbidity measurement at 350 nm. After a first measurement, 10 µl of a 1 M $CaCl_2$ solution was added to the cuvette to reach a final Ca^{2+} concentration of 10 mM. The liquid in the cuvette was gently mixed and the turbidity measured again. All measurements were performed in triplicate, at room temperature, and at an exudate concentration of 0.8 µl exudate ml^{-1}.

Atomic absorption spectroscopy

The concentration of cations (Na^+, K^+, Ca^{2+}, Mg^{2+}) in seawater and in seawater that interacted with hagfish slime was determined using flame atomic absorption spectroscopy (AAS). The cation concentrations were determined for seawater, seawater that remained in the glass after gelation and immediate removal of the slime ('unbound fraction'), and for seawater that drained from hagfish slime during five minutes ('bound and drained fraction'). Slime samples were prepared (see water retention measurements) and slime was removed using the in-house built mixing device described above. Flame AAS was performed on a Varian AA240FS Fast Sequential Atomic Absorption Spectrometer (Agilent Technologies AG, Switzerland). The hollow cathode lamp was heated for 30 minutes before measuring. For calibration, 3 different commercial standards (Merck; Titrisol) and a zero were freshly prepared with Milli-Q water and 100 µl of 32% hydrochloric acid (HCl). The stock solutions of the standards were diluted to 0.25 - 5 ppm, depending on the cation and the detection range of the individual lamp. The sampling tube was flushed with Milli-Q water between all measurements. All AAS data was measured within the confidence interval and the calibration range of the respective cation. As performed with the calibration standards, all samples were acidified with 32% HCl prior to dilution for the measurement to ensure full dissolution of the contained metals. A repeated measures ANOVA was performed with SPSS. The data fulfilled all statistical assumptions. All experiments were performed in triplicates.

Rheology

For rheology measurements either whole slime or mucin solutions were used. Whole slime and hagfish mucin solutions were prepared by pipetting a certain amount of either exudate or vesicle stock suspension into a flask or Eppendorf, followed by pouring over the liquid, closing the lid and gently turning the flask upside-down eight times.

Dynamic viscosity measurements

For dynamic viscosity measurements the mucin solution was analysed using a capillary viscometer (KPG Ubbelohde, SI Analytics GmBH, Mainz, Germany) with a capillary Nr. II with a diameter of 1.13 mm. Capillary viscometers work on the basis of the Hagen-Poiseuille law $\frac{V}{t} = \frac{\pi R^4 \Delta P}{8 L \mu}$ in which t, V, R, L, ΔP, and µ are time, volume, radius of capillary, length of capillary, pressure drop, and dynamic viscosity of fluids, respectively. The viscosity is determined by measuring the time required for a defined liquid volume to flow through a capillary tube. The sample was loaded and drawn up through the capillary by applying a vacuum with a syringe. Subsequently, the vacuum was released and the time needed for the mucin solution to pass the graduation marks was measured with a precision stopwatch. By reordering the Hagen-Poiseuille law, the kinematic viscosity v can be calculated as $v = K (\Delta t - \Theta)$ where K is the constant for the capillary (in this case $K = 0.1\ mm^2\ s^{-2}$), Δt the time used for the passage, and Θ is the Hagenbach correction (HC) time, which depends on the capillary diameter and the passage time and is provided by the supplier. The dynamic viscosity was then calculated as $\eta = v\ \rho$ with ρ being the fluid density. Mucin

concentration was about 0.02 mg ml^{-1}. All samples were measured in triplicates and at room temperature.

Shear rheology

A shear rheometer (Physica MCR501, MCR702, Anton Paar, Austria) with a Couette geometry (CC27, Anton Paar, Austria) was used for shear experiments. Amplitude sweeps were performed at a fixed frequency $\omega = 1$ rad s^{-1}. Shear viscosity was measured by applying constant shear rates of 1, 10, and 100 s^{-1} over a period of 30 min. A shear rate dependent viscosity was obtained by plotting the viscosity of the constant shear rate experiments over the applied shear rate at a given time. Measurements were performed at 10 °C.

Extensional rheology

Capillary breakup extensional rheometry (CaBER) was performed on a HAAKE CaBER 1 (Thermo Haake, Scientific Instruments) to test the extensional rheological properties of hagfish mucin solutions. 90 µl mucin solution were carefully loaded with a syringe between the two parallel cylindrical plates with a diameter D_0 = 6 mm and initial separation L_0 = 3 mm (initial aspect ratio $\Lambda_0 = L_0/D_0 = 0.5$). The top endplate was then moved upward to a final gap of L_f = 12.03 mm (final aspect ratio $f = L_f/D_0 = 4.01$) using a linear step strain of 50 ms to form a liquid filament. The subsequent decay of the liquid filament diameter D(t) was monitored with a laser micrometer at a sample rate of 5 kHz. The uniaxial extensional flow in the formed liquid filament leads to a self-driven break-up of the filament. The apparent transient elongational viscosity $\eta_{app}(t)$ was determined by measuring the change of the capillary diameter $D_{mid}(t)$ and the resulting strain rate $\dot{\epsilon}$ as a function of time:

$$\eta_{app}(\dot{\epsilon}) = \frac{\sigma R_{mid}(t)}{\dot{\epsilon}} = \frac{-\sigma}{dD_{mid}(t)/dt} \qquad \text{Equation 2}$$

,where σ is the surface tension and $R_{mid}(t)$ is the measured capillary diameter at the mid-plane. The resulting Hencky strain ε is defined as $\varepsilon = 2\ln[D_0/D_{mid}(t)]$ with D_0 being the initial diameter of the fluid thread before stretching[92,115]. Every sample was measured in triplicate. All measurements were performed at room temperature (21 °C). Images of the capillary thinning event were captured with a high speed camera (Memrecam fx RX6, nac Image Technology, USA) with a macroscope lens (Leica Z16 APO, Leica, Germany) at a framerate of 5000 frames per second and a shutter speed of 20 kHz.

Gel electrophoresis

For SDS-PAGE gel electrophoresis, 200 µg freeze dried skeins were mixed with 100 µl 1 x Laemmli loading buffer. The samples were ultrasounded for 10 min at frequency of 80 kHz (Emasonic P, Elma, Germany) and subsequently heated for 15 min at 90°C with a mixing rate of 500 rpm (Mixing Block MB102, ACTGene, USA). Before loading, all samples were centrifuged at 10'000 g (Biofuge Pico, Heraeus, Germany) to remove non-solubilized cellular debris. The gels were run on 10-20 % Criterion TGX Stain-Free Precast Gels (Bio-Rad Laboratories, USA). The reactor was filled with electrophoresis buffer, which was diluted from a 5 x stock solution (0.25 M TRIS, 1.92 M glycine and 0.5 % SDS in Milli-Q). 10 µl protein ladder (Precision Plus Protein Standards Dual Color, Bio-Rad Laboratories, USA) were loaded along with 20 µl of sample. The sample was run for 20 min at 100 V and subsequently for 12 min at 300 V. The gel was stained for 1h (0.05 % w/v Coomassie blue R250, 50 % v/v methanol, 10 % v/v acetic acid glacial and 40 %

v/v Milli-Q) and subsequently destained (10 % v/v methanol, 7.5 % v/v acetic acid glacial and 82.5 % v/v Milli-Q) on an agitation unit (Automated Gel Stainer, Hoefer, USA) for 24 h. The destaining solution was replaced several times. An image of the gel was acquired using the Molecular Imager® Gel DocTM XR+ System with Image LabTM Software 5.2.1 (Bio-Rad Laboratories, USA). The molecular weight of the bands was calculated according to the linear equation of the logarithmic weight of the protein marker versus the running distance relative to the dye front.

Production of films and fibers

Two kinds of films were produced, 'drop-cast' and 'coagulation' films. A protein dope for film production was prepared by solubilizing lyophilized skeins in ≥ 96 % formic acid for 1h to obtain a 10 % w/v stock solution[116]. Proper dissolution of the protein required intense vortexing during the first 10 min. For drop-casting 50 µl of 5% v/w dope were pipetted on a flat teflon surface, forming a film with a diameter of about 8 mm. The film was removed after drying 24 h at ambient air. Coagulation films were produced following a slightly modified protocol of Negishi *et al*.[116]. In brief, about 10 µl of the 5 % w/v protein dope were dropped on the surface of an ice cooled coagulation bath containing 100 mM magnesium chloride ($MgCl_2$) and 20 mM 4-(2-hydroxyethyl)-1-piperazineethanesulfonic acid (HEPES) at pH 7.5. Before film formation, a fine woven wire cloth with 1 mm mesh size (Haver&Boecker, Germany) and above it a thin teflon plate with holes (8 mm diameter) were immersed in the coagulation bath. The film formed in the hole of the teflon slide and was lifted out of the bath after 15 s. The underlying metal mesh ensured that the film was not stretched by surface tension during removal. For fiber production the coagulation films were picked with tweezers in the center and lifted with a speed of approx. 2 cm/s 15 s after formation. The fibers were placed on a flat teflon slide and dried at room temperature for 24 h. Natural hagfish fibers were obtained by placing hagfish slime on a teflon plate and gently applying bi-directional stretching. The aligned slime fibers were air dried for 24 h, washed with 50 mM DTT and Milli-Q and subsequently dried again for 24 h.

ATR-FTIR

Attenuated total reflectance - Fourier transform infrared spectroscopy (ATR-FTIR) was performed on an FTIR device (Varian 800 FTIR, Varian, USA) equipped with an ATR accessory (Golden Gate Standard, Specac, USA). The software Resolutions (Resolutions 4.0, Varian, USA) was used for acquisition of the ATR-FTIR spectra. The spectra were acquired in the wavenumber range of 600-4000 cm^{-1} with a resolution of 4 cm^{-1}. The number of scans was set to 64 and automatic atmospheric compensation was performed. The background was subtracted from all spectra. For qualitative comparison, the spectra were normalized between 0 and 1 by the maximum of the amide I peak. Peak deconvolution was performed with the software OriginPro 9.1.0 (Electronic Arts, USA). The amide I peak (~1650 cm^{-1}) was selected visually and the edges were defined as local minima on each side of the peak. A straight line was subtracted to correct the tilt of the amide I peak. The second derivative with a Savitzky-Golay smoothing was calculated with a polynomial order of 2 and 7 points of window. The peak deconvolution was performed using a multiple Pseudo-Voigt I peak fit and by selecting the minima of the second derivative, indicating the location of the deconvolved peaks. All fits had an R^2 of > 0.99. Choice of peak assignments to secondary structure motifs is based on the work of Hu *et al*.[117] and Zou *et al*.[118].

X-Ray Diffraction (XRD)

Small angle X-ray scattering (SAXS) and wide angle X-ray scattering (WAXS) experiments were performed at ambient temperature. **Fibers:** WAXS experiments on fibers were performed using a Bruker AXS Micro (Bruker, USA) equipped with a microfocused beam (50 W, 50 kV, 1 mA) with the l_{CuKa} = 0.15418 nm radiation in order to obtain direct information on the scattering patterns. The scattering intensities were collected by a two-dimensional Dectris 2D Pilatus 100K X-ray detector (83.8 cm × 33.5 cm, 172 µm resolution) (Dectris, Switzerland). An effective scattering vector range of 1 nm^{-1} < q < 25 nm^{-1} was obtained, where q is the scattering wave vector defined as $q = 4\pi \sin\theta / l_{CuKa}$ with a scattering angle of 2θ. **Swollen and dry films:** SAXS and WAXS experiments on dry and swollen films were performed using a Rigaku MicroMax-002$^+$ (Rigaku, Japan) equipped with a microfocused beam (40 W, 45 kV, 0.88 mA) with the l_{CuKa} = 0.15418 nm radiation collimated by three pinhole collimators (0.4, 0.3, and 0.8 mm) in order to obtain direct information on the scattering patterns. The SAXS and WAXS intensities were collected by a two-dimensional Triton-200 gas-filled X-ray detector (20 cm diameter, 200 µm resolution) and a two-dimensional Fujifilm BAS-MS 2025 imaging plate system (15.2 × 15.2 cm^2, 50 µm resolution) (Fujifilm, Japan), respectively. An effective scattering vector range of 0.05 nm^{-1} < q < 25 nm^{-1} was obtained. WAXS intensity profiles were deconvoluted by using pseudo-Voigt peak functions. Hydrated films were evaluated by using a gel-like model including a pseudo-Voigt peak function, where the resulting peak position is related to the average distance between solvent pockets (mesh-size).

Atomic Force Microscopy (AFM)

AFM imaging and indentation

AFM (atomic force microscopy) was performed on a Cypher (Asylum Research, USA). Images were acquired in tapping mode in air and water using OMCL-AC240TS cantilevers (Olympus, Japan). In water the cantilevers were driven with the Blue Drive® technology. Nanoindentation was performed using gold-coated high-precision spherical tip cantilevers (Nanotools, Germany) made of diamond-like carbon. The tip radius of each cantilever is measured in high resolution SEM and is precise down to the nanometer. Dry films were indented in air using a 50 nm radius indenter (B50-NCAu) with a spring constant of 32 nN/nm at 2 µm/s. Indentation in liquid was performed using indenters with 500 nm radius (B500-NCAu and B500-FMau) with spring constants of 38.5 nN/nm and of 1.75 nN/nm, respectively. Unless stated differently indentation in liquid was performed at 1 µm/s approach speed. The thermal method was used to determine the spring constant of the cantilevers. Before every indentation measurement, the InvOLS were determined by indenting on silica substrate. Force-volume maps were acquired containing between 120 - 1200 force curves. Drop-cast films were directly cast on silicon substrate and dried for 24 h at room temperature. Washed and dry coagulation films were placed on silicon substrates and gently hydrated with Milli-Q, which caused the films to stick and allowed subsequent repeated hydration without removal. All measurements were performed at room temperature.

Film swelling monitored by AFM

The films were hydrated in deionized water (Milli-Q), in simplified seawater (SSW) (545 mM NaCl + 10 mM $CaCl_2$) to mimic the high salt conditions faced by natural hagfish fibers as well as in 1% SSW (5.45 mM NaCl + 0.1 mM $CaCl_2$). For AFM nanoindentation and swelling height

measurements the films were hydrated in 1% SSW in order to screen surface charges. Swelling of films was assessed with AFM using force-volume mapping (FVM). Similar to imaging in tapping mode, FVM provides a height profile by determining the contact point of cantilever and sample. The combination of this 'low speed tapping' with the long approach/retrace distances avoids dragging of the sample and allows to image the same sample in air and subsequently in liquid without changing sample, or cantilever. Thus, the exact same position can be monitored before and after hydration. All FVM images were acquired on a sample edge (scratched with a scalpel) in order to always have both, sample and substrate on the same image to more accurately monitor swelling. The height images were flattened (1st order) and the difference between the medium value of the height histogram of the film to the histogram of the substrate was recorded as height. All measurements were performed on three different films at room temperature.

Surface roughness

The root mean square (RMS) roughness of the films was calculated from 5 x 5 µm AFM images, which were segmented into 25 1 x 1 µm squares in order to obtain RMS roughness values within the relevant range for indentation (indenter size = 1 µm diameter in water). The images were flattened (0 order) and the RMS roughness was calculated using Igor Pro (WaveMetrics, USA).

Calculation of (visco-)elasticity

Calculation of apparent elasticity: The apparent Young's modulus was extracted by fitting the Hertz contact model (Equation 3) to the loading part of the hydrated films and to the unloading part of the dry films of the AFM force-distance (FD) curves using Igor Pro (WaveMetrics, USA) and Matlab (Mathworks, USA). The Hertz model for a spherical indenter has the following form:

$$F(\delta) = \frac{4\sqrt{R}}{3(1-\nu^2)} E_{Hertz} \delta^{3/2} \qquad \text{Equation 3}$$

,where F is the force acting on the cantilever, δ is the indentation depth, R is the radius of the spherical indenter, E_{Hertz} is the Young's modulus, and v is the sample Poisson's ratio (assumed to be 0.5 for full volume conservation).

Calculation of viscoelasticity: Viscoelastic parameters of the hydrated films were obtained on the one hand i) directly from FD curves using an approach by Efremov *et al*.[98] and on the other hand by ii) fitting a stretched exponential model to stress-relaxation measurements. All (visco-)elasticity values were corrected for bottom effects (finite sample thickness) where required[119,120].

i) Viscoelasticity directly from FD curves: The major challenge in viscoelastic analysis of FD curves in AFM nanoindentation testing is a moving boundary condition. Pushing a hard indenter into a soft viscoelastic material results in a changing contact area with time between the indenter and the sample half-space, making the elastic-viscoelastic correspondence principle not applicable[97,98]. Lee and Radok[110] showed that if the solution of the elastic problem is known, then the time-dependent stresses and deformations for an axisymmetric indenter (i.e. the solution to the corresponding viscoelastic problem) may be found by replacing the elastic modulus after introduction of an appropriate hereditary integral operator[97]. Their method provides a time-dependent indentation depth for any load history that does not produce a decrease in contact area, i.e. the function is only valid for the approach curve[98]. A more general approach to solving the linear viscoelastic contact problem for an approach-retraction indentation cycle with a spherical rigid indenter was later presented by Ting[111]. Ting's solution can be applied to any arbitrary history of contact area and is described by following equations:

$$F(t,\delta(t)) = \begin{cases} \frac{4\sqrt{R}}{3(1-\nu^2)} \int_0^t E(t-\xi)\frac{\partial \delta^{3/2}}{\partial \xi}\partial\xi, & 0 \leqslant t \leqslant t_m \\ \frac{4\sqrt{R}}{3(1-\nu^2)} \int_0^{t_1(t)} E(t-\xi)\frac{\partial \delta^{3/2}}{\partial \xi}\partial\xi, & t_m \leqslant t \leqslant t_{ind} \end{cases}$$ Equation 4

$$\int_{t_1(t)}^{t} E(t-\xi)\frac{\partial \delta}{\partial \xi}\partial\xi = 0$$ Equation 5

Where *E(t)* is the Young's relaxation modulus (analogous to the sample relaxation function of Lee and Radok), *t* is the time of initial contact between sample and indeter, t_m is the duration of the approach phase, t_{ind} is the duration of the complete indentation cycle) and t_1 is the auxiliary function (Eq. 3). The first part of Equation 4 is valid for the indentation approach curve, during which the contact area increases ($0 \leq t \leq t_m$, t_m is the end of the approach phase). This solution is equal to the solution presented by Lee and Radok. The second part of Equation 4 is valid for the retraction curve ($t > t_m$). Here, an auxiliary function t_1 is introduced and defined by $a(t_1) = a(t)$, $t_1(t) < t_m$, which means that the contact area *a* at time *t* during the retraction phase is equal to the contact area at time t_1 during the approach phase. The t_1 values found must satisfy the formula in the Equation 4. Using the auxiliary $t_1(t)$ function, the contact area $a(t_1(t))$ and the effective indentation $\delta_1(t_1(t))$ during the retraction phase - best imagined as the indentation relative to the relaxing sample surface - can then be calculated. A time-dependent relaxation modulus *E(t)* then allows for the use of linear viscoelastic constitutive equations with Ting's model. As the relaxation modulus is a decaying function, it can be well described by rheological models such as a power-law rheology (PLR) model as used in this study[98]:

$$E(t) = E_\infty + \frac{E_0 - E_\infty}{1 + (t/t')^\alpha}$$ Equation 6

where E_0 is the instantaneous modulus, E_∞ the infinite modulus, *t'* is a small time offset (equal to $5*10^{-5}$ s in this study), and α is the power-law exponent (where $\alpha = 0$ means a solid-like behavior and $\alpha = 1$ a fluid-like behaviour). The modified PLR can be viewed as an infinite number of spring-and-dashpot combinations in parallel with removed zero time singularity, leading to a continuous relaxation spectrum and power-law decay[77,98,121].

ii) Stretch exponential fit: AFM stress-relaxation measurements were performed by indenting and leaving the indenter to dwell in the film for 10 s while the z-piezo drive is paused and cantilever deflection i.e. force is monitored over time. The relaxation curves were fitted with a stretched exponential function of the form:

$$F = F_E + F_V * exp[-(t/\tau)^\beta]$$ Equation 7

, where F_E represents stored (elastic) stresses, F_V are dissipated (viscous) stresses, τ is the relaxation time, and β is a fractional power-law exponent ($0 < \beta \leq 1$) used for 'stretching'. A stretched exponential relaxation is commonly interpreted as a 'global relaxation' of a system that contains many independently relaxing species of which each decays exponentially in time with a specific relaxation rate[122]. A stretching exponent of $\beta = 1$ results in simple exponential decay whereas smaller values of β suggest non-exponential relaxation processes that show a 'fat tail' at long times, which originates from a continuous sum of exponential decays[122,123].The stretching exponent β is considered to be related to the logarithmic full width at half maximum (FWHM) of the relaxation time probability distribution $P(\tau/\tau^*,\beta)$, where τ^* denotes a characteristic relaxation time. A physical interpretation of β is that it represents a measure of the intrinsic small relaxation-rate cutoff of $P(\tau/\tau^*,\beta)$[122]. The stretched exponential function is commonly used to describe the relaxation behavior of homogeneous glasses as well as of linear viscoelastic media[123–125].

Non-linear curve fitting was performed with the software Origin (Originlab, USA) using the Levenberg-Marquardt algorithm. For each film 17 curves were fitted, each with a peak load 90 nN as in indentation force-volume maps. Peak loads of 90 nN force resulted in average indentation depths of 43 ± 5 nm for drop-cast films and 58 ± 8 nm for coagulation films. During the 10 s dwells the spherical indenter crept about 10 nm into the films due to unavoidable elastic stresses in the cantilever, resulting in a change of indentation area. However, this change in area was found to be generally smaller than the uncertainty of the measurements and for the sake of simplicity the area was considered constant for the stretch-exponential analysis[126].

Chapter 4 - Stabilization and Functionality of Hagfish Slime Exudate

The content of this chapter has been partially published by Böni, L.J., Zurflüh, R., Widmer, M., Fischer, P., Windhab, E. J., Rühs, P. A., Kuster, S. in “Hagfish slime exudate stabilization and its effect on slime formation and functionality.” *Biology Open* 2017, *6*, 1115-1122.

Slime exudate from hagfish is obtained by mildly electro-stimulating the surrounding area of the slime pores. The sensitive exudate is immediately stabilized either in a high osmolarity buffer or by immersion in oil, however little is known about the stabilization mechanisms and duration.
Immersion in oil was first used by Ewoldt *et al*.[9]. The authors stabilized the exudate under mineral oil to study whole slime mechanics using rheology. Following a similar approach, MCT (medium-chain triglycerides) oil was found to have superior stabilization and handling properties to mineral oil[127], mainly because handling with a micropipette is easier as the sample remains fluidized.
The stabilizing effect of a high osmolarity buffer was first described by Downing *et al.*[5] who found that exudate is stabilized in 1 M $(NH_4)_2SO_4$. The stabilization criteria were further investigated by Salo *et al.*[7], who reported that hagfish exudate is also stabilized in 0.5 - 1 M sodium citrate as well as 3 M sodium tartrate and sodium acetate. Later, stabilization criteria were systematically tested by Luchtel *et al*.[6,58], who found that high osmolarity solutions of sulfate and phosphate were also able to stabilize the exudate. 0.1 M PIPES (piperazine-N,N′-bis(2-ethanesulfonic acid)), PMSF (a serine protease inhibitor), as well as small amounts of EDTA, glycerol and $MgCl_2$ were added to the stabilization buffer by Spitzer *et al.*[41]. A simpler version of this buffer (0.9 M citrate / 0.1 M PIPES, pH 6.7), to which 0.02 % NaN_3 as well as the Sigma-Aldrich protease inhibitor cocktail can be added to ensure bacterial and enzymatic stability[128] became the widely used standard, largely favored by the facilitated separation of skeins and vesicles in citrate[7]. The stabilization mechanism in buffer remains yet elusive but the presence of high molarities of di- and trivalent anions was found to be important for stabilization of mucin vesicles. In addition, the stability criteria for skeins seem intimately linked to those of the vesicles. The mucin vesicles are known to be stable for days in buffers with the appropriate ion composition and an osmolarity of about 900 mOsmol l^{-1} and higher[58] but thread skeins quickly lose their ability to unravel in CP buffer. Whereas the effect of ionic strength and ionic composition needed for stabilization of hagfish exudate[53] was studied in depth to stabilize mucin vesicles[58], the influence of time, temperature, and pH during storage of both main stabilization techniques was not investigated, although crucial for hagfish slime research. Especially, because stabilization of hagfish slime is directly linked to the complex slime formation mechanism.
In this study we promote water retention measurements as an easy, robust, and quantitative method to assess hagfish slime functionality, which is intimately linked to skein unraveling. This is of particular advantage when other techniques to gauge the material properties of fluids, gels, and soft solids such as rheology are not applicable due to difficult sample handling, low torques, or inhomogeneous structures. With this method we investigate the impact of storage time, temperature, and pH on exudate functionality and discuss putative mechanisms which reduce or even lead to a loss of the slime forming functionality, further on referred to as degradation. We found that exudate faces different pathways of degradation when stored either in oil or in buffer. Furthermore, we provide evidence that also the skeins of the Atlantic hagfish (*M. glutinosa*) - similar to the skeins of the Pacific hagfish[53] - contain a water soluble glue, which likely denatures

during storage. We propose that the denatured glue is the main cause leading to a ceased unraveling of hagfish skeins when stored in buffer over longer times. This work will support future research on hagfish slime by facilitating the choice of stabilization method and by describing the degradation processes during storage.

Water retention to assess hagfish slime functionality

Hagfish exudate at its natural concentration of about 0.02% (v/v)[8] was able to gel the whole volume of 20 ml seawater (Fig. 2 A), of which subsequently about 14 ml (initial load) could be lifted up (Fig. 2 B). For clarification, a concentration of 0.02% (v/v) refers to the volume of 'wet' exudate in water. Assuming a density of 1 g/ml[9] and taking into account that about two thirds of the exudate volume are water and solutes[8], a concentration of 0.02% (v/v) exudate corresponds a true volume expansion of about 1:15'000 or to a slime dry weight of roughly 0.0067 wt%.

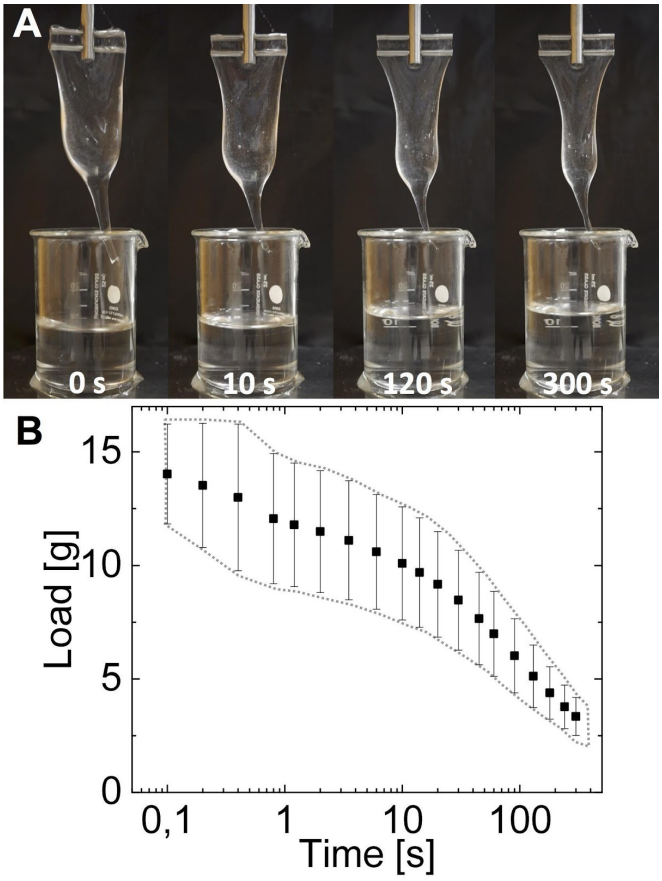

Figure 4.1: Water retention of fresh hagfish slime in seawater at its natural concentration of 0.02% (v/v). A: Hagfish slime draining over five minutes. B: Water retention of natural hagfish slime formed from fresh exudate.

After draining for about one minute under the influence of gravity, the slime lost about half of its initial load (IL). Once the water drained, the slime can hardly rehydrate and the structure irreversibly collapses (Fig. 4.2) because the threads cluster and the slime loses its sieve-like structure[8]. The IL is a good measure for the effectiveness of the water absorption and allows to conveniently compare effects such as a varying exudate concentration or structure collapse (Fig. 4.2). Other authors similarly used a 'removable mass' to assess slime functionality and investigate the influence of dithiothreitol (DTT)[129] and the influence of stirring on the slime formation[3] or

measured the water egress from the slime to investigate the physical water entrapment and sieve-like properties[8].

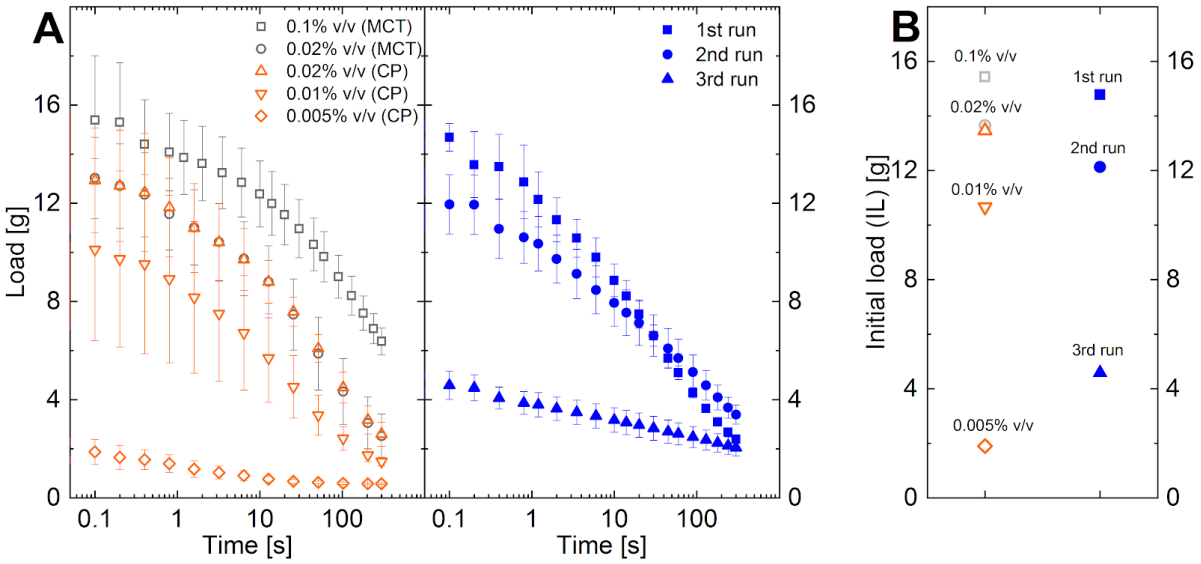

Figure 4.2: Effect of exudate concentration and repeated mixing on water retention. A left: Influence of exudate concentration on hagfish slime water retention. The tested concentrations ranged from five times the natural slime concentration (0.1% v/v - exudate per ml seawater) to ¼ of the natural concentration (0.005% v/v). **A** right: Effect of repeated measurement of the same sample on the water retention. The structure collapse results from fiber aggregation from drainage and the repeated mixing step (10 rotations around the axis) before the start of the new measurement. **B**: Initial loads of the corresponding measurements from A

The soft and wet character of biomaterials such as hagfish slime in particular often imposes substantial challenges to characterization methods applied in materials science[130]. Assessment of material properties of hagfish slime was so far mainly done by rheological measurements[9,127,128] and to a lesser extent by measuring the water egress[8,131]. Whereas rheology allows to study the mechanics and flow behaviour, the technique is limited by the softness of the slime and by potential inhomogeneities. Water retention measurements in contrast provide simple, but quantitative and robust information about the effectiveness of water uptake and the water holding capacity, which are both critical criteria for hydrogel functionality. Water retention measurements therefore permit to assess the functionality of the hagfish slime and to study effects such as storage, which is otherwise hard to assess.

Influence of stabilization method and time on slime functionality

Currently there are two main approaches to stabilize hagfish exudate - immersion in medium chain triglyceride (MCT) oil and dispersion in a high osmolarity citrate / PIPES (CP) buffer (Fig. 4.3 A). To evaluate if one method is superior to the other, water retention measurements were performed five hours after sampling (Fig. 4.3 B).

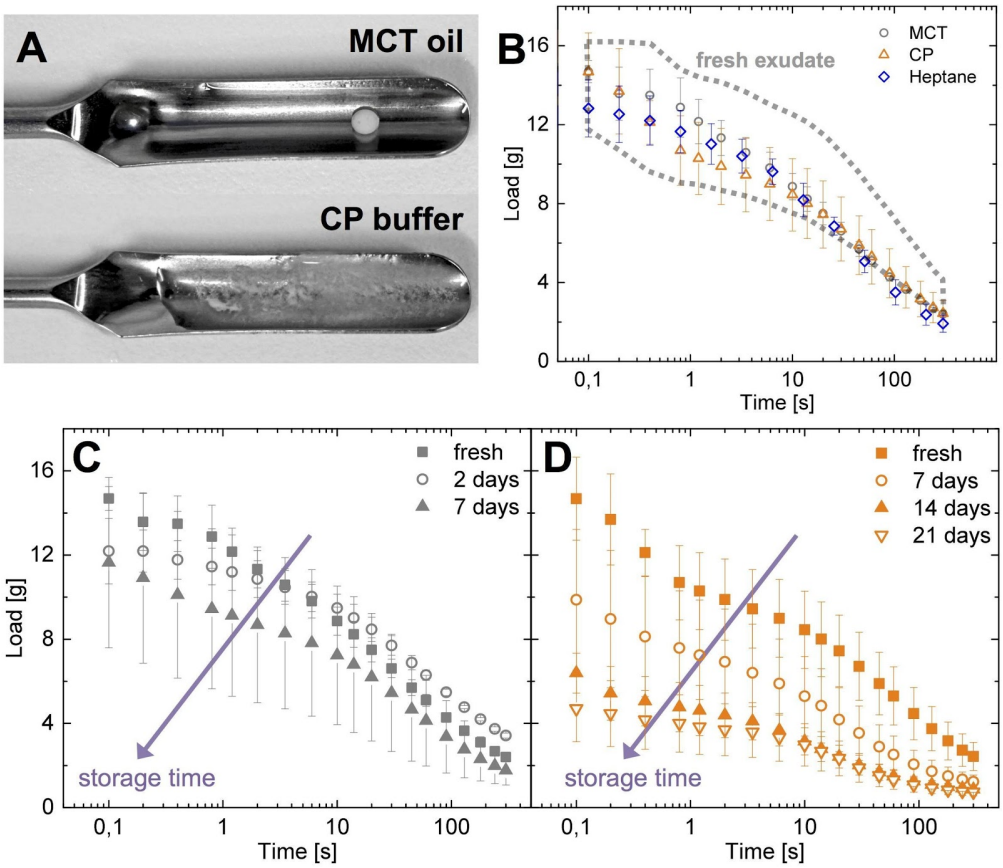

Figure 4.3: Different hagfish exudate stabilization methods and their influence on slime functionality over time at a concentration of 0.02% (v/v). A: Hagfish exudate stabilized in MCT oil and in citrate/PIPES (CP) buffer. **B**: Comparison of water retention properties of slime formed from exudate stabilized in CP buffer, MCT oil, and heptane after 5h of storage to the water retention of fresh, unstabilized exudate (dashed region). **C**: Influence of storage time on water retention of exudate stabilized in MCT oil and **D**: exudate in CP buffer.

Both stabilization methods (MCT oil, CP buffer) showed an almost indistinguishable slime functionality as they all possessed water retention properties similar to natural unstabilized hagfish slime. As a third stabilization method heptane was tested, which also showed water retention properties similar to the other two methods. Heptane is intriguing due to its volatility, allowing a removal of the stabilant at room temperature without leaving residues, which is not possible with MCT and CP. Although handling was more difficult and stability lasted only about two days, heptane is a promising short-term stabilization. In contrast to short term stability, however, extended storage resulted in a loss of functionality and showed marked differences between the MCT oil and the CP buffer (Fig. 4.3 C and D). Whereas MCT samples showed a rather sudden onset of functionality loss, the CP samples faced a more gradual breakdown. After 5 to 10 days the MCT samples started to clump and did not deploy anymore when in water. The time for the onset was strongly dependent on each individual sample as often for biological samples but also on the mechanical and temperature history of the sample. In contrast, exudate in CP buffer showed a gradual loss of functionality, which was found to be accompanied by a reduced skein unraveling. However, after a storage of two weeks the water retention properties markedly decreased, which could be linked to a reduced skein unraveling. From these observations it can be inferred that the principal mechanism of degradation is different for either stabilization method. This hypothesis was further suggested by the finding that the storage lifetime of a MCT sample could be extended when it was transferred to CP buffer before clumps occurred, giving it a second life. Stabilization and storage of slime exudate is crucial in hagfish slime research. We therefore

studied the two putative degradation mechanism by varying temperature and pH to determine the influence of storage on the exudate samples.

Temperature induced mucin vesicle swelling and rupture

Exudate (20 µl covered with 200 µl MCT oil) was heated in an Eppendorf tube in a water bath to 37, 42, and 50°C for five minutes to test the effect of temperature on hagfish exudate stability and on slime formation (Fig. 4.4 A). Whereas heating to 37°C had a minor impact, heating to 42 and 50°C resulted in an almost completely inhibited slime formation. Heating MCT exudate under a microscope revealed that the sample gelled as soon as the heat wave reached the vesicles, suggesting that the vesicles swelled and ruptured at elevated temperatures (Fig. 4.4 B and C).

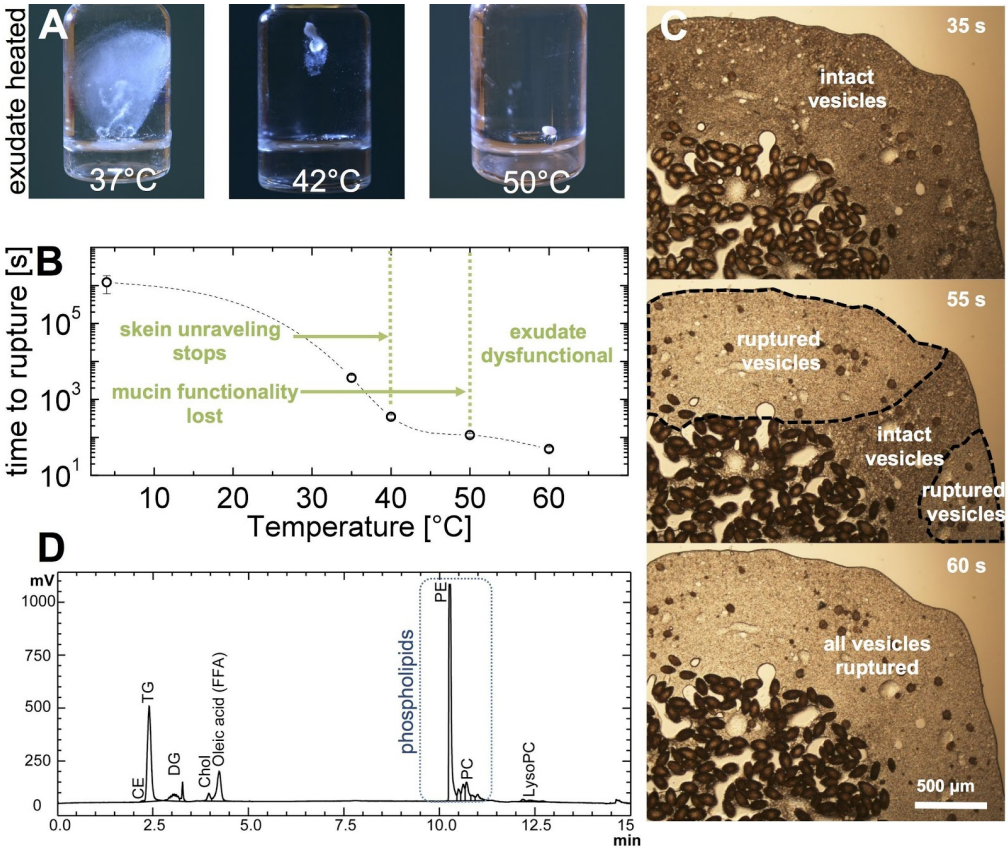

Figure 4.4: Effect of temperature on hagfish exudate and slime functionality. A: Effect of heating MCT stabilized exudate for 5 minutes on slime formation. **B**: Hagfish mucin vesicle swelling and rupture time as a function of temperature. For vesicle rupture MCT stabilized exudate was used. The data point at 4°C refers to a sample stored in the fridge and indicates the time until clumping occurred in the fridge. The green text and the green dashed lines denote observations for exudate that was heated in CP buffer. The dashed line serves as a guide for the eye. **C**: Microscopy image sequence of vesicle bursting at 60°C. The dashed areas outline the regions where mucin vesicles burst. **D**: HPLC lipid analysis of hagfish mucin vesicles (CE: cholesteryl ester, TG: triglycerides, DG: diglycerides, Chol: Cholesterol, FFA: free fatty acid, PE: phosphatidylethanolamine, PC: phosphatidylcholine, LysoPC: lysophosphatidylcholine)

The ruptured vesicles released their mucin, forming a firm gel with the little available liquid originating from the residual fluid. The gel fails to swell rapidly when in water and also prevents a subsequent unraveling of the gel-embedded skeins. It is likely that the surrounding MCT oil favours swelling and rupture of the vesicles at elevated temperatures given their putative phospholipid bilayer membrane[58]. To investigate the existence of a phospholipid bilayer, lipid analysis was

performed (Fig. 4.4 D). Substantial amounts of phosphatidylethanolamine (PE) and phosphatidylcholine (PC) and minor amounts of cholesterol (Chol) and lysophosphatidylcholine (LysoPC) were found, adding further evidence for the presence of a phospholipid membrane[58]. A surrounding non-polar phase such as MCT oil likely favors an exchange of membrane phospholipids with the oil phase, leading to a break in vesicle membranes. This effect is more favored at higher temperatures[132,133], as membranes become softer when temperatures come close to the melting temperature of the lipids[134]. The lipid analysis also showed the presence of triglycerides (TG), diglycerides (DG), and free fatty acids (FFA). Salo *et al.*[7] found that hagfish mucin vesicles contain about 4.8% lipids. As speculated by the authors, it is likely that non-membrane lipids are needed for the formation of a functional mucin gel. A positive effect of lipids on mucins is known as they can associate to mucins by hydrophobic interactions via the hydrophobic domains of mucin glycoproteins[68,135]. Thereby, lipids were found to increase the viscosity and viscoelasticity of mucin [68,136] and support their capability to form gels[137]. The appearance of the heated and clumped sample was similar to old (> 2 weeks) MCT samples, which were also gelled. However, the clump formation during storage in MCT oil is more likely to be a slow osmotic driven swelling and rupture of mucin vesicles, given that the residual fluid of the exudate does not have obvious stabilizing effects on vesicles[6]. It should be noted that clumping can also be induced when the samples are mechanically stressed, e.g., with a micropipette.

Vesicles stabilized in CP buffer do not rupture when mechanically stressed with a micropipette, when stored in the fridge for over six months or when heated to 50°C. The high ionic strength of the buffer likely keeps the glycoproteins in a stiff, condensed state, which makes merging of adjacent vesicles energetically unlikely. The polyanionic nature of mucins makes their conformation highly sensitive to ionic strength[138], which strongly reduces swelling of anionic gels at elevated salt levels[139,140]. Also, the high ionic strength of the CP buffer could stabilize the membrane due to a binding of the buffer ions on the phospholipids[134]. Although the vesicular structure did not visually break at 50°C, the mucin probably denatured and aggregated inside the vesicle and lost the ability to swell, as the ability to form a viscous solution when mucin vesicles were mixed with water was lost. When the sample was heated to 42°C the vesicles were still able to form a viscous solution. Furthermore, heating exudate in CP to 42°C completely inhibited skein unraveling, which was not observed for 37°C. These results are in line with the findings of Bernards *et al*.[53], who still observed skein unraveling at 35°C. Our observations show that also the unraveling of *M. glutinosa* skeins is highly temperature sensitive. We suggest that heat sensitivity of the skeins either originates from the presence of a protein glue that denatures at elevated temperatures and thus cannot mediate unraveling anymore.

Influence of pH on storage and on slime formation

The pH of the CP buffer does not match the physiological pH values of hagfish blood (≈ pH 8[141]), the residual fluid of the exudate (pH 7.3[6]), nor the pH of seawater (≈ pH 8). We therefore investigated if an increased pH of the CP buffer has beneficial effects on storage (Fig. 4.5 A).

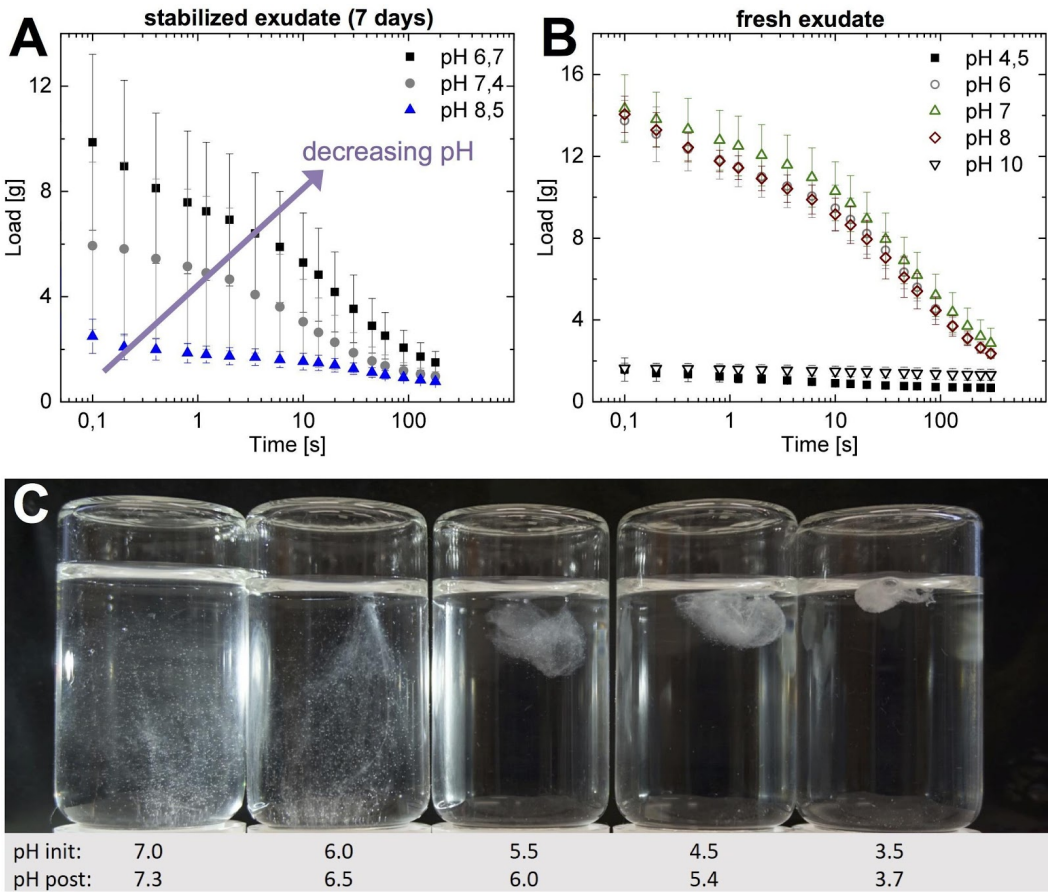

Figure 4.5: Influence of pH on exudate storage and slime formation. A: Influence of pH of CP buffer on slime functionality (4 µl of hagfish exudate from MCT oil were mixed into 200 µl of CP buffer of different pH values and measured after 7 days of storage). **B**: Water retention measurements of hagfish exudate from MCT oil in seawater at different pH values. **C**: Hagfish exudate from MCT oil mixed into seawater at different pH values (pH init). The pH of the seawater slightly rose after the addition of hagfish exudate (pH post value)

From the tested pH values (pH 8.5, 7.4, and 6.7), pH 6.7 - being the commonly used pH for CP buffer - showed the highest initial load, the highest degree of skein unraveling and thus the best slime functionality after seven days of storage. In contrast, it was found that when fresh MCT stabilized exudate was mixed into seawater or phosphate buffer between pH 6 and pH 9 (Fig. 4.5 B, C, and Fig. 4.6 A), the slime showed similar water retentions, implying that the reduced functionality at higher pH originates from the storage. At pH extremes (pH 4.5 and pH 10) no functional slime formed. At low pH the skeins did not unravel and aggregated with the mucins (Fig. 4.6 B). At high pH the mucins formed a tacky solution and many skeins did not unravel resulting in a weak network which was unable to entrap water when lifted out of the water.

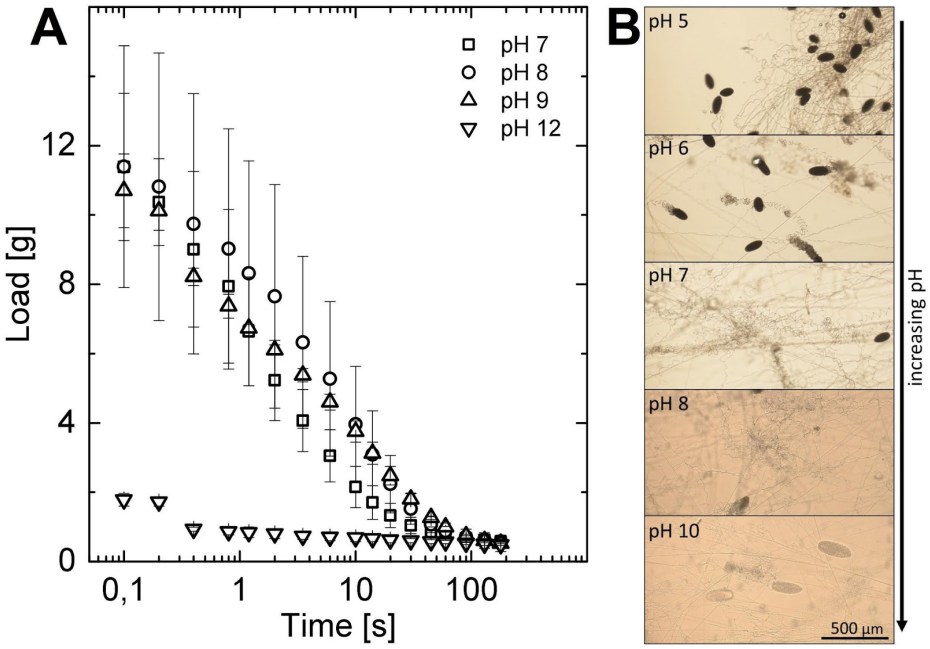

Figure 4.6: Effect of pH (in phosphate buffer) on water retention and skein unraveling. A: Effect of pH adjusted by 25 mM phosphate buffer on water retention. **B**: Light microscopy images of slime formed in the 25 mM phosphate buffers at different pH values showing the influence of pH on skein unraveling and network formation.

These results show that skein unraveling is pH dependent and that an increased pH of the CP buffer decreases slime functionality by limiting the amount of unraveled skeins. We have two hypotheses why a lower pH stabilizes the exudate better. First, pH 6.7 and possibly even lower to about pH 6 could be beneficial for mucin gel condensation inside the vesicle. Mucin granules are considered to have a low intraluminal pH (≈ pH 6)[142–144]. A low storage buffer pH, potentially close to the isoelectric point (pI) of mucin, is likely beneficial in keeping the mucin condensed. Close to the pI the number of counterions is minimal and therefore the osmotic pressure in and around the mucins decreases, resulting in a limited swelling capacity[139,145]. A similar observation was made for mucin granules from human cervical cells, which showed a significantly decreased swelling velocity at pH 6.5 compared to pH 7.4[146]. Increasing the pH gradient from the CP buffer to the vesicle intragranular pH could thus result in compromised integrity of the mucin meshwork inside the granule[142,147] and cause partial swelling. These would inhibit vesicle swelling at the time of slime deployment and thus also limit skein unraveling, as both processes are suggested to be intimately linked[23,58]. The second hypothesis is that a higher pH denatures the seawater soluble glue of the skeins faster. As most of the skeins are stripped from their plasma membrane when secreted through the slime pore[5] they lack protection when exposed to the stabilization buffer. It is likely that the protein glue slowly denatures and becomes insoluble at elevated pH during storage.

Extended storage in buffer denatures seawater soluble glue of thread skeins

Fresh stabilized hagfish skeins spontaneously unraveled in seawater (Figure 4.7 A). The absence of flow and the high local viscosity due to the concentrated mucin around the skein likely slowed the unraveling down. The spontaneous unraveling suggests the existence of a seawater soluble glue[53] in *M. glutinosa* skeins, which dissolves and mediates unraveling by releasing the stored spring energy of the thread. Further evidence for the existence of a seawater soluble glue is

provided in scanning electron microscopy (SEM) pictures in Figure 4.7 B. The pictures show a skein in the process of unraveling. In the inter-thread spacings filamentous structures could be seen, which were also observed for *E. stoutii* skeins[53]. At high magnification the filamentous structures look like they are part of the rough surface of the skein, which is about to dissolve. Old skeins that were exposed to CP buffer for longer times fail to unravel in water, even in the presence of strong flow. However, when those old skeins were subjected to a trypsin solution they unraveled naturally similar to freshly harvested skeins, i.e. starting at the apical end of the skein (Fig. 4.7 C)[53]. As observed by Bernards *et al.*[53], we also observed that trypsin removed the glue faster than digesting the thread.

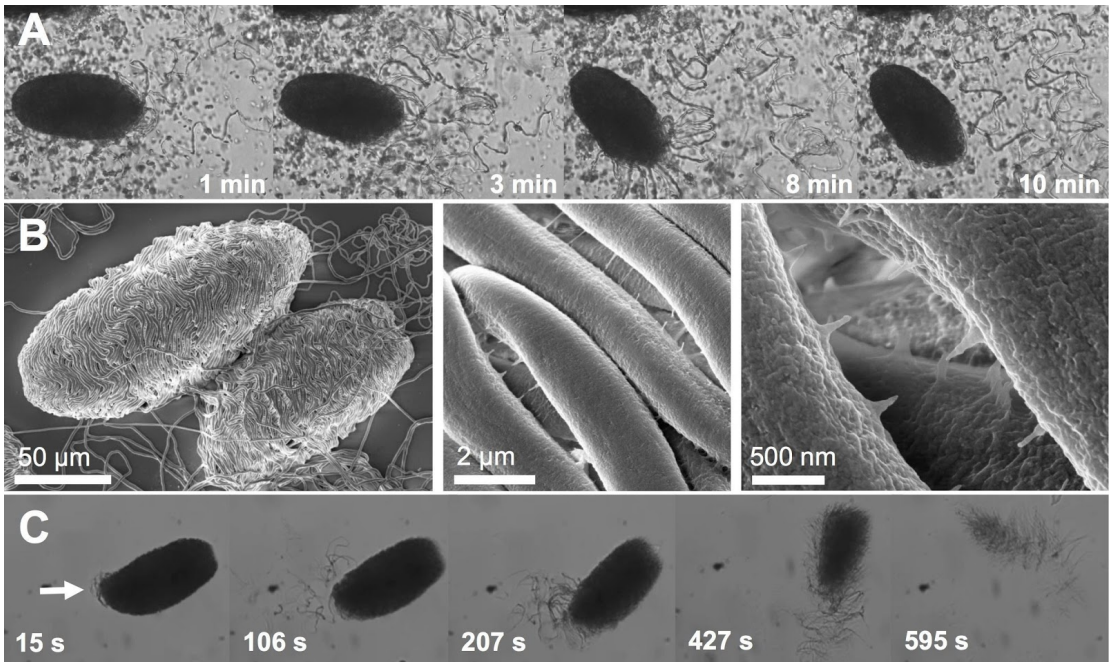

Figure 4.7: Spontaneous unraveling of *M. glutinosa* skeins is mediated by a water soluble protein, which becomes insoluble during storage in buffer. A: Spontaneous unraveling of a functional M. glutinosa skein surrounded by mucin vesicles in seawater in the absence of flow (MCT oil stabilized sample). **B**: SEM of *M. glutinosa* skeins that were unraveled with Milli-Q water without stirring on a SEM slide (left). The unfinished unraveling shows small bridging filaments between the thread parts (middle, close up right). **C**: Old skein unravels in the presence of trypsin. The unraveling starts at the apical end of the skein (arrow).

We suggest that the protein glue denatures during storage and therefore becomes insoluble, being the main cause for a ceased unraveling after prolonged storage in CP buffer. Trypsin, cleaving on the C-terminal of lysine and arginine amino acid residues[148] seems to be able to digest the denatured protein glue, thus re-initiating unraveling in water. It is possible that the glue is denatured by oxidation, by high ionic strength, or by other unfavorable conditions. The fact that elevated temperatures and non physiological pH inhibit skein unraveling support the existence of a protein glue, as the protein is likely to denature. An alternative hypothesis is that adjacent loops of the thread stick to each other during storage, thereby inhibiting unraveling. The trypsin-driven unraveling would also support this mechanism as trypsin could digest the parts of the thread that are stuck together and liberate stored strain energy. Here we like to note that our findings stand in slight contrast the current theory of Winegard and Fudge[23] who state the unraveling of *M. glutinosa* skeins requires mucin strands and flow. Our movies revealed that neither flow nor mucin strands (the old skeins were washed with Milli-Q and DTT prior to trypsin unraveling) are required for unraveling. We do not doubt the necessity of flow and mucin strands for the formation of a functional slime network but we propose that flow and mucin strands are rather needed to

propagate the spontaneous unraveling by mucin strands attaching to the unraveling threads and not for initialization of unraveling. However, further investigations to decouple the influence of single parameters such as flow, mucin, and glue dissolution on skein unraveling and on the complex mechanism of slime formation are needed.

Conclusion

In this study the two main stabilization methods for hagfish exudate - immersion in MCT oil and dispersion in a high osmolarity citrate/PIPES (CP) buffer - were compared. An overview of the major advantages and disadvantages of both stabilization method is shown in Table 4.1.

Table 4.1: Advantages and disadvantages of the two major exudate stabilization methods

	CP buffer	**MCT oil**
advantages	inhibition of bacterial and enzymatic degradation separation of skeins and vesicles long term storage of vesicles	accurate concentration in natural environment (residual fluid) no additional ionic strength
disadvantages	high ionic strength skeins cease to unravel difficult concentration determination	sensitive to mechanical stress and room temperature no bulk separation of skeins and vesicles no inhibition of bacterial and enzymatic degradation possible

Using water retention measurements to assess the functionality of hagfish slime, it could be shown that for short storage times (< five hours) both stabilization methods produced slime networks equal to fresh unstabilized hagfish exudate. As a novel stabilization method heptane was tested, which also preserved the functionality but was more difficult in handling than MCT oil as it had a drying effect on the exudate. Nevertheless, heptane could be used for applications where the stabilant is to be removed as it quickly evaporates. Therefore, depending on the purpose of exudate stabilization, a different stabilization technique has to be chosen.
In this work we studied the boundary conditions necessary for a successful stabilization of exudate for laboratory experiments. Longer storage times caused the samples to degrade, whereby MCT oil and CP buffer showed different breakdown mechanisms. MCT samples formed clumps after about five to seven days, probably due to osmotic driven swelling and rupture of the mucin vesicles. The mucin vesicles and the thread skeins were found to be highly sensitive to elevated temperatures, which possibly accelerates vesicle rupture. Rupture is likely favored by the non-stabilizing ion composition of the surrounding residual fluid and by phospholipids in the membrane, as they interact with the surrounding oil phase, causing leakage of the mucin and a subsequent gelation of the system. The gelled system does not form a slime anymore when in contact with seawater as the thread skeins are trapped in a dense mucin gel matrix. CP buffer stabilized samples, on the other hand, showed a gradual loss of functionality over time, which

could be linked to reduced skein unraveling. At long buffer exposure times, less skeins unraveled and therefore less water was retained. We propose that a seawater soluble glue, which holds the threads together and mediates unraveling denatures during storage in the buffer and thus likely becomes insoluble. Evidence for the presence of such a glue as similarly observed for *E. stoutii* skeins[53] was provided by trypsin induced unraveling of old skeins as well as by electron microscopy images. The suggested increasing insolubility likely causes a gradual loss of skein unraveling and thus decreases slime functionality. When the pH of the CP buffer was raised from pH 6.7 to pH 8.5 the functionality further decreased. It could be shown that the negative influence of the higher pH was only observed after storage but not when fresh exudate was mixed into seawater of higher pH. The reasons why a higher storage pH reduces slime functionality are elusive but it is likely that a higher pH denatures the water soluble glue faster or has inferior stabilizing properties on the mucin vesicles.

Our findings underline the importance of rigorous cooling of MCT exudate samples and show that a stabilization buffer pH of 6.7 and possibly lower is beneficial to preserve the functionality of CP exudate samples. The observed degradation processes provide valuable guidelines for the choice of appropriate stabilization for hagfish exudate and will foster the uncovering of the complex mechanisms of slime formation.

Chapter 5 - Effect of Ionic Strength on Hagfish Slime Formation

The content of this chapter has been partially published by Böni, L.J., Zurflüh, R., Baumgartner, M. E., Windhab, E. J., Fischer, P., Kuster, S., Rühs, P. A., in "Effect of ionic strength and seawater cations on hagfish slime formation." *Scientific Reports* 2018, *8*, 9867

Hagfish slime constitutes a polyanionic mucin hydrogel that synergistically interacts with a fiber network in fragments of a second, rapidly forming a fibrous hydrogel in high ionic strength seawater (≈ 0.7 M[149]). The ability of a polyanionic gel to expand and swell vastly and rapidly in a high ionic strength solution is astonishing, because high salt levels generally counteract swelling of polyelectrolyte gels[145,150]. Polyelectrolyte gels can exhibit striking swelling degrees as high as 10^3 in ion-free water relative to their dry weight, making them the preferred material for superabsorbents[151]. The swelling potential of these charged gels is defined by a balance between the elastic energy of the network counteracting swelling and the osmotic pressure of the ions as well as the electrostatic repulsion of the polymer-bound charges driving swelling[145,150,152]. The swelling capacity of polyelectrolyte gels is therefore much greater than that of neutral polymer gels because of the mutual electrostatic repulsion of polymer-bound charges as well as the osmotic pressure contributions of the counterions confined in the gel[153]. However, in the presence of salt electrostatic interactions in the gel are screened, causing a deswelling[150,154]. By contrast, hagfish slime forms in seawater in just a matter of seconds and entraps vast amounts of water.

Intrigued by the rapid and efficient swelling of hagfish slime in its natural high ionic strength environment, we investigate how hagfish slime formation is affected by the ionic strength and the cationic composition of water. The effect of ionic strength and ionic composition of the buffers used for hagfish exudate stabilization was studied before[5,7,58] where it was found that high osmolarity buffers containing divalent anions (sulfate, citrate, phosphate) above a critical osmotic pressure of about 800 mOsmol l^{-1} stabilize hagfish exudate and thus prevent swelling of the gel. Other studies focused on the unraveling of skeins as a function of ionic strength, showing that skeins of the Pacific hagfish (*E. stoutii*) unraveled most at NaCl concentrations between 1 - 2 M[53]. Less proportions of bundles unraveled at lower (0.25, 0.5 M) and higher (2.5, 3, 4 M) NaCl solutions. In the same study the authors also found that seawater was superior to NaCl solutions in dissolving a glue that holds the skeins together and thus probably mediates unraveling once in water. In two other studies Herr *et al*.[6,60] investigated the swelling and rupture of hagfish mucin vesicles in solutions containing different mono- and divalent salts and inorganic osmolytes. However, the effect of divalent salts and ionic strength on the formation and functionality of whole hagfish slime were so far only scantily investigated. Fudge [155] showed that the removable mass of whole slime formed in distilled water and in 0.45 M NaCl solutions is substantially lower than in seawater. Also, the effect of NaCl solutions on skein unraveling was partly studied for *E. stoutii* skeins but the dynamic interactions of individual ion species during slime formation and especially their effect on the functionality of the resulting slime network are unknown.

In this work we combined material- and morphological characterizations to study the ionic strength dependant dynamics of hagfish slime. We show that ionic strength seems crucial for timing the slime formation via a controlled unraveling of the thread skeins. We further investigate the role of divalent seawater cations and show that their presence is vital in order to entrap large volumes of water in high ionic strength environments. In a last part we assess the flux of seawater cations (Na^+, K^+, Mg^{2+}, Ca^{2+}) during slime deployment, casting light on the complex cation dynamics during

slime formation. Our insights might be valuable in the design of novel, bioinspired dynamic hydrogels that form rapidly in a high ionic strength environment with potential applications such as water desalination[156].

Effect of seawater and Milli-Q on water retention

The effect of ionic strength on hagfish slime was evaluated by mixing freshly harvested hagfish exudate into Milli-Q water and seawater, representing the complete absence of ions and the natural environment for hagfish slime formation, respectively. The resulting fiber network was investigated under the microscope and the water retention of the slime was measured. Milli-Q water resulted in the formation of a confined and compact slime mass, showing a close arrangement and narrow spacings between the slime threads instead of a widespread and expanded network as observed in seawater (Fig. 5.1 a). The slime formed in Milli-Q did not span the entire available water volume of 20 ml upon deployment in the glass flask, which resulted in a condensed 'blob'. Furthermore, almost all skeins unraveled in Milli-Q, which stands in contrast to observations in seawater where skeins have been shown to remain coiled[23]. Although more skeins unraveled in Milli-Q, the slime showed a substantially reduced ability to entrap water (Fig. 5.1 b). Slime in Milli-Q initially retained 7.5 g of water, which is roughly 50% less compared to the 14.7 g retained in seawater (Fig. 5.1 c). We suggest that this effect is caused by altered network formation dynamics. In the following sections, we will discuss the effects of ionic strength and seawater cations on skein unraveling, vesicle decondensation, and mucin viscosity and will suggest their implications on whole slime formation and functionality.

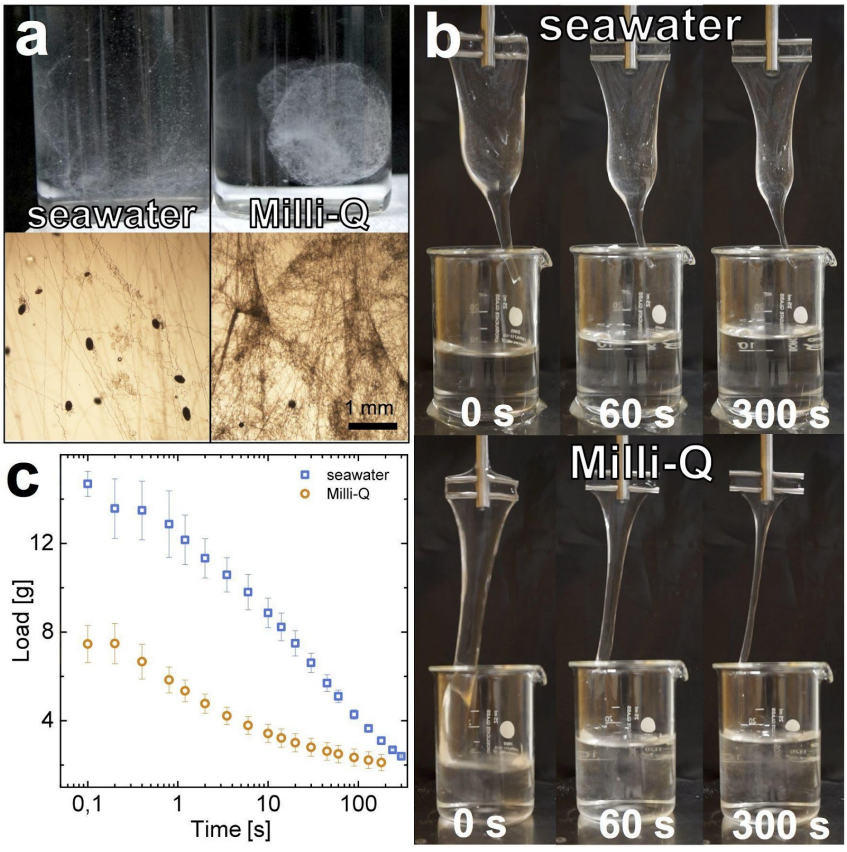

Figure 5.1: Effect of seawater and Milli-Q on hagfish slime thread network and water retention properties. (**a**) Hagfish slime formed with seawater (left) and Milli-Q (right). In seawater the expanded thread network spans the entire volume whereas in Milli-Q a confined 'blob'-like network is formed. (**b**) Images of slime draining during water retention measurements. (the image

series in the top line in (b) was previously published[157]). (**c**) Water retention measurements of slime formed in seawater and Milli-Q.

Unravelling dynamics of thread skeins in Milli-Q and seawater

Skein unraveling dynamics in ion-free Milli-Q are less controlled and faster than in seawater. Figure 5.2 a shows an image sequence of a skein unraveling in Milli-Q. The skein swells radially and completes unravelling in about two seconds, even in the absence of substantial external flows. Similar to seawater, the unraveling started at the apical tip of the skein[53,157], but then the skein continued to uncoil from both sides in an uncontrolled manner. As the uncoiling is localized to the position of the skein, a confined and narrow thread mesh remains on the uncoiling spot. In contrast, unraveling in seawater can take several minutes when observed under the microscope[53,157] (Fig. 5.2 b) and the uncoiling threads are able to span a larger area, especially in the presence of flows. A direct comparison of the skein unraveling characteristics in seawater and in Milli-Q is shown in Fig. 5.2 c. The slower unraveling of skeins of the Atlantic hagfish (*M. glutinosa*) compared to skeins of the Pacific hagfish (*E. stoutii*) in seawater was similarly observed by Bernards *et al.*[53], who suggested that a slime that deploys too fast could have drawbacks for burrowing animals such as the Atlantic hagfish.

In Milli-Q the combination of radial swelling and uncontrolled unraveling from two sides probably causes the uncoiling skeins to tangle. Tangled threads are limited in their ability to spread out after they have unraveled, which in turn impairs the formation of a widespread and expanded network, resulting in a lower water retention.

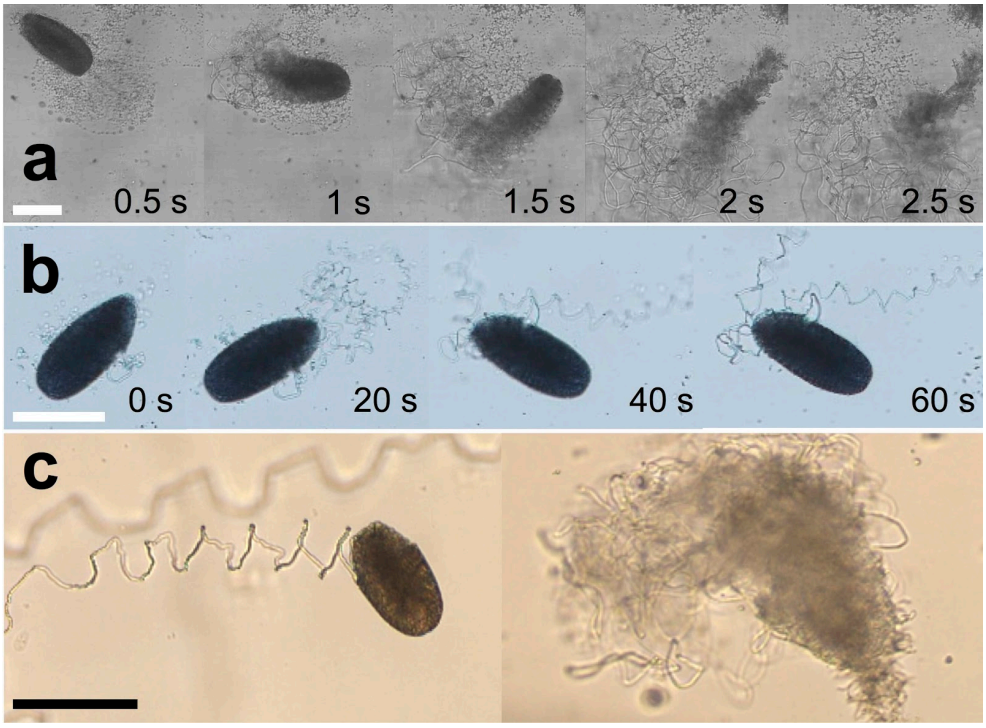

Figure 5.2: Characteristic unraveling times of single *M. glutinosa* skeins in ion-free Milli-Q water and in seawater observed under a light microscope. (**a**) Image series of a skein unraveling in Milli-Q captured with a high speed camera. (**b**) Skein unraveling in seawater. (**c**) Comparison of skeins unraveling with seawater (left) and Milli-Q (right), showing the radial swelling in Milli-Q and the controlled unraveling from the apical tip in seawater. Scale bars = 100 µm.

Ionic strength determines skein unraveling

Seawater and Milli-Q resulted in distinct network properties and skein unraveling. We studied the effect of ionic strength on skein unraveling and found that ionic strength slows down unraveling speed and reduces swelling of the skeins. Radial swelling and uncontrolled, fast unraveling of skeins was observed in low-ionic strength sodium chloride solutions (10 mM NaCl, I = 0.01 M) and in diluted seawater (10% seawater, I = 0.06 M), similar to Milli-Q (not shown). The presence of increased ionic strength in the form of sodium chloride (100 mM NaCl, 500 mM NaCl), seawater, or artificial seawater lacking certain cations in contrast resulted in controlled (only from the apical end) and slow unraveling of the skeins (not shown). We have two hypotheses how a high ionic strength could slow down and control skein unraveling. The two hypotheses are not mutually exclusive and both give a reasoning to slower unraveling in a high ionic strength environment.

First, the fast unraveling and radial swelling of the skeins in ion-free water could be caused by thread swelling given the large osmotic gradient. Salt dependence in thread skein uncoiling between distilled water and seawater was already observed and a dependence of uncoiling on seawater-induced swelling of thread skeins was suggested[4,129]. Milli-Q could cause an excessive swelling of the keratin-like[42,44,129] hagfish slime threads. Unlike in hard α-keratins, where intermediate filaments (IFs) are embedded in a isotropic, high-sulfur matrix[158], hagfish slime threads constitute matrix-free IFs and are therefore highly sensitive to hydration[10,55]. Fudge and Gosline[55] showed that hagfish threads increased 45% in diameter compared to the dry state when hydrated with deionized water. As spontaneous unraveling of the skeins is considered to be propelled by a stored strain energy in the coiled thread, it seems probable that an excessive swelling of the thread adds to this stored entropy-elasticity. The osmolarity of seawater - as well as the high osmolarity of the residual fluid (888 mOsm) of the slime exudate[6] - could reduce the swelling of the threads compared to Milli-Q and thus limit the strain energy, resulting in a slower and controlled unraveling, which can then be accelerated by external mixing flows and attaching mucus strands.

The second hypothesis is that ionic strength reduces the dissolution speed of the seawater-soluble glue, which was found to mediate unraveling in *E. stoutii* skeins[53] and similarly observed on *M. glutinosa* skeins[157]. It is possible that the glue dissolves faster-in the presence of low ionic strength solutions and that its dissolution speed is reduced at high ionic strength. Deionized water seems to be sufficient to loosen the glue from binding to itself, as already shown in electron microscopy images[157]. However, a low ionic strength could prevent a further dissolution of the glue from the threads as observed by Bernards *et al*.[53]. Both hypotheses could also explain why skeins are stable in high-osmolarity stabilization buffers[5,7,58]; given a suggested increased insolubility of the glue and/or an osmotically dehydrated slime thread with reduced strain energy.

Regardless if one or both suggested hypotheses are considered the main reason for the observed differences in skein unraveling, the different unraveling patterns governed by ionic strength have implications on whole slime functionality.

Effects of ionic strength on slime network formation

Similar to skein unraveling, the effect of ionic strength on whole slime functionality was studied by mixing hagfish slime exudate with solutions of various sodium chloride (NaCl) concentrations and dilutions of natural seawater. The presence of 10 to 100 mM NaCl resulted in a substantially increased initial load compared to Milli-Q (Fig. 5.3 a) and the fiber network did not show a clump formation after mixing, supporting the beneficial effect of ionic strength. The observed differences

between the treatments were too large to be accounted for simply by differences in the density of the different salt solutions. Although a low ionic strength (10 mM NaCl and up to 10% seawater) showed skein swelling under the microscope, the salts had beneficial effects on the water retention. However, a high ionic strength solely based on sodium chloride (I = 0.5 M) - being close to the ionic strength of natural seawater (I = 0.6 - 0.7 M) - resulted in a collapsed and dysfunctional slime. Although single skeins did not swell and unraveled controlled under the microscope, no widespread fiber network formed (Fig. 5.4) and no water was retained.

This stands in contrast to seawater, where the slime shows a functional network and superior water retention properties despite a high ionic strength (Fig. 5.3 b). Even in the presence of 1% seawater (I < 0.01 M) the initial load was increased to ≈ 12 g compared to ≈ 7 g in Milli-Q and ≈ 10 g in 10 mM NaCl (Fig. 5.3 b). 5% seawater retained the most water initially over 100% seawater. These findings imply an important role of other seawater cations such as Ca^{2+} and Mg^{2+} for slime functionality in a high ionic strength environment, which will be discussed in the following section. Furthermore, it suggests that slime network functionality is not determined by skein unraveling and ionic strength alone and that the dynamics of vesicle rupture and mucin viscosity might be similarly crucial.

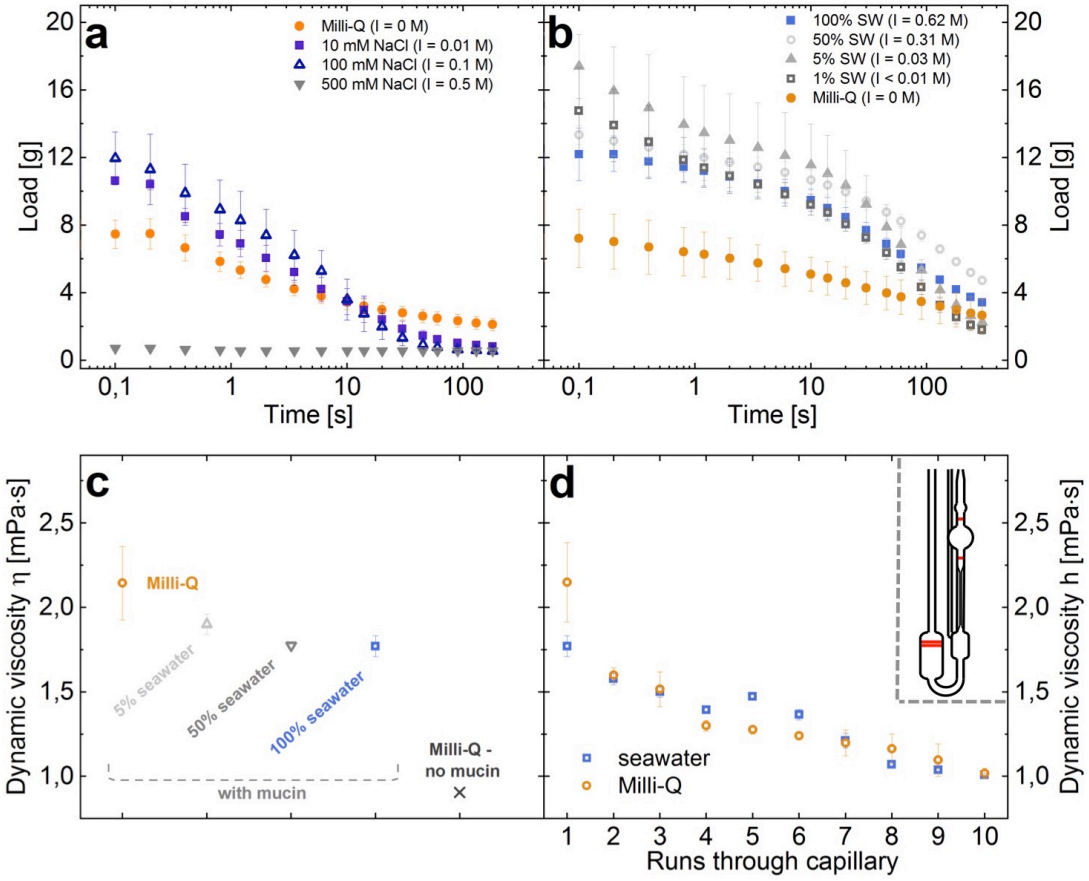

Figure 5.3: Effect of ionic strength on the water retention properties of hagfish slime and on mucin viscosity. (**a**) Water retention in different concentrations of sodium chloride (NaCl). (**b**) Water retention of hagfish slime formed in dilutions of seawater. For comparison between NaCl and seawater measurements, the ionic strength I is indicated in brackets. (**c**) Dynamic viscosity of hagfish mucin in Milli-Q, seawater, and diluted seawater at a concentration of 0.02 mg/ml measured at room temperature. Pure Milli-Q is given as a reference. (**d**) Mucin viscosity as a function of runs through the capillary of the viscometer, showing the mechanical sensitivity of hagfish mucin towards shear. The inlet shows a schematic drawing of an Ubbelohde capillary viscometer.

Mucin viscosity measurements (Fig. 5.3 c) showed that in Milli-Q hagfish mucin had the highest viscosity (2.14 mPas). At increased ionic strength as the case in 5% and 100% seawater the viscosities dropped to 1.86 mPas and 1.77 mPas, respectively. Theses results are in good agreement with the findings of Fudge *et al.*[8] who measured a viscosity of 1.41 mPas in seawater and about 1.54 mPas in Milli-Q at 9°C. The higher viscosity of mucin in 5% seawater compared to 100% seawater could explain why 5% seawater showed a higher initial load over 100% seawater in water retention measurements (Fig. 5.3 b). A higher viscosity means a higher resistance to flow, suggesting that liquid should be better retained. A higher viscosity combined with the presence of small amounts of salts in 5% seawater and their beneficial effect on skein unraveling seem to lead to a slime with superior water retention properties in comparison to slime formed under natural conditions. However, this does not infer that slime formed in 5% seawater also has superior defense properties. Although Milli-Q showed a higher viscosity than all dilutions of seawater, water retention in Milli-Q was inferior to seawater (Fig. 5.1 c). In this case the negative effects of the proposed tangling of the uncoiling skeins on network formation probably outbalances the slightly positive effect of viscosity on water retention.

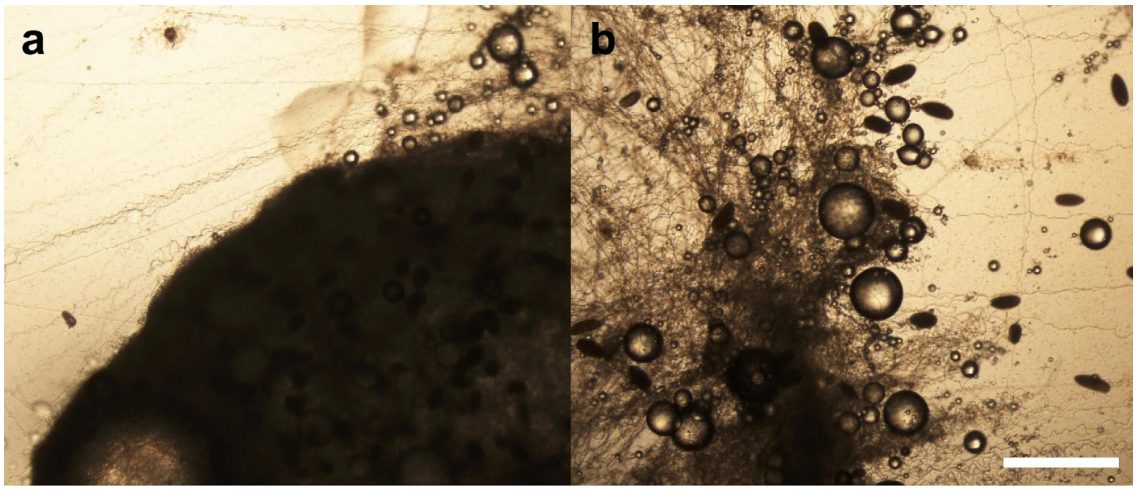

Figure 5.4: Light microscopy images of hagfish slime formed with 500 mM NaCl (**a**) and with artificial seawater without divalent cations (**b**) showing the dense and collapsed fiber network and the remaining coiled skeins. Scale bar = 500 µm.

The lower mucin viscosity in seawater compared to Milli-Q probably originates in increased electrostatic charge suppression[159,160] of the high ionic strength in seawater. Similar effects were shown for porcine gastric mucin (PGM), which does not gel at high ionic strengths (> 0.1 M)[160] and for human sputum, which shows reduced spinnability, rigidity, and viscoelasticity after treatment with hypertonic saline solutions[161–164]. Polyelectrolyte gels such as mucins are shown to stiffen as they swell in low salt solutions because the counterions in the gel network increase the internal pressure [165], thus increasing in viscosity. Furthermore, hagfish mucin viscosity showed a sensitivity towards mechanical shear (Figure 5.3 d), regardless whether in seawater or in Milli-Q. The sensitivity of hagfish slime towards mechanical stress is well known[3,166] and was similarly shown for hagfish mucin using a rotational shear rheometer[128]. These results support previous observations that hagfish mucin seems to aggregate under shear[128] and suggest that network cross-links could be disrupted. For the capillary rheometry experiments the mucin solution had to be pulled up through the glass capillary in order to prepare the measurement, meaning the mucin solution inevitably already experienced one shear event prior to the measurement. This infers that the viscosity of natural hagfish mucin immediately after secretion could be substantially higher than reported so far.

Divalent seawater cations (Ca^{2+} and Mg^{2+}) are crucial for whole slime functionality

The importance of divalent seawater cations (Ca^{2+} or Mg^{2+}) to efficiently entrap water in a high ionic strength environment was investigated using artificial seawater (ASW) and modifications thereof, lacking specific cations. Water retentions of hagfish slime formed with natural seawater and with ASW did not show substantial differences (Figure 5.5 a), despite the differences in cationic composition (Table 5.1).

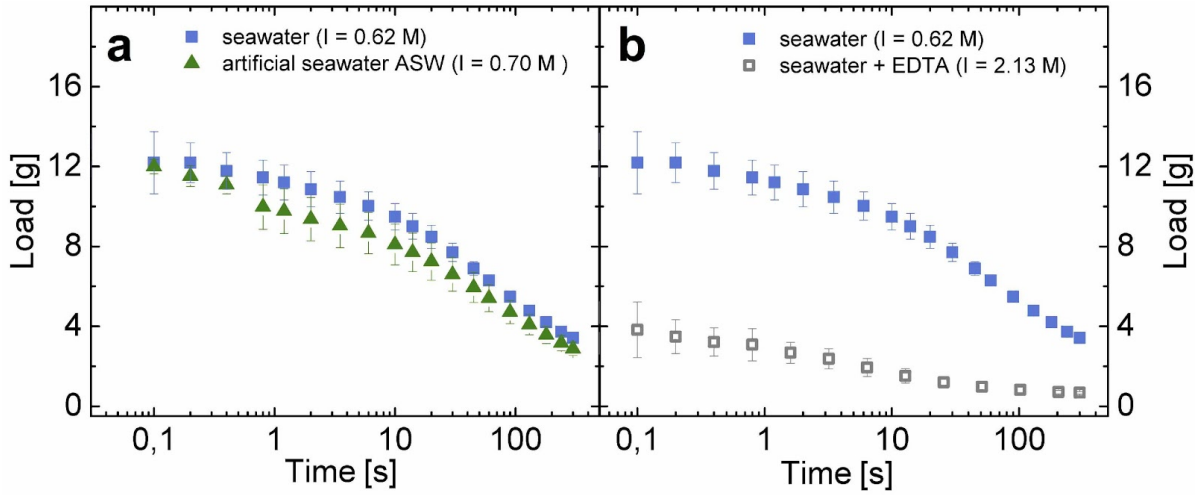

Figure 5.5: Water retention in seawater and artificial seawater (ASW) **(a)**. Water retention in seawater and in seawater with EDTA (150 mM) **(b)**. The pH of seawater with EDTA was adjusted to pH 8.0 using a 10 M NaOH solution in order to minimize the dilution.

Table 5.1: Comparison of the cationic composition of coastal seawater from Ålesund (Norway) with the recipe for artificial seawater (ASW) by Kestner *et al.*[112] in millimoles / liter (mM).

	coastal seawater (mM)	artificial seawater (mM)	difference (%)
Na^+	427.2	468.1	+8.7%
K^+	9.8	9.1	-7.6%
Ca^{2+}	7.5	10.3	+26.8%
Mg^{2+}	38.6	53.3	+27.6%

In contrast, ASW lacking divalent cations Ca^{2+} and Mg^{2+} did not form a functional slime network (Fig. 5.6 a, Fig. 5.5 b), i.e. no water was entrapped as similarly observed for the 500 mM NaCl solution (Fig. 5.3 a). Also, when EDTA - being a strong chelator of di- and trivalent cations - was mixed into seawater, the initial entrapped load dropped significantly (Fig. 5.5 b). In contrast, ASW lacking monovalent seawater cations (Na^+ and K^+) but containing the divalent seawater cations (Ca^{2+} and Mg^{2+}) resulted in a slime that efficiently entrapped and retained the water, similar to seawater. We found that when one of the two major divalent cations was present at its natural concentration like in seawater (10 mM Ca^{2+}; 50 mM Mg^{2+}[112]), a functional slime network was formed, which entrapped and retained water (Fig. 5.6 b). The beneficial effect of calcium ions was found to allow slime formation beyond ionic strengths occurring in natural seawater. In the presence of 10 mM Ca^{2+} functional slime networks formed in solutions containing up to 3 M NaCl

(Fig. 5.6 c), corresponding to about 4-5 times the ionic strength occurring in natural seawater. However, slime formation eventually failed at 4 M NaCl. Similarly, Bernards *et al.*[53] showed that skein unraveling is inhibited in 4 M NaCl in Pacific hagfish slime. The initial load slightly decreased with increasing NaCl molarity, which could originate in a lower mucin viscosity due to charge screening and/or in the higher density of the higher molarity fluids. These measurements show the extreme resilience and the limits of hagfish slime to high salt conditions and underline the importance of calcium.

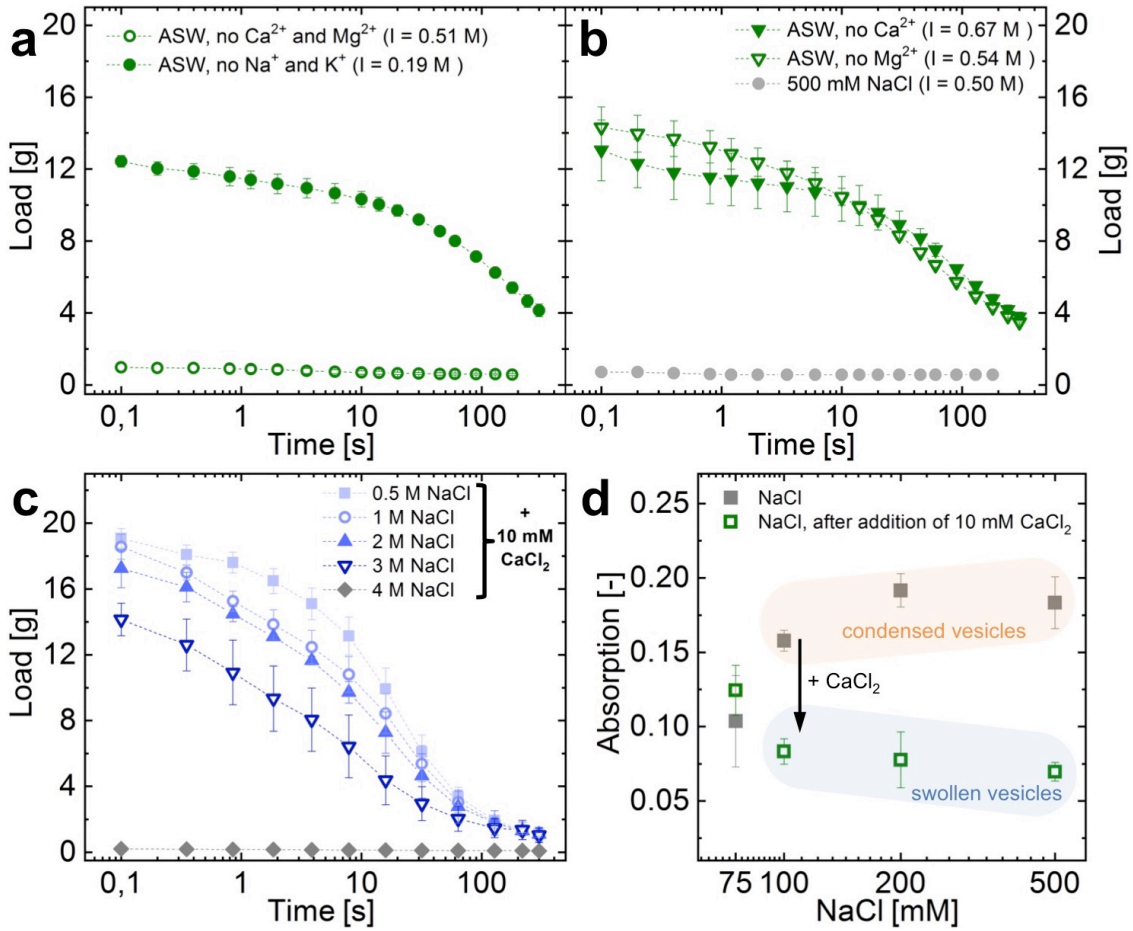

Figure 5.6: Effect of ionic composition of various versions of artificial seawater (ASW) on slime functionality. (**a**) Water retention in ASW without divalent cations (Ca^{2+} and Mg^{2+}) and ASW without monovalent cations (Na^{+} and K^{+}). (**b**) Water retention in ASW either without Ca^{2+} or Mg^{2+}, showing that one divalent ion is sufficient for functionality at a high ionic strength. If none are present at a comparable ionic strength, no water is retained (500 mM NaCl). For comparison the ionic strength (I) for every measurement is provided in brackets. (**c**) Water retention in NaCl solutions containing 10 mM $CaCl_2$. (**d**) UV-VIS turbidity measurements of hagfish exudate mixed with NaCl solutions in the absence of calcium. The turbidity at NaCl ≥ 100 mM originates in the presence of condensed vesicles and vanished once 10 mM $CaCl_2$ are added.

The crucial role of the divalent cation Ca^{2+} for mucin vesicle rupture was in depth investigated by Herr *et al.*[60]. The authors showed that Ca^{2+} is required for the swelling and rupture in approximately 60% of vesicles in seawater strength osmolarity and suggested that Ca^{2+}-activated transporters in the vesicle membrane are responsible for the need of calcium. The remaining 40% ruptured also in the absence of Ca^{2+}. All vesicles ruptured when exposed to distilled water[6]. Our observations are in line the findings of Herr *et al.*[60] and show that calcium is needed for complete

vesicle decondensation already at NaCl concentrations approximately ≥ 100 mM (Fig. 5.6 d). The turbidity at 75 mM NaCl did not significantly change upon calcium addition, suggesting that most vesicles swelled even in the absence of calcium. At 50 mM the solution was already viscous and many skeins unraveled, making turbidity measurements difficult (not shown). However, the onset of viscosity and unraveled skeins suggest that in these conditions most vesicles swelled and ruptured.

These findings imply that a low ionic strength (approx. ≤ 100 mM) allows a hypo-osmotic swelling and rupture of most mucin vesicles similar to Milli-Q but results in a controlled skein unraveling as the ionic strength could be sufficient to suppress excessive thread swelling. Combined, this seems to form a somewhat functional fiber network that retains more water than Milli-Q (Fig. 5.6 b). At a high ionic strength (approx. ≥ 100 mM) vesicle decondensation is limited to about 40% of the vesicles. The reduced amount of ruptured vesicles and mucin strands does not seem to be able to sufficiently drive the unraveling of the skeins. A strongly impaired and collapsed network forms with many skeins remaining coiled, resulting in an almost absent water retention. Therefore, at high ionic strength the presence of Ca^{2+} seems crucial to rupture all the vesicles within the deployment time frame, allowing to transmit mixing forces to the threads[23] and thus form a functional slime network.

The presence of 50 mM Mg^{2+} resulted in an only slightly inferior water retention to Ca^{2+} (Fig. 5.6 b). Although it was found that Mg^{2+} only increased rupture in vesicles at about double the seawater concentration in seawater strength osmolarity, it seems that for whole slime functionality Mg^{2+} has a similar effect to Ca^{2+}. However, the origin of this beneficial effect is so far elusive. The similar water retentions between seawater and dilutions of seawater (Fig. 5.3 b) imply that hagfish slime functionality is not limited to a narrow window of ion composition as long as specific divalent ions (Ca^{2+} and Mg^{2+}) are present at concentrations similar to seawater. It was shown that > 3 mM Ca^{2+} resulted in a significant increase in vesicle rupture[60]. Although in 1% / 5% seawater there is only about 0.1 / 0.5 mM Ca^{2+}, there might be a beneficiary effect of having additionally 0.5 / 2.5 mM Mg^{2+} present. Additionally, the low osmolarities of these dilutions could support a hypo-osmotic vesicle rupture and at the same time reduce thread swelling, allowing for controlled unraveling without tangling.

Dynamic interactions of hagfish slime with seawater cations

Since hagfish slime deploys rapidly, it must distinctly interact with ions in the direct environment. To capture the dynamic processes between hagfish slime and seawater cations, the cation flux was investigated immediately after and five minutes after slime formation. Three fractions of liquids (a) seawater (Norway), the (b) unbound and the (c) bound & retained fraction were analyzed (Fig. 5.7). Hagfish slime significantly depleted potassium ions (K^+) from seawater and released calcium ions (Ca^{2+}). It was found that most K^+ was depleted in the unbound fraction (- 24 ppm, $p < 0.02$). Some K^+ was again added to fraction (c) after five minutes of draining as fraction (c) showed an only 19 ppm ($p < 0.04$) lower concentration compared to seawater. Calcium followed an opposite trend as the unbound fraction showed some more calcium (+ 15 ppm, $p < 0.08$) whereas the bound and drained fraction showed significantly more calcium compared to seawater (+ 23 ppm, $p < 0.02$). Sodium and magnesium levels did not change significantly.

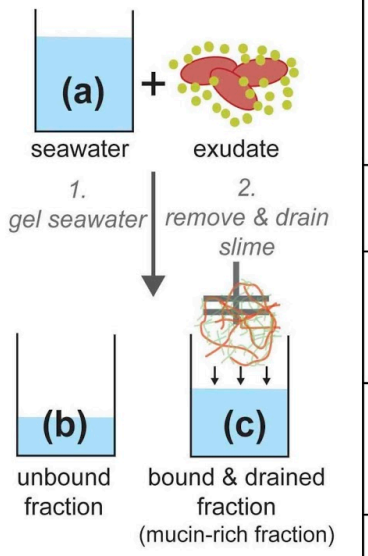

	(a) seawater (Norway)	(b) unbound fraction	(c) bound and drained fraction
Na^+	9825 ppm	10003 ± 338 ppm	10335 ± 897 ppm
K^+	383 ppm	359 ± 3 ppm ($p < .02$)	364 ± 4 ppm ($p < .04$)
Ca^{2+}	302 ppm	317 ± 4 ppm ($p < .08$)	325 ± 3 ppm ($p < .02$)
Mg^{2+}	938 ppm	942 ± 4 ppm	963 ± 25 ppm

Figure 5.7: **Dynamic cation concentrations during slime formation.** The concentration of seawater cations (Na^+, K^+, Ca^{2+}, Mg^{2+}) of three seawater fractions - (a) seawater, (b) unbound seawater, and (c) bound and drained mucin-rich seawater - were analysed. The figure on the left represents a schematic drawing of the experiment. Concentrations are in parts per million (ppm).

The depletion of K^+ from seawater suggests that K^+ is involved in an ion-exchange process during slime formation rather than for mucus gelation. The elevated Ca^{2+} levels in the fractions (b) and (c) (Figure 5.7) raise the possibility that a K^+/Ca^{2+} exchange process is involved in mucus decondensation during vesicle rupture, suggesting that the calcium is added by the ruptured vesicles. Skeins are unlikely to contribute substantial amounts of intracellular calcium when they unravel because cytoplasmic calcium levels are typically very low, and the skein develops within the cytoplasm of gland thread cells[4,5]. Apart from the skeins, Ca^{2+} can only be added by the vesicles as it is almost completely absent in the residual fluid[6]. A high intragranular calcium ion content of *M. glutinosa* mucus vesicles was suggested by Herr *et al.*[6]. The authors proposed that vesicle swelling is driven by a 'jack-in-the-box' mechanism, in which typically Ca^{2+}-ions shield the charges of condensed polyanionic molecules such as mucin inside a vesicle[167]. This cation is Ca^{2+} in the case of mice mucin vesicles[144] but can also be histamine for heparin or lysozyme for proteoglycans[167]. Once exposed to seawater, vesicle decondensation is triggered and Ca^{2+} is replaced by a less effective shielding cation such as Na^+ or K^+, causing repulsion between the negatively charged mucin polymers and thus fast swelling of the gel[168]. Our observations of dynamic cation concentrations in slime deployment support the suggestion of Herr *et al.*[6] that hagfish mucin inside the vesicle is kept in a condensed state by Ca^{2+}. Also, it is possible that Ca^{2+} is exchanged for K^+ during vesicle swelling, as similarly reported by Nguyen *et al.*[169] for mucus granules. The small potassium increase in fraction (c) compared to (b) supports the possible role of K^+ as a counterion in mucin decondensation. The K^+ ions do not seem to be strongly bound by the slime and drain again back into the solution. However, given the fact that sodium is present in seawater at 25x the concentration of potassium and therefore the diffusion of sodium would be faster, it seems unlikely that potassium exchange for calcium would evolve in preference to sodium. Therefore, probably both, potassium and sodium are exchanged for calcium during decondensation but the changes in sodium level could not be measured (see caveat further down) or the sulfonic groups of the mucin have a slight preference for potassium.

Furthermore, the fact that the mucin-rich fraction (c) in Figure 5.7 contains higher calcium levels than fraction (b) suggests that Ca^{2+} binds to hagfish mucin and helps it to gel. The affinity of invertebrate mucus for calcium ions was shown before for mucus of the freshwater snail[170]. Ca^{2+}-ions knowingly forms reversible cross-links and create salt-bridges between mucin chains, thus forming networks[171–173]. Therefore, the putative gelled mucin network interspaced in the thread network allows to entrap water. Furthermore, competitive binding of divalent cations over monovalent cations to sulfonated polyelectrolytes such as hagfish mucin[7] is also well known[174–176]. The calcium probably bound to the mucin in a counterion condensation process[177–179] and drained from the slime mass together with some of the mucin.
What is the amount of calcium that keeps the mucin condensed in the vesicle? 4 µl of exudate added about 0.3 mg - 0.46 mg calcium ions to the seawater. Calculating with an exudate density of about 1 mg/µl[9] results in 75 - 115 µg Ca^{2+} per mg exudate. Considering that 66% of the exudate are residual fluid and 17% each are mucin vesicles or skeins[8] about 0.68 mg mucins were added to the seawater. If all Ca^{2+} originates from the mucus vesicles 44 wt% - 68 wt% of the total mucus dry mass would be calcium. Calcium was shown to reach high intragranular levels between 2.5 - 3.6 moles calcium / kg dry mass mucus in the giant mucin granules of a slug (*Ariolimax columbianus*)[167], corresponding to about 10 - 14.4 wt%. Considering that hagfish mucin must swell extremely fast in a defense situation against the high osmotic gradient of seawater, a roughly three to four times higher concentration than reported in slug mucin vesicles does not seem unlikely.

A caveat to the presented data lies in the high levels of sodium and magnesium in seawater, which limited an holistic insight in the dynamic ion flux during slime formation. Both calcium and potassium occur at concentrations of roughly 300 - 400 ppm whereas magnesium and sodium are present at more than double and ten-fold this concentration, respectively. We worked with concentrations close to the natural concentrations of hagfish exudate (1 mg exudate on 5 ml seawater[8]). Cation concentrations of 300 - 400 ppm result in a exudate / cation mass ratios of about 1/1.5-2 per cation as is the case for Ca^{2+} and K^{+}. In contrast, this ratio is roughly 1/5 for Mg^{2+} and almost 1/50 for Na^{+}. It is possible that the concentrations of Mg^{2+} and Na^{+} varied in the investigated fractions but their variation remained hidden in the small ratio of exudate / ion concentration. Future investigations such as measuring the calcium content only in the mucus and the skein fraction of the exudate or using dilutions of seawater and investigating the vesicles and skeins separately could help to provide a more detailed analysis of intragranular Ca^{2+} levels and ion flux during slime formation.

Conclusion

In this study we demonstrate the crucial role of ionic strength and seawater cations - especially Ca^{2+} - for the formation dynamics and functionality of hagfish slime. The findings are summarized and schematically depicted in Figure 5.8. We suggest that sufficient ionic strength controls the dynamics of skein unraveling and slime network formation.

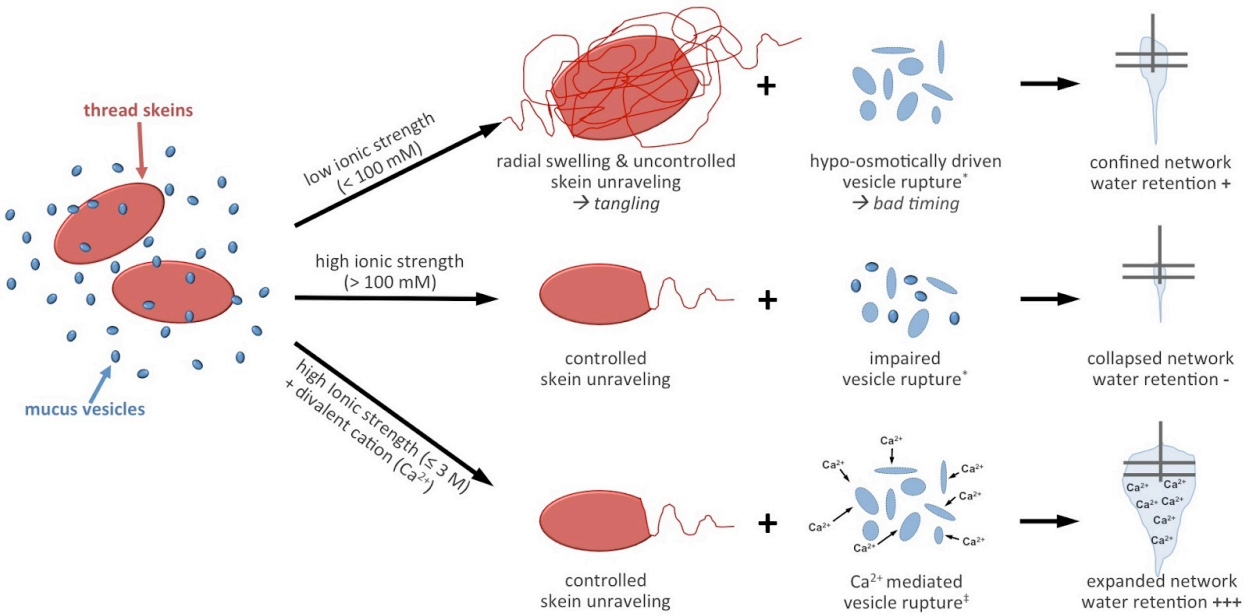

Figure 5.8: Schematic representation of the suggested role of ionic strength and divalent seawater cations (Ca^{2+}) for the formation and functionality of hagfish slime. A low ionic strength causes the thread skeins to swell radially and unravel uncontrolled from both sides, causing tangling of the threads. The vesicles rupture due to the large osmotic gradient. Tangling combined with immediate vesicle rupture creates a confined thread network that fails to entrap large amounts of water. At a high ionic strength skein unraveling is controlled but vesicle rupture is impaired. A dense and collapsed network forms, resulting in an almost absent water retention. At a high ionic strength with Ca^{2+}-ions present, skeins unravel controlled, vesicles rupture Ca^{2+}-mediated, and the mucin probably gels. A widespread and expanded slime network forms that entraps large amounts of water as observed in seawater, resulting in a functional defensive hydrogel. Citations in the figure: *[6]; ‡[60]

A low ionic strength caused a confined and narrow thread network in contrast to the widespread and expanded network formed in seawater. The thread skeins swelled and unraveled uncontrolled from both sides, probably causing tangling of the threads and thus preventing a widespread network. It is possible that the fast unraveling in ion-free water originates in an excessive swelling of the intermediate filament slime thread, which would possess increased stored strain energy. More stored strain energy would lead to a less controlled and faster unraveling. However, as the mucin vesicles ruptured in the hypo-osmotic environment of deionized water, a somewhat functional network that entraps about 50% of water in comparison to seawater can be formed in the absence of ionic strength.

At increased ionic strength (approx. > 100 mM) a collapsed network formed that failed to incorporate water although the thread skeins unraveled controlled. We assume that as a consequence of impaired mucin vesicle rupture at high ionic strength - in the absence of calcium ions - an effective skein unraveling is limited as less mucus strands can attach to the threads to transmit mixing forces, leaving many skeins coiled. Only in the presence of divalent seawater cations Ca^{2+} and Mg^{2+} a functional slime network is realized at seawater strength osmolarity. Whereas the reasons for the beneficial effect of Mg^{2+} remain elusive, Ca^{2+} was shown to be important to mediate a complete and well-timed vesicle rupture, which supports skein unraveling in the high ionic strength environment, creating an expanded network. The presence of calcium allowed the formation of a functional slime network up to 3 M NaCl, corresponding to 4-5 times the ionic strength of seawater. Furthermore, Ca^{2+} could be necessary for an ionic gelation of hagfish

mucin, which is supported by cation concentration measurements. These measurements further suggest that *M. glutinosa* mucin vesicles release intragranular Ca^{2+} during the rapid decondensation and swelling of hagfish mucin. Based on the findings in this work we propose that calcium has three distinct roles in hagfish slime: mucin condensation within vesicle, mucin decondensation via Ca^{2+}-activated transporters in the vesicle membrane at high ionic strength[60], and mucin gelation in the deployed slime.

Our results show that a functional defensive slime that entraps and retains water can only be formed in the presence of divalent seawater cations Ca^{2+} or Mg^{2+} at a high ionic strength. The insights on the interactions of hagfish slime with seawater ions will improve our understanding of the complex cascade of physico-chemical events underlying the formation of hagfish defensive slime and might support the design of bioinspired fibrous polyelectrolyte hydrogels that efficiently and rapidly form in high ionic strength environments.

Chapter 6 - Hagfish Slime Rheology

The content of this chapter has been partially published by Böni, L.J., Fischer, P., Böcker, L., Kuster, S., Rühs, P. A., in "Hagfish slime and mucin flow properties and their implications for defense." *Scientific Reports* 2016, *6*, 30371.

Hagfish are preyed upon by a variety of aquatic animals, exposing the fish and the formed slime to feeding mechanisms such as biting or suction (Fig. 6.1 a). Suction feeders rapidly expand their buccal cavity, thereby creating a unidirectional flow of water that engages the prey and draws it into the mouth[180,181]. As shown by Zintzen *et al.*[2], in all observed cases of predation, the hagfish were able to free themselves from the attacker by gill-clogging[3], suggesting that their defense mechanism is very efficient and crucial for their survival. Being such an outstanding defense, the slime has a major drawback for the hagfish. If they were not able to free themselves from their own slime, they might self-asphyxiate. Therefore, hagfish can tie a sliding knot with their own body to strip off the slime and thus avoid self-entanglement (Fig. 6.1 b)[3,11,182,183]. Escaping slime by knotting seems important as hagfish do not only secrete slime when attacked, but also when feeding or injured[11].

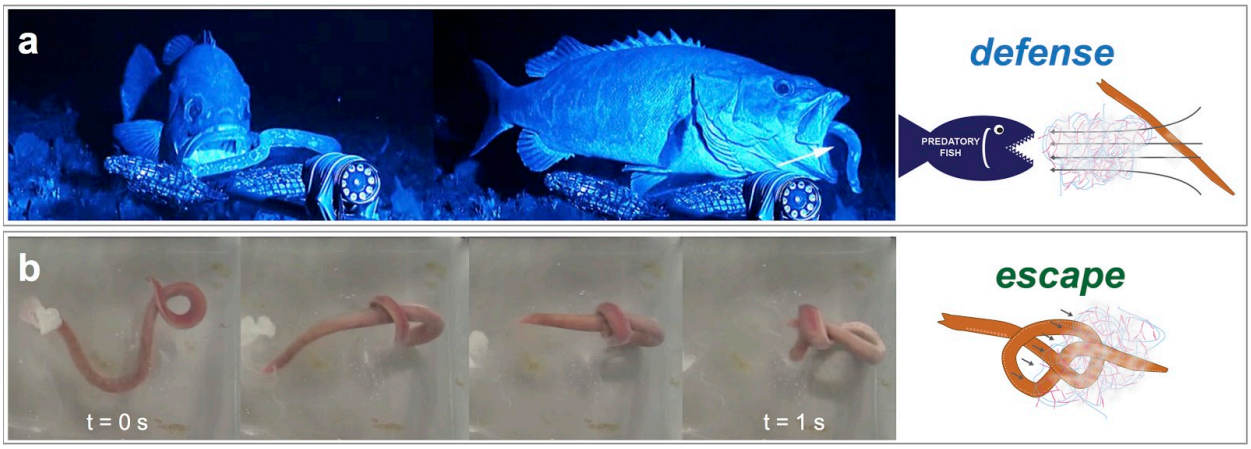

Figure 6.1: Hagfish defense and escape. (**a**) During predation hagfish instantly form large quantities of slime as a defense mechanism. Predation often occurs through suction feeding where the prey is sucked into the mouth by a strong elongational flow. The arrow depicts jets of slime that were projected into the predator's mouth upon suction feeding (Adapted and reprinted by permission from Macmillan Publishers Ltd: Scientific Reports, Zintzen *et al.*[2], copyright 2011). (**b**) Entanglement and self-asphyxiation is avoided by sliding a knot across the body to shear off the slime and escape.

Despite the remarkable properties of hagfish slime, the flow behavior behind its defensive properties and the individual contributions of each slime component are largely unknown. The rheology of slime was studied previously[9,127,128], however the flow properties of the slime were not linked to its main purpose, i.e. its protecting capacity. Therefore, we studied the rheological properties of hagfish slime and hagfish mucin in elongational, shear, and oscillatory flow to investigate the role of hagfish slime in defense and escape. The slime has a unique network structure, as small exudate concentrations (0.01% v/v) are sufficient to develop resistance features against flow such as viscosity and elasticity. Using a rheological approach, we propose that the flow properties of the slime seem beneficial to its ability to clog the gills of predators (thickening in

elongation), and its ability to be shed by hagfish that get trapped within the slime (thinning in shear).

Outline

The flow behavior of hagfish slime was measured with rheology to study its implications for the defense mechanism. In the first part the influence of the threads on the slime network properties were studied. In the second and third part the effect of shear and elongational forces on the slime were investigated. Based on our measurements, the apparent shear thinning and elongational thickening flow properties were linked to biological implications for hagfish defense and escape strategies.

Hagfish slime viscoelasticity

One of the most striking features of hagfish slime is the low concentration needed to gel vast quantities of water[8,9]. We therefore investigated the rationale behind the natural economic use of material by gradually increasing the slime concentration and studied the contribution of threads and mucins to the network properties. With oscillatory rheology, the network properties of hagfish slime and mucin were measured at exudate concentrations from 0.01 to 0.08% v/v and compared to naturally occurring concentrations of mucin in 0.01% v/v slime. Please note that an exudate concentration of 0.02% v/v equals a slime protein dry weight of 0.0066 wt% (fibers and mucin in equal parts of 0.0033 wt% each), based on the fact that about 66% of the exudate are water and solutes and that an exudate density of 1 g/ml can be assumed[8]. An exudate concentration of 0.01 to 0.02% v/v, being the natural concentration[8], is sufficient to develop elastic features with a higher storage modulus G′ than loss modulus G″ (Fig. 6.2 a).

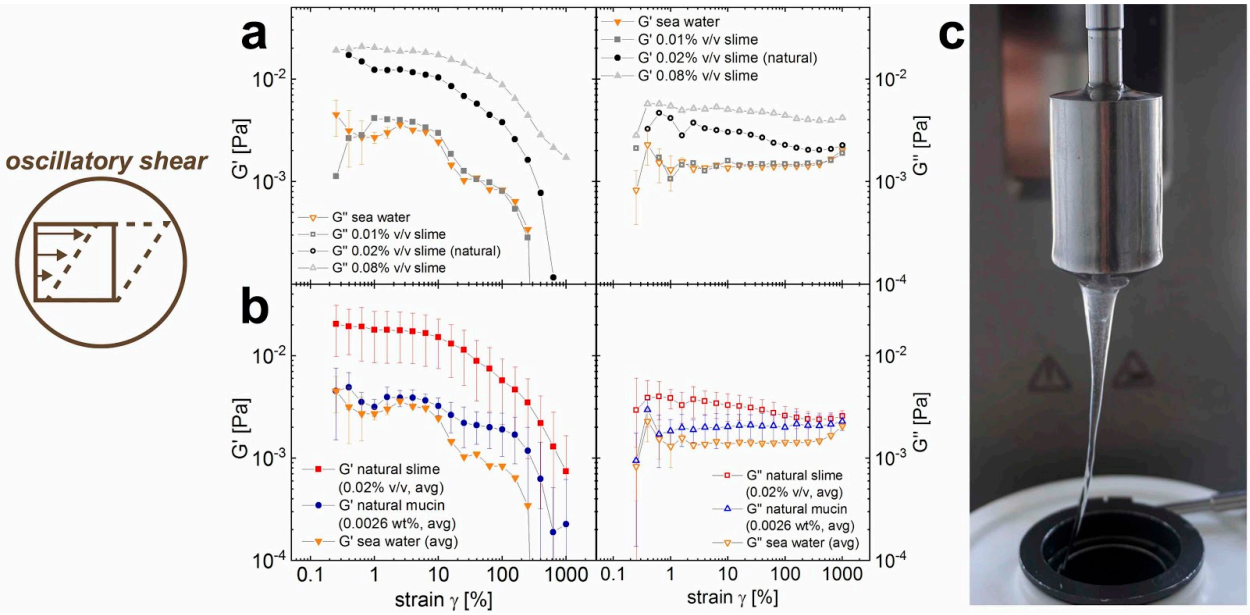

Figure 6.2: Oscillatory shear rheology of hagfish slime and mucin. (**a**) Amplitude sweep of hagfish slime (G′ left and G″ right) at varying concentrations (0.01 to 0.08 % v/v, 0.01% v/v being the natural slime concentration) at a fixed angular frequency of ω = 1 rad/s. (**b**) Amplitude sweep (G′ left and G″ right) of five averaged measurements of hagfish slime (0.02 wt% being the natural concentration), hagfish mucin (0.0026 wt% being the natural mucin concentration), and seawater as a reference at a fixed angular frequency of ω = 1 rad/s. (**c**) In oscillation and simple shear the rheological properties of hagfish slime were measured with a Couette geometry.

This is unique, as most biological hydrogels require a much higher concentration to exhibit gel-like features[184]. A concentration of 0.01% v/v exudate was found to be the lowest functional concentration as it visibly still gelled the entire system but showed a viscoelastic signal close to water, which also exhibits an apparent elastic modulus due to surface tension effects (Fig. 6.2b left). Ewoldt *et al*.[130] reported the considerable rheological challenges (sample and instrument inertia, instrument resolution, boundary effects) in determining the underlying material functions of soft and water-based bio-materials, such as hagfish slime. However, although in this study a more than fourfold lower exudate concentration was used than by Ewoldt *et al*.[9] (0.83 mg/ml by Ewoldt *et al*., corresponding to 0.083% v/v), an almost identical softness for hagfish slime ($G' \approx 0.02$ Pa) was measured. When the concentration was increased to 0.08% v/v, the linear viscoelastic modulus G' still remained largely constant. This finding suggests that hagfish slime is an inherently soft material, regardless the concentration.
In 0.01 wt% slime (mass exudate per mass water), about 20% is mucin[8], therefore we evaluated to what extent the mucins contribute to the rheological response. We found that the apparent elasticity of the mucin fraction (20% of 0.01 wt%) is nearly identical to seawater. This can be seen in the substantially higher moduli of the slime compared to mucin in Fig. 6.2 b showing the average of five measurements for slime, mucin, and water, respectively. At a concentration of 0.0026 wt% the mucins do not seem to form a network across the entire slime or the used measurement technique is not sensitive enough. This data supports the theory of Fudge *et al*.[8], who suggested that hagfish mucins do not form a cross-linked network throughout the slime but are rather heterogeneously distributed in discrete networks. Therefore, to have a viscoelastic network, the threads seem to be important for the overall viscoelasticity.

Shear thinning of hagfish slime

Hagfish have to escape their own slime to avoid suffocation. They can form a sliding knot with their body to shear off the slime. The influence of simple shear flow on the slime properties is measured at shear rates of 1, 10, and 100 s^{-1} corresponding to the range of natural shear rates: Assuming a hagfish body length l = 0.2 m, a knotting time of t = 1 s, and a gap range between the sliding surfaces of h = 0.001 – 0.01 m. This equals a sliding velocity of v = l/t = 0.2 m/s . According to $\dot{\gamma} = v/h$ this corresponds to an average shear rate of $\dot{\gamma} \approx 20$ - 200 s^{-1} during knot sliding.
As hagfish slime is highly sensitive to its mechanical history[8,166], no pre-shear experiments were performed. Hagfish slime shows an apparent shear thinning behavior (Fig. 6.3 a left and Fig. 6.3 b) but in contrast to some other shear thinning solutions, with shear thinning being an intrinsic property of a homogeneous material, the slime viscosity decreases even at constant shear rates.

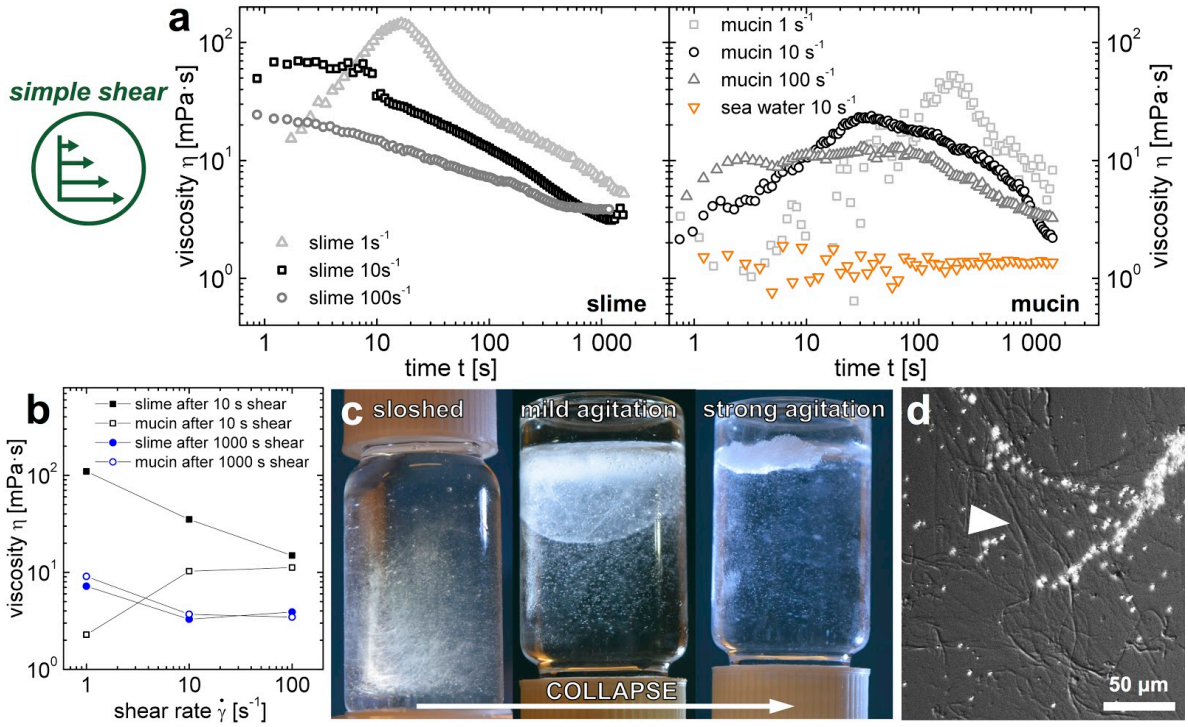

Figure 6.3: Shear induced collapse of hagfish slime and aggregation of mucin. (**a**) Simple shear of hagfish slime (left) and hagfish mucin (right) mimicking the flow properties during knot sliding at exudate concentrations of 0.02% v/v for slime and 0.0026 wt% for mucin, respectively. Hagfish slime viscosity was measured at constant shear rates (1, 10, 100 s^{-1}) over a period of 30 minutes. (**b**) The viscosity values plotted as a function of shear rate, showing the apparent shear thinning behavior of hagfish slime and the influence of time on the viscosity. (**c**) Agitation causing a collapse of the slime network by thread association. (**d**) Differential interference contrast (DIC) micrograph of a mucin floc after shear of a mucin solution, showing mucin aggregated into thread-like structures (arrowhead).

This effect can be attributed to the coiling of threads around the geometry[9] and thread association, leading to a collapse of the slime network (Fig. 6.3 c) and consequently to a phase separation of a condensed gel network separating from watery remains. A collapse of the network due to shear is also visible in Fig. 6.3 a right where the mucin fraction was measured without threads. We propose that the mucin fraction is not stable against shear, forming aggregates (Fig. 6.3 d), which lowers the viscosity. The tendency of mucins to aggregate and thus cause a gel-sol transition is known and mainly attributed to intermolecular hydrophobic interactions among protein segments[62,185]. We propose that given their large size and their high protein content[7], shear flow causes hagfish mucin to aggregate by facilitating inter-molecular hydrophobic interactions. The aggregating mucin fraction supports a collapse of the slime network by thread association. This collapse can be circumvented, as was shown in a previous study[127], with a network stabilized by negatively charged biopolymers.

Elongational thickening during suction feeding

When hagfish are predated through suction feeding[2,186] the slime is stretched by elongational, unidirectional flow[187–189]. A list of suction feeding fish preying on hagfish is presented in Table 6.1.

Table 6.1: Selection of suction feeders preying on hagfish

Predator / Predator family	Preys on hagfish	Uses suction feeding
Polyprion americanus (Atlantic wreckfish)	Zintzen *et al.*[2]	Brick Peres *et al.*[190]
Congridae (Conger eels)	Zintzen *et al.*[2]	De Schepper *et al.*[191]
Squalidae (Spiny dogfishes)	Zintzen *et al.*[2]	Wilga *et al.*[192]
Otaria flavescens (Southern sea lion)	Jørgensen *et al.*[186]	Berta *et al.*[193]
Gadus callarias (Codfish)	Jørgensen *et al.*[186]	Muller *et al.*[188]
Phoca vitulina (Harbour seal)	Jørgensen *et al.*[186]	Marshall *et al.*[194]

In addition, extensional flow is also likely to be important for the development and formation of the slime[23]. Extensional measurements with hagfish slime threads revealed that threads are very elastic in extension[32,56,195]. Additionally, distinct elastic features of hagfish mucins can be observed in hagfish slime. To address the effect of the mucin fraction, we measured the extensional rheology at the natural concentration of hagfish mucin and at lower concentrations to determine their role in the flow properties of hagfish slime (Fig. 6.4 a) using capillary breakup extensional rheology (CaBER). A strike time of 50 ms corresponding to a natural prey-sucking time was chosen[187,188].

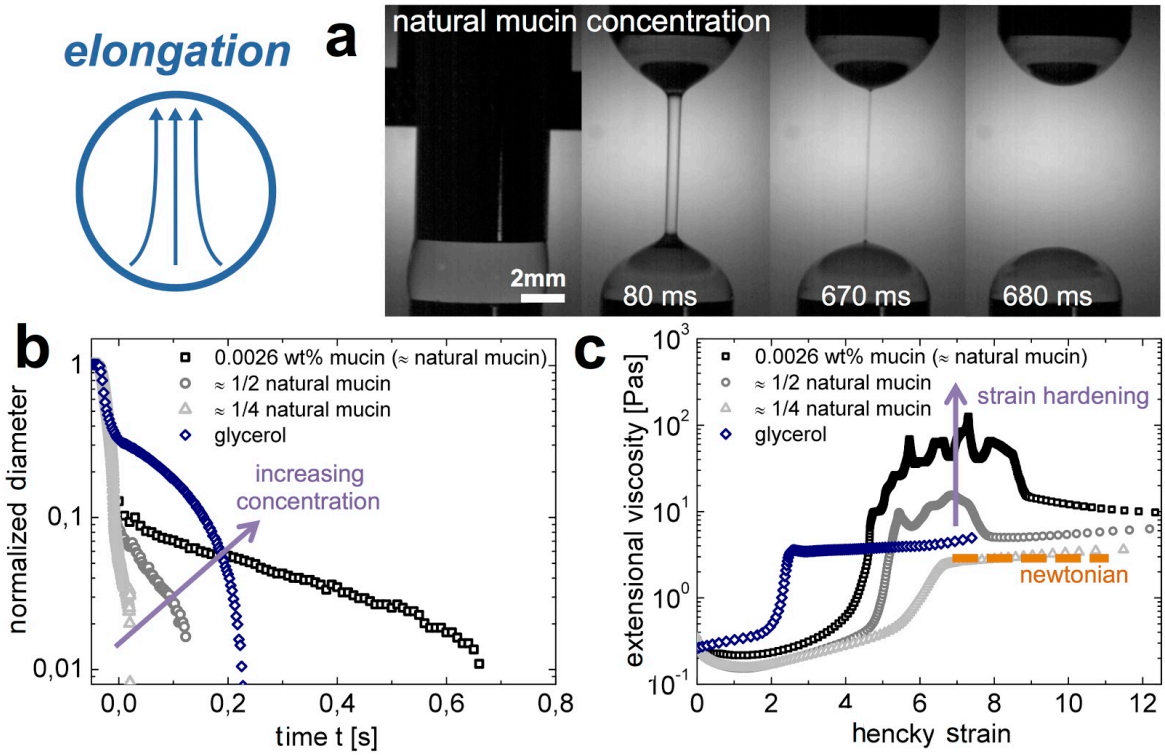

Figure 6.4: Capillary breakup extensional rheology (CaBER) measurements mimicking the extensional flow experienced by hagfish slime during suction predation. (**a**) A liquid filament thinning event of hagfish mucin (natural concentration) at t: 0, 80, 670, 680 ms. (**b**) The normalized filament diameter of hagfish mucin at a natural concentration, 50%, and 25% of the natural concentration as a function of time. Glycerol is provided as a Newtonian standard. (**c**) Extensional viscosity of hagfish mucin as a function of Hencky strain based on the data provided in (**b**). The orange dashed line indicates a Newtonian profile as observed for glycerol.

In Fig. 6.4 b the liquid filament thinning events of three mucin concentrations in seawater are shown. At the natural mucin concentration, a delayed breakup of the liquid filament can be observed. By contrast, a lower mucin concentration (25% of the natural mucin concentration)

coincides well with a Newtonian profile, suggesting that this concentration is very dilute and the mucin thread thinning is mainly ruled by capillary forces and given the low concentration possibly also by surface tension forces. A loss of elastic stresses and a Newtonian behavior with a decreasing mucin concentration is also observed in the corresponding extensional viscosity curves in Fig. 6.4 c. A pronounced strain hardening or an increase in extensional viscosity with strain is observed, which is attributed to a strong resistance of flexible polymer molecules to extensional flow[196]. Strain hardening is a known phenomenon for mucus systems[197–200] and is thought to arise from peculiarities of the extension kinematics, and to be related to a deferred disentanglement process[79]. A similar strain stiffening of hagfish slime was described by Ewoldt *et al*.[9] from oscillatory shear measurements, who likewise suggested that mucins, as non-linear elastic network components, are strain-stiffening. As shown in Figure 6.4 b,c, a strain hardening can be observed when the concentration of mucin is increased as strain hardening depends on the molecular weight and concentration of polymer in solution[196]. In the case of hagfish slime (with threads), mucin is entrained in defined regions due to the threads. We suggest that in combination with the elastic threads, the viscosity is even further increased, causing an elongational thickening during extensional stresses. The resulting resistance against flow has a strong influence on the elastic behavior of hagfish slime as presented in Figure 6.2. An increased viscosity thus might reduce the water flow at the predators' gills, supporting gill clogging.

Conclusion and Biological Implications

Hagfish are able to form viscoelastic slime networks at very low exudate concentrations (0.01% v/v) with distinct rheological properties in oscillation, simple shear, and extension. The low concentration allows for an economic use of exudate but results in a short-lived and soft gel. Nevertheless, the short-longevity of the slime may be of advantage for the hagfish as it can escape from its own slime. Furthermore, the slime forms within milliseconds, allowing for a fast response upon attack without large energetic triggers for slime development, which is in contrast to most hydrogels that require substantial energy input for network formation. We suggest that the balance between gel structure and time/energy needed to form this structure is favorable for the defense situation. Using a rheological approach, we propose that not only the viscosity but also the elasticity of hagfish slime is largely determined by the mucin fraction and its synergistic interplay with the threads. So far only the viscous behavior of hagfish mucins was reported[8]. Although we could not detect mucin elasticity using oscillatory rheology, we base our assumption on their distinct extensional elastic properties. Hagfish mucins, being large biopolymers[7], are known to attach to the threads[23]. By this anchoring additional network points are created, thus decreasing the overlap concentration of the mucin dispersion. We propose that the threads provide long range properties such as extensibility and cohesiveness of the slime, prevent mucin wash-out[3,8,128], and allow the mucin to exhibit viscoelasticity by supplying anchoring points. Thus, when combined with the threads, the mucin fraction can establish viscoelastic properties, despite the low natural concentration.

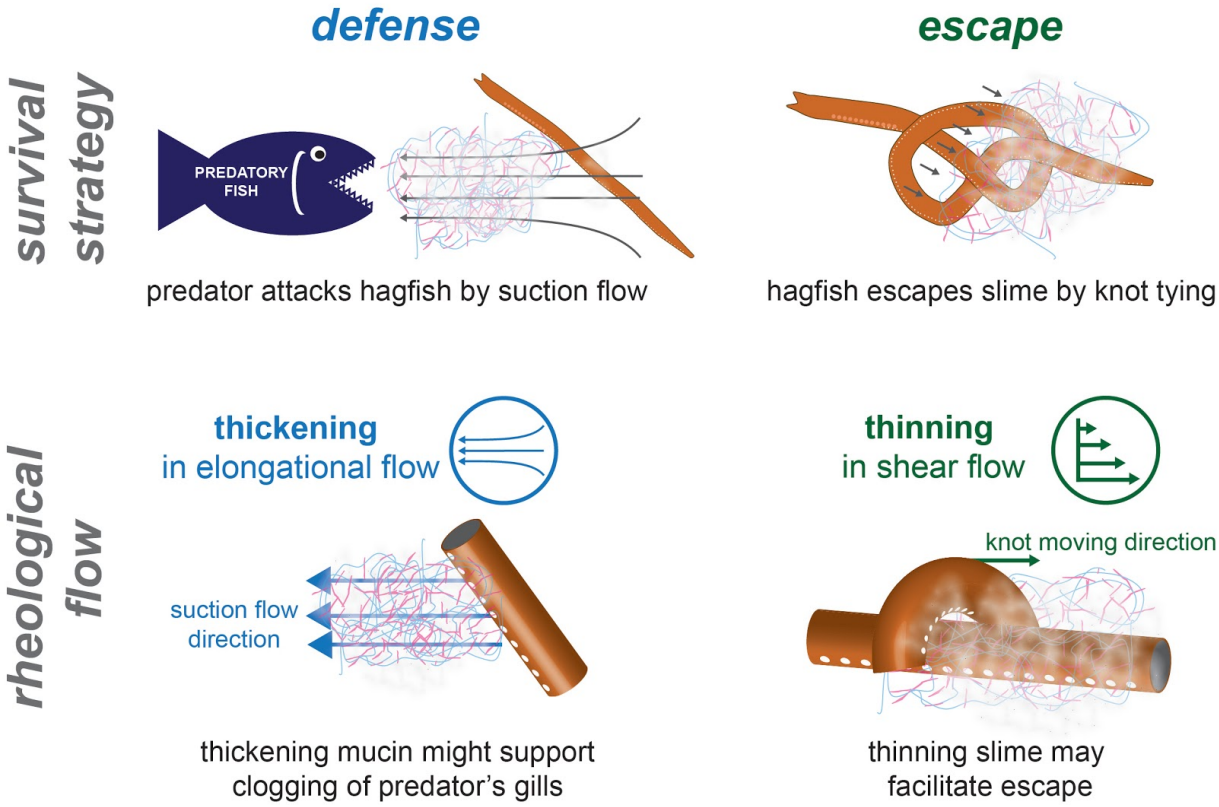

Figure 6.5: Hagfish survival strategies and their underlying flow principles. During predation, hagfish secrete and form large quantities of slime as a highly effective defense mechanism. Many predators hunt by suction feeding, where a strong unidirectional elongational flow draws in the prey. When the slime is subjected to elongational flow, the viscosity of the hagfish mucin increases, which might support clogging of the predator's gills. Facing suffocation and entrapment in their own slime, hagfish shear off the slime by moving a knot across their body. The applied shear leads to a viscosity decrease and a collapse of the slime, which may facilitate the escape and prevent self-asphyxiation.

The slime flow behavior in shear and extension seem beneficial for the biological survival strategies of hagfish slime (Fig. 6.5). Predators attacking hagfish often use suction feeding[2]. We propose that suction flow has two effects on the slime. First, flow supports the slime formation[23]. Second, extensional flow, created through suction feeding induces an increase in extensional viscosity of hagfish mucin. An increased viscosity reduces the water flow and thus could support gill clogging. Furthermore, the cohesiveness provided by the threads could also be important for predator gill clogging or to defend against biting predators[3]. To avoid self-asphyxiation, hagfish are able to form a knot with their body to release themselves from their slime[182]. The shear thinning behavior of the slime may be helpful in this situation. Yet, other flow phenomena such as lubrication and slip might also be important. Shear forces eventually lead to a collapse of the slime network, which is supported by mucin aggregation.
However, some questions and limitations of this study remain to be addressed in order to draw further conclusions on the functions in life and the selective pressures that have led to the slime's physical properties. Knowing the relative amounts of extension to shear during suction feeding events will provide deeper insights in the opposite behavior of the slime under the respective flow conditions. Additionally, the timing of slime formation and possible changes of the slime during formation might be critical as the slime could enter the mouth of a predator in an incompletely deployed state. Therefore, further studies will extend the basis for hypotheses on the evolution of

hagfish slime as a defense mechanism. In summary, we propose that hagfish slime flow properties, thickening in elongation and thinning in shear, may be beneficial for both, escape and defense. Besides the biological significance, the synergistic effect between macroscopic extensible threads and microscopic extensible mucin molecules might allow the formulation of novel, bio-inspired, and functionalized hydrogels with an enormous water holding capacity.

Chapter 7 - Biomimetics

The content of this chapter has been partially published by Böni, L. J., Sanchez-Ferrer, A., Widmer, M., Biviano, M. D., Mezzenga, R., Windhab, E. J., Dagastine, R. R., and Fischer, P., in "Structure and nanomechanics of dry and hydrated intermediate filament films and fibers produced from hagfish slime fibers." *ACS Applied Materials & Interfaces* 2018, *10*, 40460–40473

A rich source of keratin-like Intermediate filaments (IFs) can be found in hagfish slime threads [40–44], commonly referred to as hagfish fibers or hagfish threads. IFs are a major structural element of animal cells, playing an important role in cell mechanics by acting as stress absorbers, imparting integrity, and by mediating mechanotransduction processes[24–29]. IF have a diameter of approximately 10 nm and share a common architecture characterized by of a central α-helical coiled-coil 'rod' domain, flanked by a largely amorphous N-terminal 'head' and C-terminal 'tail' domain of variable length and sequence[30]. Given their open molecular architecture and their unique assembly plan[27], IFs possess unique mechanical properties[31–33] by combining extreme extensibility[34–36], flexibility[37], and toughness, making them much more flexible and resistant to large deformations than other cytoskeletal polymers such as F-actin and microtubules[36,38,39].

Hagfish threads consist of axially aligned IFs, which condense to a solid 1 - 3 μm diameter fiber that can be up to 15 cm long[4,5,8,40]. Hagfish IFs comprise three thread keratin (TK) proteins (α, β, and γ)[43], whereby β is likely a post-translationally modified version of γ[41]. They are classified as IFs because they contain a central rod domain with heptad repeat motifs of apolar residues, rod subdomains shared with other IF proteins, a 'stutter' of the heptad repeat in subdomain 2B, conserved sequences at each end of the rod domain, and non-helical N- and C-terminal domains that connect to the central rod domain [22,42,44]. Hagfish IFs were termed 'keratin-like' due features in the head and tail domains that are similar to keratin[42,44]. TKα was found to be a type II keratin homolog and TKγ possesses features of type I keratins, but also contains structural similarities to type III IFs, which include desmin and vimentin[22,45]. Furthermore, TKα and TKγ were found to self-assemble into hetero-dimeric IF like nanofibrils in vitro[43,46,47].

Hagfish fibers still comprise the only known example of extracellularly secreted IFs. As in all other known cases, IFs occur strictly intracellularly[5,48]. Mechanical properties similar to spider silk[10], as well as the high protein concentration (supposed to approach 1000 mg/mL in hydrated threads[55]), and the ability to isolate relatively large (several grams) quantities[40]) make hagfish fibers an intriguing natural source of invertebrate IFs.

Recently, macroscopic fibers were produced from naturally sourced[116] and bacterially expressed[46,47] hagfish IFs from the Pacific hagfish (*E. stoutii*). Whereas these studies focused on the mechanical performance of the dry reconstituted fibers, little is known about the ability of reconstituted IF materials to hydrate and the associated changes in mechanical properties. Hydration differs strongly for hard and soft α-keratins and is a key property of IFs. In hard α-keratin such as hair and nails, the approx. 10 nm IF fibrils are embedded in an isotropic, high-sulphur matrix[158], keeping them in a largely hydration-free state[55], and thus forming strong composite materials[201,202]. In soft α-keratin as found in the stratum corneum (soft outer layer of skin), hydrated IFs are - apart from their mechanical role - crucial for water conservation[195]. In contrast to F-actin and microtubules, which exist in a dynamic equilibrium with soluble pools of monomers within cells, IFs are much less soluble[195,203], and therefore potentially constitute a good source of functional protein for biomaterials with applications in liquid environments.

In this study we investigated the mechanical properties and protein secondary structure of IF films produced from hagfish fibers in the dry and hydrated state. Using naturally sourced IFs from thread skeins of the Atlantic hagfish (*M. glutinosa*), two different methods were used to produce films: i) drop casting, and ii) coagulation on a magnesium chloride bath as first described by Negishi *et al.*[116]. The films were compared for their secondary structure assessed by Fourier transform infrared spectroscopy (FTIR) and X-ray diffraction (XRD), as well as their surface morphology using AFM imaging. Films were then hydrated and structural changes (swelling height, network mesh-size) as well as viscoelasticity assessed by nanoindentation were monitored and compared to the dry state. In a last part, biomimetic fibers with aligned β-sheets similar to natural hagfish fibers were produced and implications of IF viscoelasticity on the production of such bioinspired materials are discussed. Our observations provide valuable insights into the mechanics of condensed IF systems and their response to hydration and will support the design of novel bioinspired IF materials.

Isolation of intermediate filament protein from hagfish skeins

Intermediate filament (IF) proteins were obtained from hagfish thread skeins - coiled up hagfish fibers - from the Atlantic hagfish (*M. glutinosa*). The skeins were separated from the mucin vesicles via filtration, washed with Milli-Q water, dialysed and freeze-dried. The isolated dry skeins (Figure 1a) and mucin (Figure 1b) were checked for purity using SDS-PAGE gel electrophoresis (Figure S2a,b,c) and FTIR (Figure 1c). In SDS-PAGE, the skeins showed a major double band with molecular weights of 62 kDa and 67 kDa, which agrees well with the findings from Koch *et al.*[42,44] who reported a molecular weight of 66.6 KDa for the α-subunit and 62.7 for the γ-subunit of the IF heterodimer for the Pacific hagfish (*E. stoutii*). Additionally, two minor bands are visible at about 53 kDa and 58 kDa. They could originate from small amounts of microtubules (α- and β-tubulin of approx. 50 kDa[204]), which occur within skeins that are not fully mature[40,49].

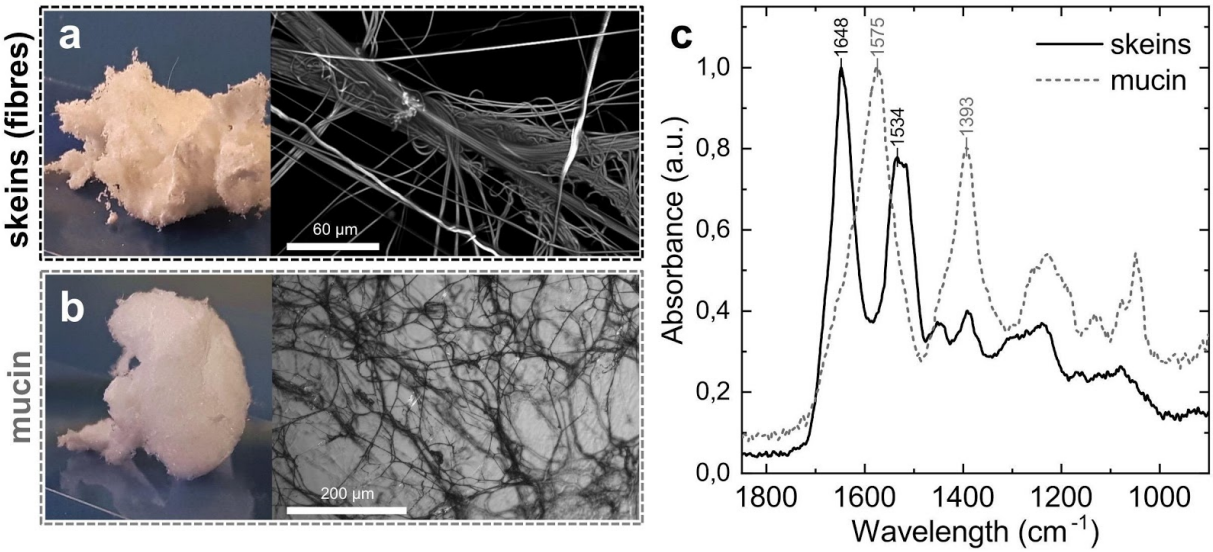

Figure 1: Separation hagfish fiber intermediate filament (IF) protein from hagfish mucin. (a) Photograph of freeze-dried hagfish skeins on a microscopy slide (left), and confocal scanning laser microscopy (CLSM) of hagfish slime fibers (uncoiled skeins) in water (right). **(b)** Photograph of freeze-dried hagfish mucin on a microscopy slide (left) and corresponding CLSM image (right). **(c)** ATR-FTIR spectra of freeze-dried skeins and mucin (the spectra were normalized to their highest peak for comparison).

Mucin showed a major band at 89 kDa and a minor band at 37 kDa and one component that did not enter the gel, as similarly observed for mucin isolated from the Pacific hagfish[7,43]. The major band at 89 kDa is in good agreement with findings of Spitzer *et al.*[43] but differs from findings of Salo *et al.*[7]. Both components - skeins and mucins - showed distinct FTIR spectra (Figure 1c), supporting their successful separation. The skein fraction showed a spectrum characteristic for proteins with an amide I peak around ~1648 cm^{-1} and amide II peak around ~1534 cm^{-1}. In contrast, the mucin fraction had a clearly different spectrum with a major peak around 1575 cm^{-1} and 1393 cm^{-1}. Hagfish mucin is considered a large, highly sulfated glycoprotein[7,205].

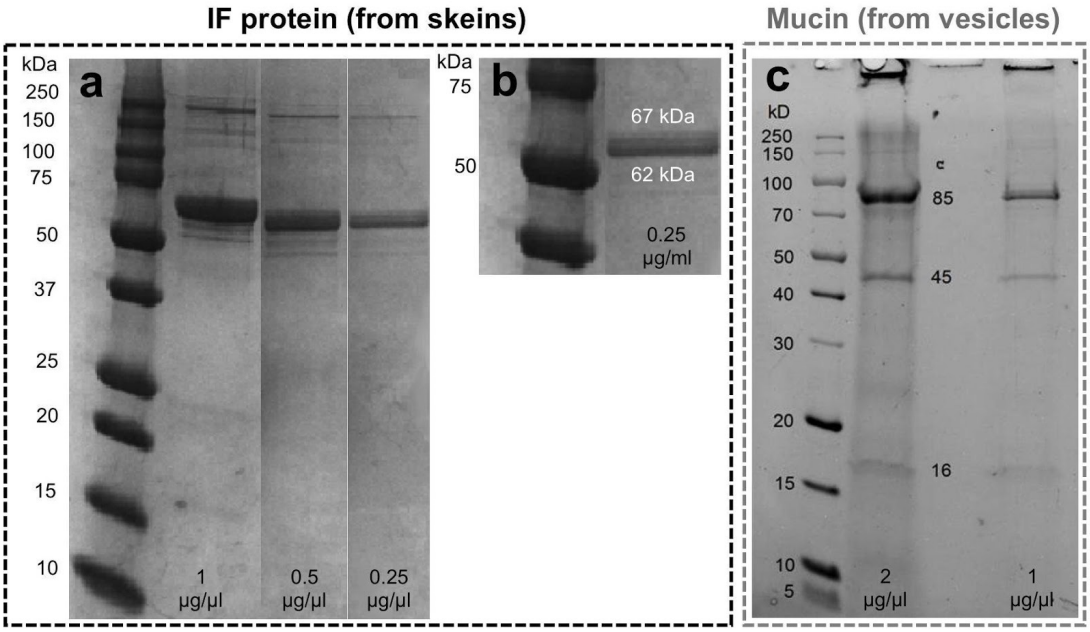

Figure 2: SDS-PAGE of freeze-dried hagfish skeins and mucin. (a) Skeins (hagfish fiber intermediate filament protein) at various concentrations consistently show a double band around 62 to 67 kDa. **(b)** Magnification of double band from (a) at a sample concentration of 0.25 µg/µl. **(c)** Dialyzed hagfish mucin

The peak around 1575 cm^{-1} shows shoulders at the amide I and II position, indicating the presence of protein but shifted, probably because of sugars bound to the protein backbone. The prominent peak around 1393 cm^{-1} could result from protein side-chain COO^-. The peak around 1230 cm^{-1} could originate from the antisymmetric S=O stretch vibration from sulfates, which is typical for highly sulfated carbohydrates[206] and was also observed for sputum[207]. The peak around 1050 cm^{-1} is an indication for carbohydrates such as N-acetylglucosamine, N-acetylgalactosamine, and sialic acid bound to mucins[207]. These peaks were also observed for other mucins such as porcine gastric mucin, bovine submaxillary mucin[208–210] and invertebrate mucins[211,212], and agree well with the reported sugars in hagfish mucin[7,205].

Hagfish IF films are rich in β-sheets

Separated and freeze-dried skeins (IF protein) were solubilized in formic acid and two different approaches were used to produce films: i) drop-casting, and ii) coagulation on the surface of an ice-cold buffer bath containing $MgCl_2$ (Figure 3a). Both films were partly transparent. Whereas drop-casting produced thick, self-supporting, and highly birefringent films (Figure 3b,d), coagulation resulted in thin, brittle, and weakly birefringent films (Figure 3c,e). The stronger birefringence of the drop-cast film likely originates in the increased thickness and could additionally be favoured by a higher β-sheet content. FTIR peak deconvolution revealed that both films mainly

consisted of β-sheets (~1620 cm^{-1}), random coils (~1650 cm^{-1}), and a smaller amount of β-turns (~1680 cm^{-1}) (Figure 3f,g). The drop-cast film contained higher amounts of beta-population (61%) compared to the coagulation film (49%), and lower amounts of random coils (39%) compared to the coagulation film (49%).

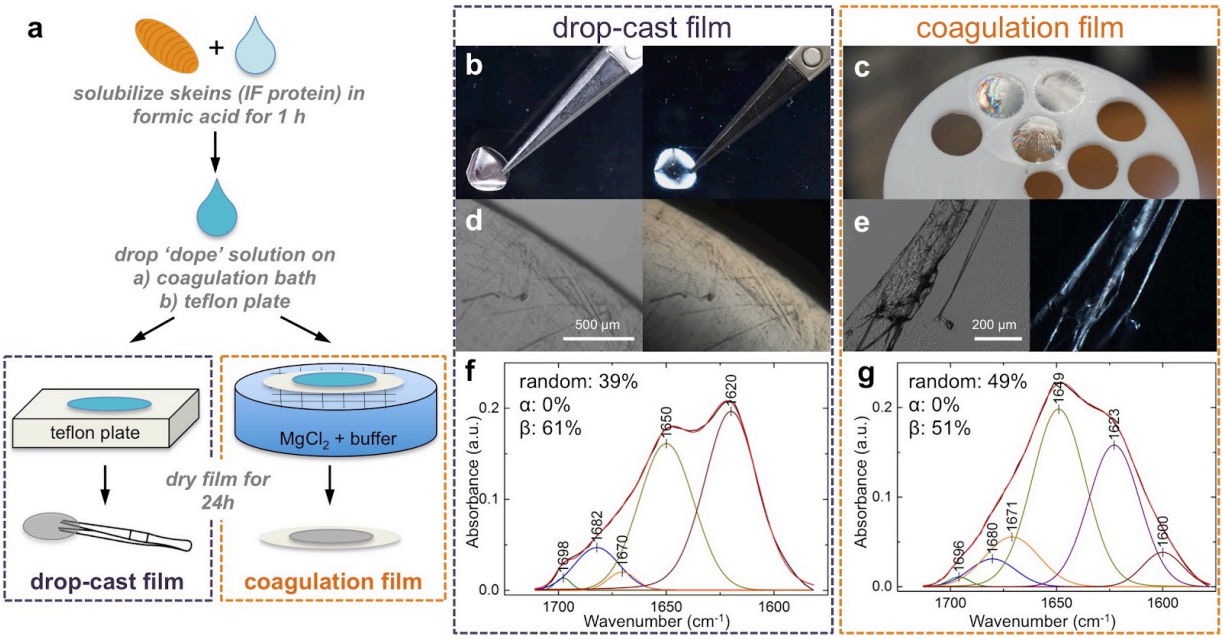

Figure 3: Production, morphology, and protein secondary structure of films produced from hagfish fibers. (a) Film production from solubilized hagfish fibers. Hagfish IF protein is solubilized in formic acid and then either coagulated on a buffer containing $MgCl_2$ or drop-cast on a teflon plate. From the buffer the film is removed with the help of a fine supportive metal mesh that is placed under a thin teflon plate with holes. Both films are air dried for 24 h. Drop casting forms self-supporting films, which show strong birefringence **(b)** in contrast to the coagulation method, which forms thin films **(c)**. Birefringence assessed with polarized light microscopy **(d,e)**. For the thin coagulation film birefringence is only visible when several layers are on top of each other (scale bars are located on the films). FTIR peak deconvolution of a drop-cast **(f)** and coagulation film **(g)**.

Whereas β-sheet rich structures were similarly found for fibers produced from natural and recombinant[46] hagfish protein - where coagulation films were drawn from the water surface into macroscopic fibers - no α-helices were observed in this study. Negishi *et al.*[116] reported α-helices identified by Raman spectroscopy. However, their deconvoluted spectra would alternatively allow to identify the peaks at 1654 cm^{-1} and 1655 cm^{-1} as random coils instead of α-helices - given that peaks between 1647 and 1655 cm^{-1} are often assigned to random coils, and peaks between 1656 and 1662 cm^{-1} are often assigned to α-helices[117] - and wide angle x-ray scattering (WAXS) measurements did not show the presence of α-helices either. Based on circular dichroism measurements Fu *et al.*[46] suggested that α-helices (coiled-coils) are present in hagfish IFs when they are solubilized in formic acid but undergo an α-helix to β-sheet (α-β) transition at the water/air interface during picking up the film and drawing it into a fiber. Conformational changes of proteins at interfaces are a well-known phenomenon[213]. However, given that stretching of the films was largely avoided during lifting the films from the water surface and that drop-cast films were not subjected to any stretching strains except maybe surface tension effects during drying raises the question whether α-helices are at all present in materials produced by solubilizing hagfish fiber protein in formic acid. The absence of α-helices thus remains elusive so far but could be linked to

the strongly chaotropic nature of formic acid or maybe the freeze-drying step in sample preparation[214].

Nano surface topology of IF films

The height of coagulation films was typically in the range of 1 µm and is limited by the spreading of the dope droplet at the buffer interface and the subsequent film formation. A film thickness of 3 - 5 µm for drop cast films was targeted for AFM measurements (Figure 4a,b) but in contrast to coagulation films the height of drop-cast films can be tuned by protein concentration, cast volume, or by using a mold that can easily reach up to 50 - 100 µm. Both films appeared flat at the micron scale but showed distinct differences in surface morphology at the nanoscale (Figure 4c,d,e,f). The drop-cast film was denser and substantially smoother than the coagulation film and occasionally showed shallow and round dents that probably stem from surface tension stresses during air-drying. The coagulation film had a more nano-porous and nano-rough surface, which seems a result of the immediate solidification at the $MgCl_2$ buffer surface.

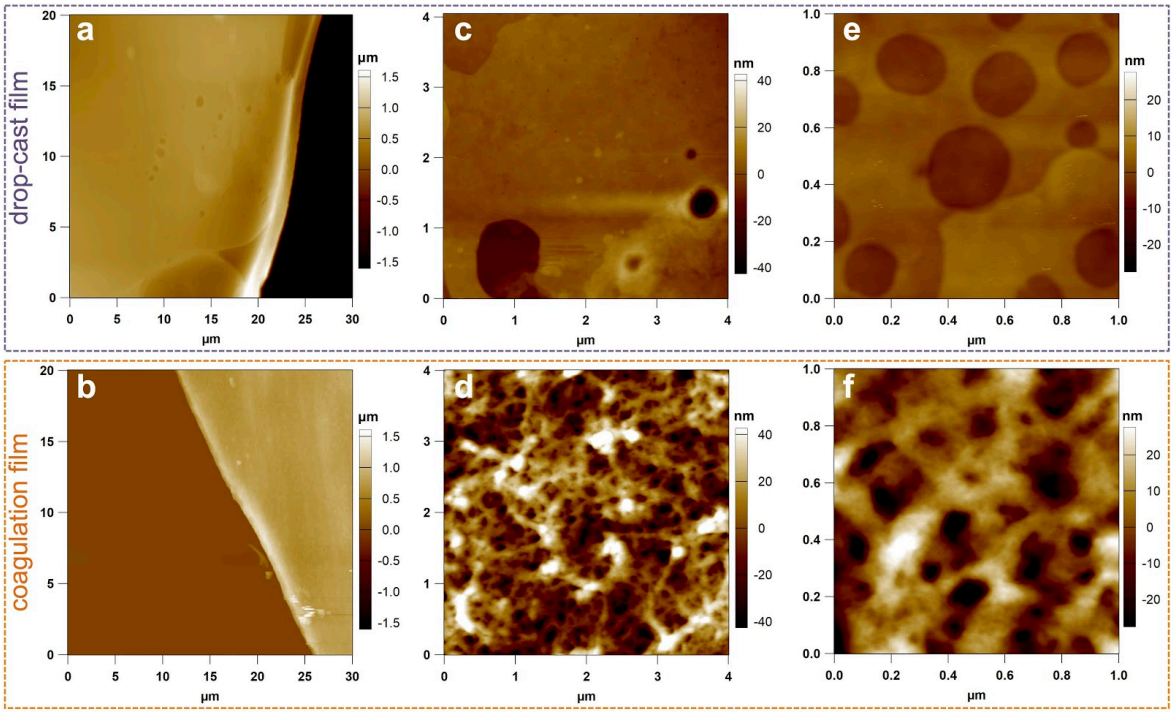

Figure 4: AFM height images showing the micro- and nano-topography of dry hagfish protein films. Drop-cast (a) and coagulation film (b) show a smooth surface at the micro-scale. At the nano-scale the drop-cast film (c,e) is considerably smoother than the coagulation film (d,f).

Hagfish IF films readily hydrate and swell in water

The reconstituted films readily hydrated and swelled when immersed in water, similar to native hagfish slime fibers[10,55]. Immersion in deionized water (Milli-Q), as well as in higher ionic strength solutions, did not dissolve the IF films - a hallmark feature of IFs[215] - and the birefringence was conserved (Figure 5a). Hydration in 1% simplified seawater (SSW; 5.45 mM NaCl + 0.1 mM $CaCl_2$) resulted in immediate swelling of the films, whereby the drop-cast films increased 55±9% and coagulation films increased 73±13% in height (Figure 5b). In contrast to the coagulation film, hydration did not change the surface roughness of the drop-cast film (Figure 5c, Figure 6).

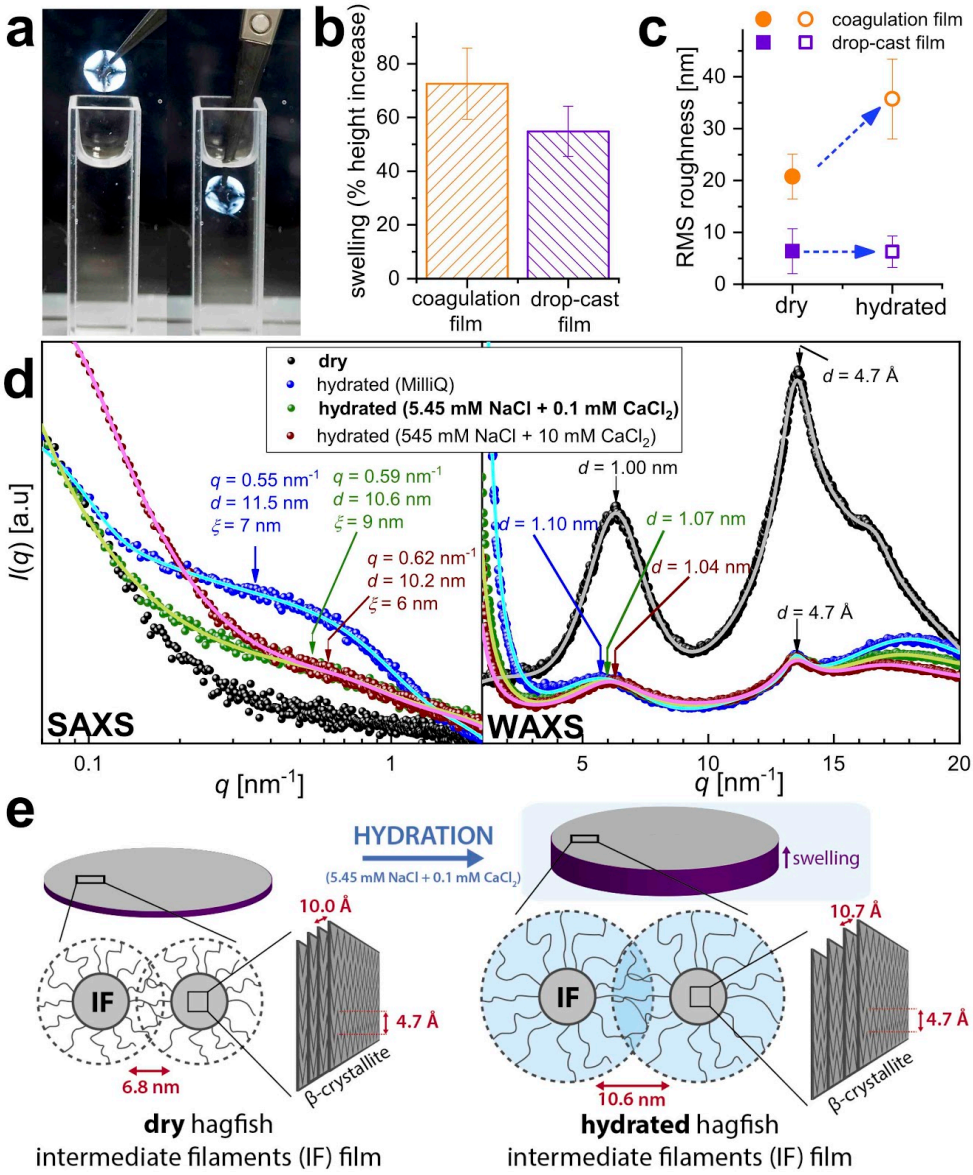

Figure 5: Hydration of intermediate filament protein films. (a) Hydration of a drop-cast film between cross-polarizers, showing birefringence for the dry and the hydrated state. **(b)** Swelling of the hydrated films, depicted as the height change percentage compared to the dry films. **(c)** Change in surface root mean square (RMS) roughness upon hydration (data based on images shown in Figure 3 and Figure 6). **(d)** Small angle (SAXS) and wide angle (WAXS) X-ray scattering profiles of dry and hydrated drop-cast films. For the hydrated films different salt concentrations were measured, whereby 5.45 mM NaCl + 0.1 mM $CaCl_2$ are the salt concentrations also used in AFM measurements in liquid. **(e)** Model depicting the hydration of hagfish IFs. The films are made of randomly oriented IFs. The amorphous C-terminal tail domains radiate perpendicular to the IF cylinder axis in a bottlebrush configuration. In the illustration the tail domains are end-grafted to a plane rather than a filament cylinder for simplicity. Upon hydration, the tail polymers stretch out and the brush height grows with polymer length.

Wide angle x-ray scattering (WAXS) measurements of dry films (Figure 5d) showed the presence of β-crystallites, indicated by the two peaks corresponding to 4.7 Å (inter β-strand) and to 10.0 Å (inter β-sheet)[216] distances and thus supporting the FTIR findings. Upon hydration, the peak at 4.7 Å remained unchanged, while the second peak at 10.0 Å increased to 11.0 Å when hydrated with Milli-Q water, showing a lager inter β-sheet distance. These results demonstrate that the

β-crystallites do not dissolve and supports the observation that birefringence does not vanish upon hydration. The main broad peak in the WAXS profile at ca. q = 18 nm^{-1} for the swollen samples – indication of water molecules -, as well as the occurrence of a characteristic length d = 11.5 nm (Milli-Q) in small angle x-ray scattering (SAXS) measurements (Figure 5d) suggest that swelling mainly happens in the amorphous C-terminal tail domains of the IFs as already suggested for hagfish fibers[10]. The characteristic length likely represents an inter-IF distance and can be attributed to the average mesh-size of the gel system when films are hydrated. The mesh-size could be influenced by a bottle-brush configuration of the tail domains that are known to radially graft IFs (Figure 5e), whereby in average 16 IF tails radiate from the filament backbone every 22 nm, resulting in a distance of 6.6 nm between two neighbouring tails[33,217,218].

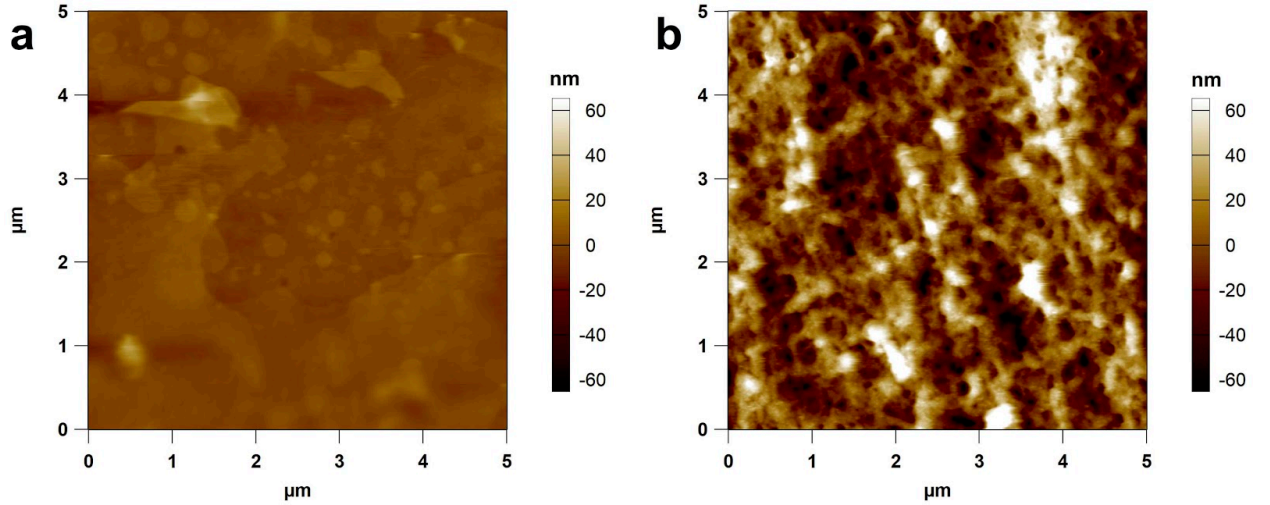

Figure 6: AFM images of a drop-cast film (**a**) and coagulation film (**b**) in liquid (5.45 mM NaCl + 0.1 mM $CaCl_2$).

X-ray measurements further suggest a polyelectrolyte behavior of hagfish IFs, which can be seen in the decrease of the average mesh-size *d* and of the inter β-sheet distance upon salt addition (Figure 5d). The mesh-size decreased from *d* = 11.5 nm in Milli-Q to *d* = 10.6 nm in 1% SSW to *d* = 10.2 nm in 100% SSW, implying that charge screening effects at high salt levels reduce the expansion of the IF tail domains and thus probably cause the IF film to swell less. Polyelectrolyte properties of IFs are well known, especially for neurofilaments (NFs) as they are considered to regulate the steric and electrostatic repulsions between the amorphous sidearms and thus affect both single NFs as well as NF networks[218–223] Also, hagfish thread skeins were found to display salt dependent properties[4,224] Threads uncoiled substantially faster when subjected to Milli-Q compared to seawater, which was considered to result from an increased swelling of the hagfish fiber in Milli-Q[225].

A mesh-size for the dry films can be estimated by relating the average mesh-size of a hydrated film (d = 10.6 nm) to its macroscopic swelling ratio V/V_0. Using the swelling ratio of 1.55 for the drop cast film, an average mesh-size of *d* = 6.8 nm for the dry film is obtained. These results suggest that the entropic brush of tail domains, which maintain the inter-filament spacing expands from 6.8 nm to 10.6 nm upon hydration in 1% SSW, and thus causes swelling in hagfish IF films[218,226]. A schematic model depicting the structural changes occurring during hydration of hagfish IF films is shown in Figure 5e.

Elastic modulus of dry and hydrated films

Mechanical properties of the films were assessed using AFM nanoindentation. Representative force-distance (F-D) curves in air (dry films) and in water (hydrated films, in 1% simplified seawater) with the respective Hertz fits to obtain the Young's modulus are shown in Figure 7a. The reported elastic moduli in this study are referred to as 'apparent', as a result of the sudden load during indentation. Dry films had high apparent elastic moduli ($E \approx 10^9$ Pa), which decreased about thousand fold upon hydration ($E \approx 10^6$ Pa) (Figure 7b). A thousand fold decrease in stiffness upon hydration is in line with observations for other matrix-free soft keratins such as stratum corneum and hagfish fibers[55]. The drop-cast films had a higher elastic modulus than the coagulation films, in both dry and hydrated state, which could be due to its increased β-sheet content and its higher density as the coagulation films appear porous. The elastic moduli of the dry films (5.1 GPa for coagulation films; 7.7 GPa for drop-cast films) agree well with the value reported for dry hagfish fibers in extension ($E \approx 8$ GPa[56]), and are in the range of elastic moduli determined by indentation for other dry keratins such as the cortical component of wool (4 GPa[227]), hair (7.4 GPa[228]), or fingernails (4.6 GPa[229]. Furthermore, the elastic moduli of the hydrated films (E = 6.1 MPa drop-cast films; E = 3.9 MPa coagulation films) agree well with elastic moduli reported for hydrated hagfish fibers (6 MPa)[10], as well as for other IFs such as vimentin (9 MPa[230]) but are a bit lower than values determined for single vimentin IFs in extension (27 MPa[39]).

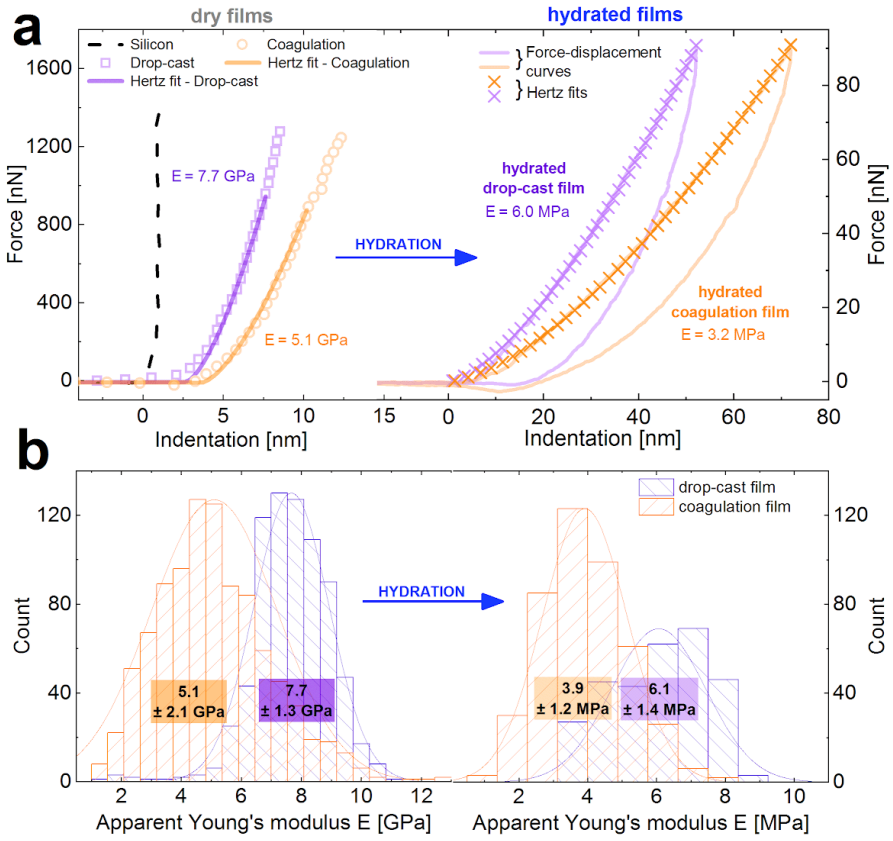

Figure 7: AFM force-distance (F-D) curves obtained from spherical indenters on dry and hydrated intermediate filament films. (a) Representative F-D curves obtained by indenting dry (left) and hydrated (right) hagfish protein films. The F-D were fitted with the Hertz model using the approach curve (hydrated films) and the retrace curve (dry films) to obtain an apparent Young's modulus. **(b)** Histograms depicting the elastic modulus E from dry and hydrated films.

Viscoelasticity of hydrated IF films

Apparent elastic moduli were obtained using the Hertz fit, assuming a purely elastic response of the deformed material. This criterion was satisfied for the dry films, but the F-D curves on the hydrated films clearly showed energy dissipation, recognizable by a hysteresis loop between the approach and retraction curve (Figure 7a). Hysteresis was similarly observed in uniaxial extension experiments with hydrated hagfish fibers[10]. The hysteresis loops did not show fatigue after repeated indentation (Figure 8), implying that there is no permanent plastic deformation.

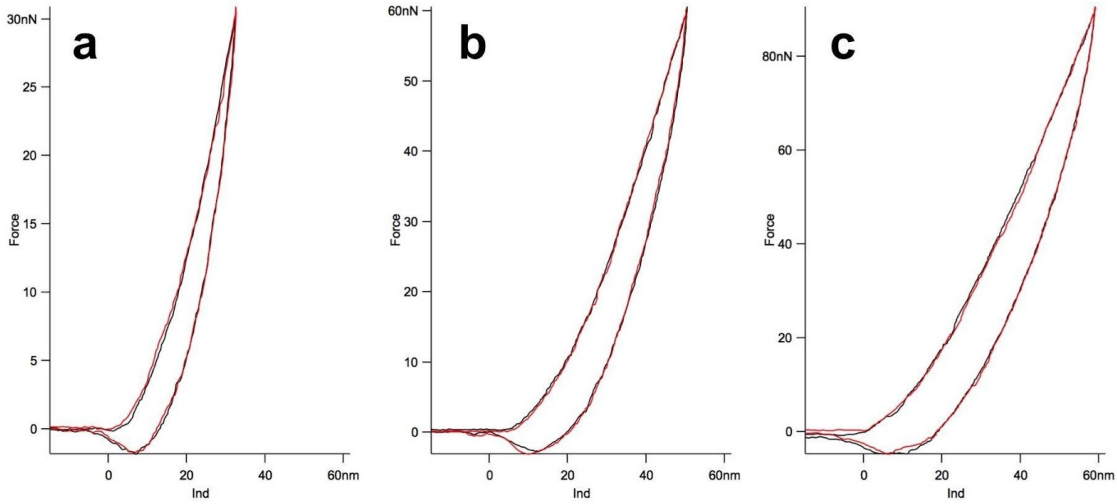

Figure 8: Repeated indentation on the same spot at increasing trigger force on a coagulation film. Red curve - 1st indentation, black curve 6th indentation for increasing trigger forces (a) < (b) < (c). The hysteresis loop does not change with repeated indentations on the same spot, showing that there is no permanent plastic deformation.

Therefore, a behavior similar to tough hydrogels[231] as well as viscoelasticity[100,232] were observed. Viscoelasticity is well-known for IFs[201,230,233] and indentation curves showing a similar recoverable hysteresis were observed for hydrated collagen fibrils[234] and stratum corneum[235], cells[98], as well as polyacrylamide, PVA hydrogels[98,236,237], and PDMS[238,239]. In order to assess the viscoelastic behavior of the hydrated IF films, two different approaches were used. On the one hand, constitutive viscoelastic parameters were extracted directly from AFM F-D curves using a method developed by Efremov *et al.*[98], where the indentation speed was varied (Figure 9). On the other hand, viscoelastic properties were assessed from stress-relaxation measurements (Figure 10), where the effect of maximum load was investigated.

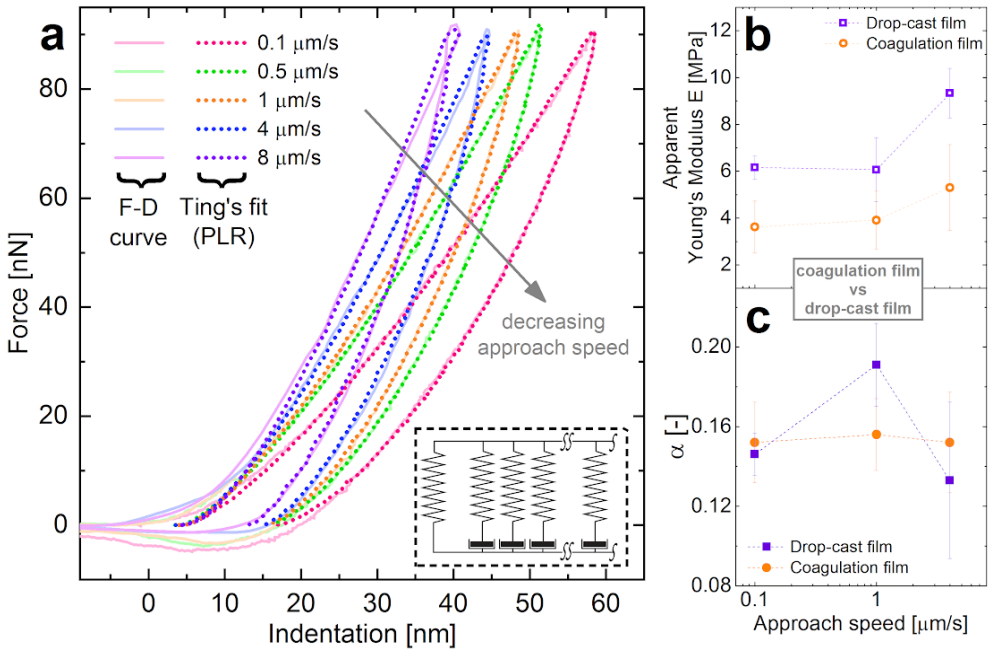

Figure 9: Effect of cantilever approach speed and cantilever size on viscoelastic properties of hydrated hagfish IF films. (a) Force-distance (F-D) curves on a hydrated coagulation film. The respective power-law rheology (PLR) fits using Ting's model[111] are overlaid (dotted lines). The inlet shows a schematic drawing of the modified PLR model depicting the serial connection of spring-and-dashpot elements. **(b)** Effect of cantilever approach speed on the apparent elastic modulus. **(c)** Effect of cantilever approach speed on the power-law exponent α for a coagulation and drop-cast film. Every point in (b) and (c) represents an aggregation of a minimum of 120 force curves acquired by force-volume mapping.

Increasing the cantilever approach speeds lead to a decrease in indentation depth (from approx. 60 nm at 0.1 µm/s to 40 nm at 8 µm/s) in F-D measurements (Figure 9a) and caused an increase in apparent elastic moduli of roughly 50% (Figure 9b), both evidence for viscoelasticity[101,239]. The apparent elastic moduli at a cantilever approach speed of 0.1 µm/s (3.6±1.1 MPa for coagulation films; 6.1±0.5 MPa for drop-cast films) increased about 50% when the speed was 40 fold increased to 4 µm/s (5.3±1.8 MPa for coagulation films; 9.3±1.1 MPa for drop-cast films). The power-law rheology (PLR) model (in depth explained in the methods section) fitted the F-D curves well over the range of investigated cantilever approach speeds and showed a predominantly soft-solid response, revealed by a power-law exponent α - where $\alpha = 0$ means a solid-like and $\alpha = 1$ a fluid-like behaviour. The power-law exponents of both films ($\alpha = 0.19 \pm 0.02$ for drop-cast films; $\alpha = 0.16 \pm 0.02$ for coagulation films) were similar and did not vary substantially with speed. The derived instantaneous moduli E_0 (22±3 MPa for drop-cast films; 12±3 MPa for coagulation films) were higher than the apparent elastic moduli for both films, which could infer an underestimation of elasticity at very short experimental times. At a speed of 8 µm/s the F-D curves showed a slight 'twist' at peak indentation, suggesting artifacts caused by hydrodynamic effects or limitations in the AFM feedback loop due to the constant sampling rate of 2 kHz.

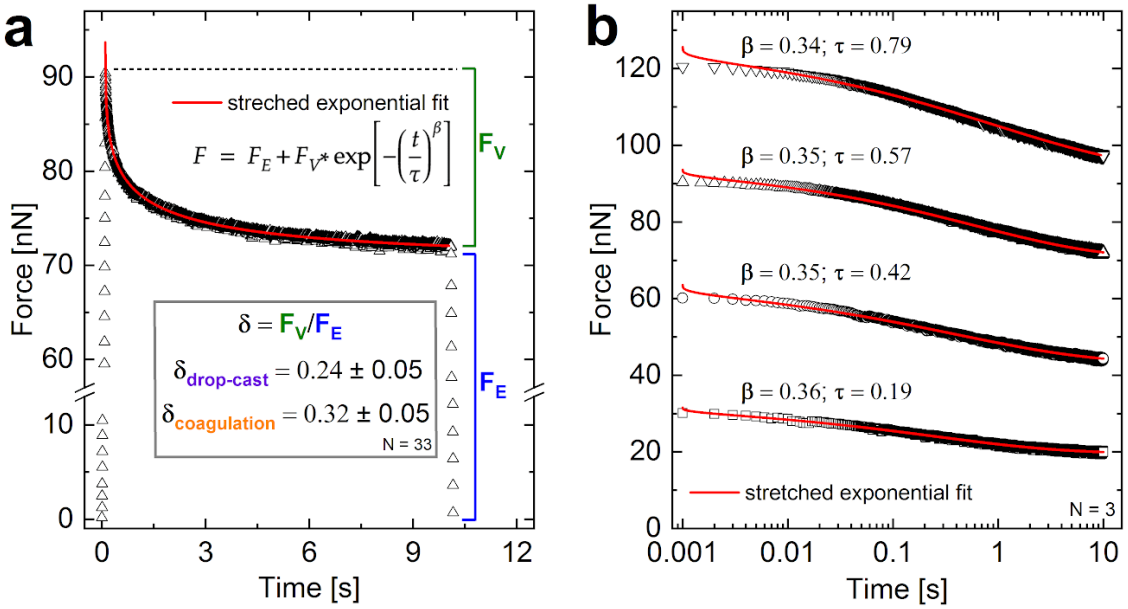

Figure 10: AFM stress-relaxation measurements on a hydrated hagfish IF film and the corresponding stretched exponential fits (red lines). (a) Stress relaxation of a coagulation film from an initial load of about 90 nN. The inlet depicts the calculation for δ - a parameter to relate elastic F_E and viscous F_V forces similar to the rheological loss factor tan δ. **(b)** Stress relaxation measurements performed at increasing initial peak load (strain).

The stretched exponential model fitted the relaxation behavior of both hydrated IF films well (Figure 10a), yielding a fractional power-law exponent β = 0.45±0.07 and a relaxation time τ = 0.40±0.07 s for the drop-cast film and β = 0.31±0.03 and τ = 0.75±0.22 s for the coagulation film. The lower β for the coagulation film suggests a broader distribution of underlying relaxation times[122], which could be due to its more heterogeneous and rough structure. Its heterogeneous and presumably less dense structure could also be a reason for the higher relaxation time τ. Small discrepancies between the fit and the measurement data can be observed at very short times, which probably stem from experimental difficulties such as simultaneously detect short and long times and the challenge to impose an instantaneous step strain[240]. A parameter $\delta = F_V/F_E$ was defined that relates the stored elastic F_E to dissipated viscous stresses F_V - similar to the loss factor tan δ = E''/E' in rheology - was calculated from the relaxation measurements (Figure 10a, inlet). Drop-cast films showed a δ = 0.24±0.05, suggesting that they retain more stored elastic stresses than the coagulation films (δ = 0.32±0.05) after 10 s relaxation - corresponding to a theoretical oscillatory frequency of 0.1 Hz. These values supports the finding that hydrated hagfish IF films show viscoelastic solid-like behavior and dissipate viscous stresses under load. Increasing loads in stress relaxation measurements did not affect the stretch exponent β but resulted in increased relaxation times τ (Figure 10b). This implies that strain (in the tested range) does not affect the overall relaxation mechanism of the many independently relaxing structures. However, higher strains increase the time these structures require to relax, implying the relaxation of physical bonds rather than chemical cross-links. The more physical entanglements are stressed the more time they require to dissipate this stress. The PLR model also fitted the stress relaxation measurements well and yielded similar power-law exponents ($0.05 < \alpha < 0.2$) for increasing step loads (Figure 11a,b) as obtained from the F-D curves using Ting's model. However, the less parametrized stretched-exponential model was found more resilient to describe the stress-relaxation behavior. The challenge to impose an instantaneous step load especially for AFM in liquid environments as well as the possibility that residual stresses in the bent cantilever co-relax

with the hydrated film during the long dwells (10 s) and thus cause a superimposed relaxation - which is less the case in the faster F-D measurements - seem to affect the PLR model more and therefore the stretched-exponential model was chosen to describe the stress-relaxation in the dwell measurements.

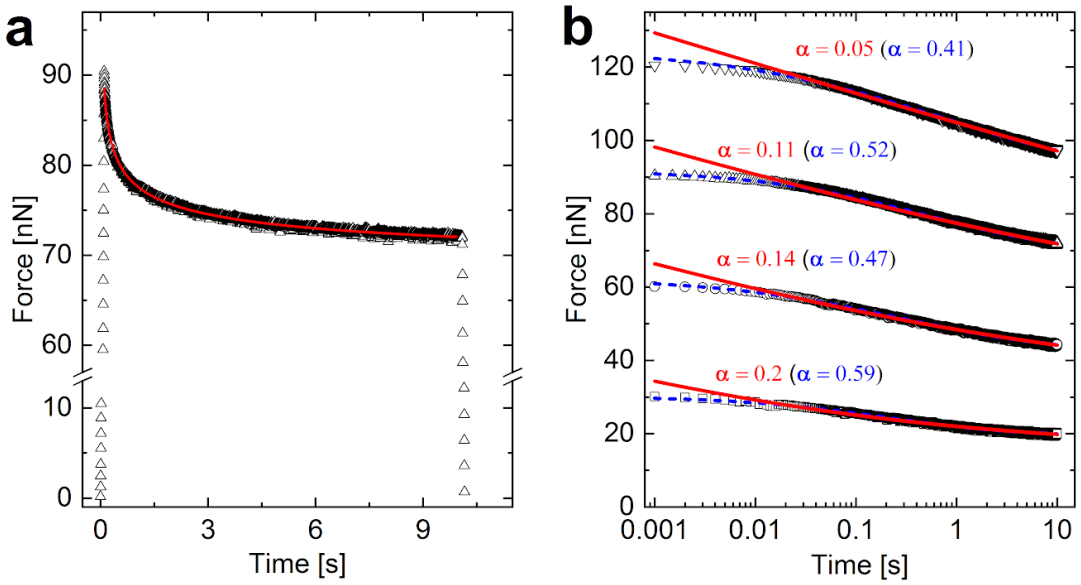

Figure 11: Power-law rheology (PLR) model fitted to AFM stress-relaxation measurements on a hydrated hagfish IF film (coagulation film). (a) Stress relaxation from an initial load of about 90 nN with fitted PLR model. **(b)** Stress relaxation measurements performed at increasing initial peak load (strain) and the corresponding PLR fits. The red lines depict fits where *t'* was held constant at $5*10^{-5}$, similar to the PLR fits used for the F-D curves. The blue lines represent fits where t' was let run free for the fitting, which resulted in better fits but also in substantially higher alpha values (in brackets).

Based on the mechanical and structural findings, we propose that the hagfish IF films possess an amorphous matrix constituted by the IF tail domains with embedded β-sheet clusters from the central part of the IFs. It is challenging to distinguish whether the structure is a connective β-sheet matrix with amorphous domains or a connective amorphous matrix with β-sheet clusters only from FTIR and X-ray measurements. However, the thousand-fold reduction in elasticity upon hydration strongly favours latter model, as a β-sheet matrix is unlikely to soften this substantially. Furthermore, the finding that larger strains require more time for the system to relax suggests that the contact points in hagfish IF films are the physical, which is likely due to the entangled and overlapping IF tail domains.

Hydrated IF films do not exhibit strain stiffening

It was further tested if increasing strain provokes strain stiffening in hydrated IF films in indentation measurements. Spanning a range between 20 - 250 nm indentation depth no strain stiffening was observed (Figure 12a). The apparent elastic modulus (Figure 12b), as well as the power-law exponent α from the PLR fit (Figure 12c) remained constant except for the smallest indentation, and when the indenter was changed from a spring constant of 1.75 nN/nm to 38.5 nN/nm in order to achieve larger indentations and still operate in the linear range of cantilever deflection.

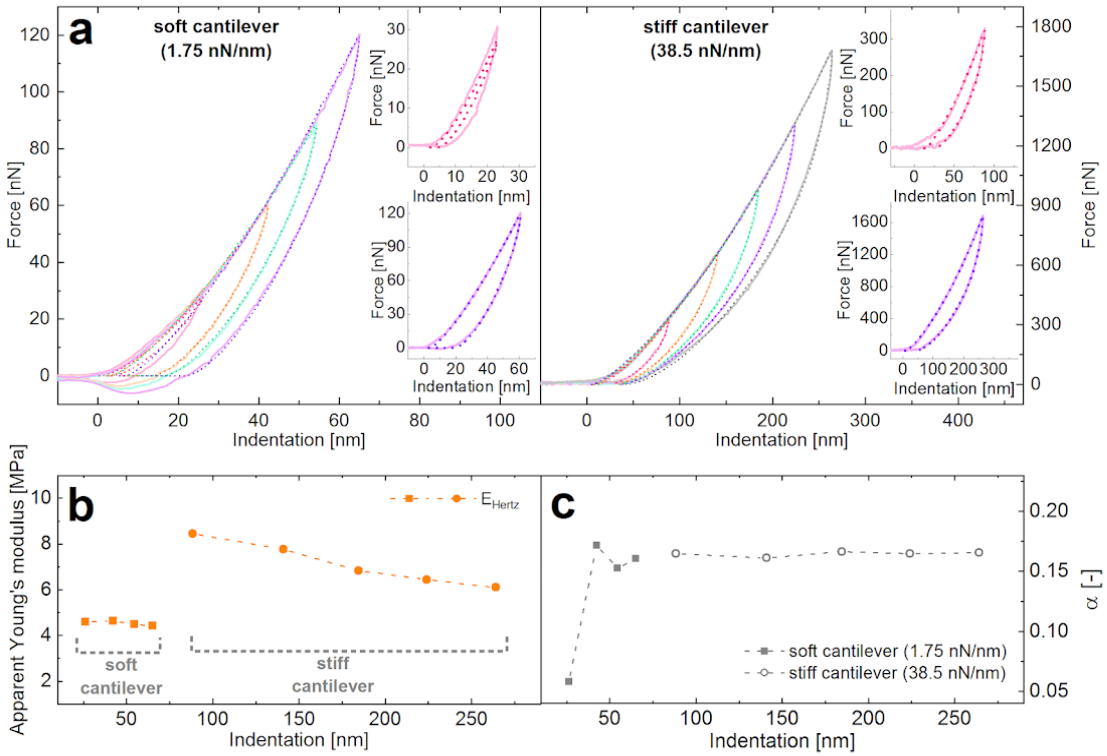

Figure 12: Effect of increasing indentation depth (strain) for two differently stiff cantilevers on the mechanical properties of hydrated coagulation film. (a) Force-distance curves (solid lines) performed at increasing peak forces on a hydrated coagulation film, overlaid with the PLR fit. The graph on the left shows curves obtained with a soft cantilever (1.75 nN/nm) and the graph on the right shows curves obtained using a stiff cantilever (38.5 nN/nm). Both cantilevers had a radius of 500 nm. **(b)** Elastic modulus and **(c)** power-law exponent *α* based on data shown in (a).

It is likely that surface roughness of the coagulation film as well as the small cantilever deflection caused inaccuracies at the smallest indentation depth. The small change of moduli upon cantilever change could be due to minor deviations in the deflection calibration of the cantilever. Strain stiffening was described for IF hydrogel networks[217,230,233,241] and is caused by an entropy loss associated with the stretching of filaments in between cross-links of the (hydrogel) network[217]. For strain hardening to occur the contact points must be sufficiently strong in order to stretch the filament strands as otherwise the links break and the strands relax[241,242]. The contact points (*i.e.*, overlapping and entangling IF tail domains) in hagfish IF films likely keep the films together, prevent dissolution, and are mainly responsible for the viscoelastic response. However, as only β-sheets are observed, it is possible that the increased rigidity of β-sheets compared to the more flexible α-helical coiled-coils[243,244] prevents stretching of the IF. The physical contact points of the 'tail-domain matrix' might be too weak to stretch the β-sheets. Furthermore, it is possible that indentation is less prone to induce strain stiffening as it exerts compression rather than stretching. Compression might require higher strains, *i.e.*, deeper indentations in order to achieve the same amount of stretching than shear or extension.

Implications of viscoelasticity for biomimetic fiber production

Coagulation films can be lifted up from the water interface of the $MgCl_2$ buffer and pulled into macroscopic fibers[116] (Figure 13a). The fibers reached lengths up to 12 cm, which is about five

times longer than reported previously[46] and in the range of natural hagfish fibers (10 - 20 cm[4,5]). The hydrated film formed a 'curtain' that is stretched at the air-water interface upon pulling (Figure 13b). The stretching caused an alignment of the otherwise randomly distributed IFs along the fiber axis (Figure 13c) similar to natural hagfish fibers (Figure 13d) as shown by WAXS measurements. The WAXS pattern of the reconstituted fibers (inter β-strand spacing of 0.46 nm; inter β-sheet spacing of 0.94 nm) strongly resembled the patterns of natural stretched hagfish fibers (inter β-strand spacing of 0.46 nm; inter β-sheet spacing of 0.94 nm) and also showed a silk-like alignment of the β-crystallites along the fiber axis as reported for IFs in natural hagfish fibers[10,40]. The alignment of the IF β-crystallites was assessed by the order parameter *S* (Figure 13e,f), which provides a measure of the long-range crystalline order of a material and is defined as the second Legendre polynomial $S = \frac{1}{2} < 3cos^2\phi - 1 >$, where ϕ is the angle between the axis of an individual molecule and the director of the crystal averaged over the complete ensemble[245]. The order parameter ranges from a perfect parallel orientation (S = 1) to a perfect perpendicular orientation (S = -0.5) and is S = 0 for unoriented material[246,247]. For both the reconstituted and the natural fibers order parameters of $S \approx 0.3$ in the low q-range (15 nm^{-1} < q < 17 nm^{-1}) and $S \approx 0.5$ in the high q-range (5.6 nm^{-1} < q < 7.6 nm^{-1}) were found, implying a nematic-like alignment of the β-strands (high q; from 15 to 17 nm^{-1}) and β-sheets (low q, from 5.6 to 7.6 nm^{-1}).

We suggest that a combination of viscoelasticity and the interaction of the film with the water interface are crucial for the production of such long biomimetic fibers with aligned β-sheets. The viscoelastic properties allow stretching and relaxation during stretching, which seems important to manufacture long fibers without removing the film from the surface at once. Furthermore, strong interactions probably due to hydrogen bonding between the film and the water interface are crucial to achieve a substantial stretching of the 'curtain' and thus create long fibers with aligned IFs. We found that tiny residues of surfactants in the buffer prevented the pulling of long fibers, underlining the importance of the interaction of the film with the water interface. Also, we found that in contrast to a previous work which found that a secondary drawing of the reconstituted fibers increased IF alignment[46], IF alignment was only minimally improved by 'double drawing' in this work. This shows that if the film strongly interacts with the buffer surface, it is sufficiently stretched and thus most IFs are aligned already during pulling from the interface.

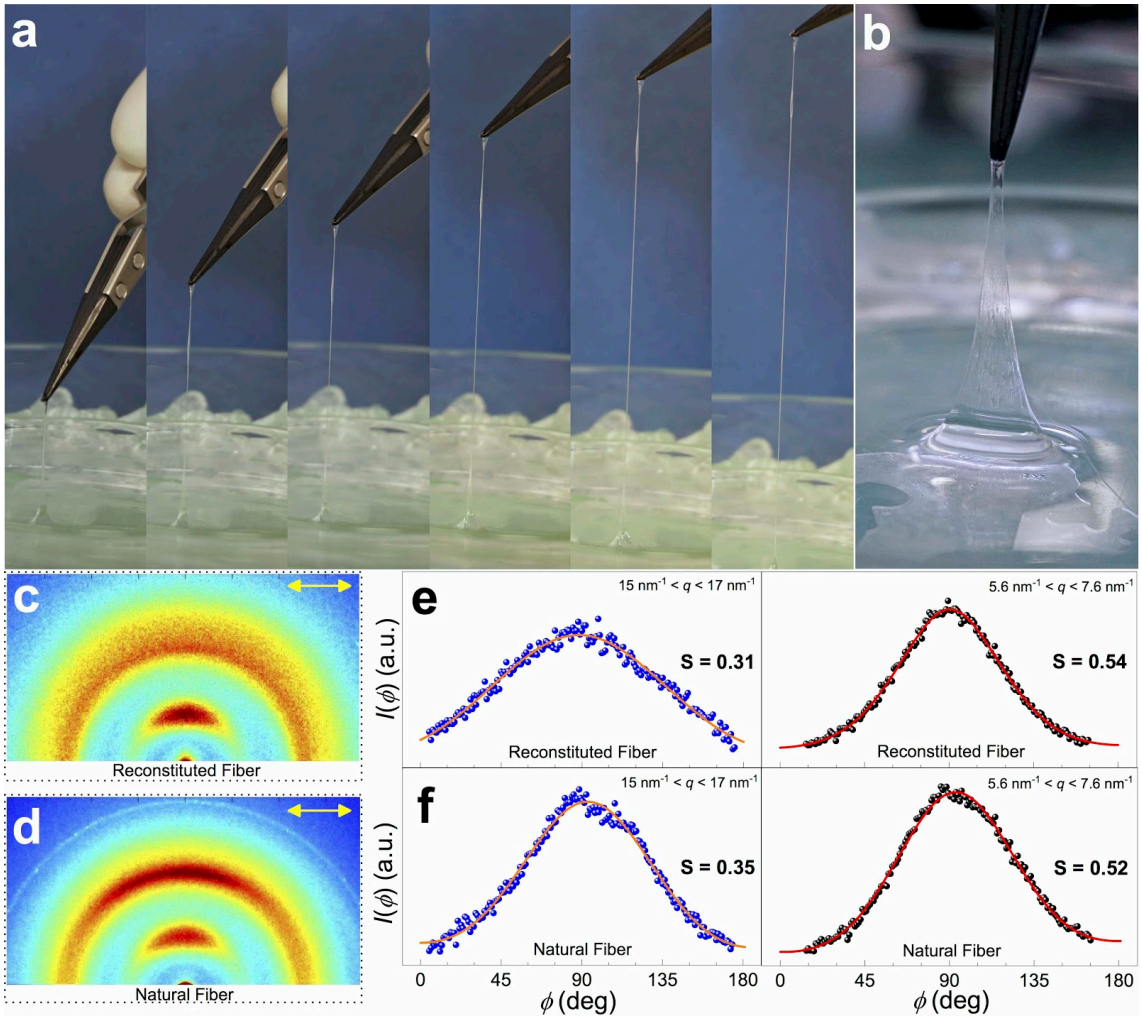

Figure 13: Implications of viscoelasticity on the production of biomimetic fibers. (a) Drawing a coagulation film from the $MgCl_2$ buffer surface into a long fiber. **(b)** Close-up of the coagulation film 'curtain' during fiber pulling. The curtain is stretched at the water interface, causing the randomly distributed IFs to align with the fiber axis. **(c,d)** 2D WAXS patterns of reconstituted and natural hagfish fibers showing the axial alignment of β-sheets. The yellow arrow denotes the fiber axis direction. **(e,f)** Azimuthal intensity distribution of the WAXS profiles and the derived order parameter *S*, showing showing the silk-like alignment of the IF β-sheets in both the reconstituted and the natural hagfish fibers.

Conclusion

Intermediate filament (IF) films from hagfish fiber protein were produced by drop-casting and coagulation on a $MgCl_2$ buffer. Drop-casting yielded self-supporting, smooth, and dense films rich in β-sheets (61%) whereas coagulation formed thin, porous films with a nano-rough surface and a lower β-sheet content (51%). Both films were birefringent due to the randomly distributed β-crystallites of the IFs. When immersed in water the films immediately swelled, resulting in a height increase of 55 and 73% in for the drop-cast and the coagulation film, respectively. Small and wide angle X-ray scattering revealed that the β-crystallites remained stable upon hydration and that swelling presumably happens in the C-terminal tail-domains of the IFs. These amorphous tails are considered to be radially grafted to the IFs in a bottle-brush configuration, which hydrates and increases in diameter and thus causes swelling. X-ray measurements further revealed a polyelectrolyte behavior of hagfish IFs as the average mesh-size of the IF network as well as the

inter β-sheet distance decreased upon increase of salt concentration due to charge screening, with Milli-Q showing a larger average mesh-size of 11.5 nm compared to simplified seawater (SSW) with an average mesh-size of 10.2 nm.

Using AFM nanoindentation it was observed that hydration in 1% SSW caused a roughly thousand-fold decrease in apparent elastic modulus from 10^9 to 10^6 Pa. The apparent elastic moduli for the drop-cast films (E_{dry} = 7.7 GPa, $E_{hydrated}$ = 6.1 MPa) were higher than those of the coagulation films (E_{dry} = 5.1 GPa, $E_{hydrated}$ = 3.9 MPa), which could be due to their higher β-sheet content and the presumably lower density of the porous coagulation films. The hydrated films displayed distinct viscoelastic behavior characteristic for soft-solid and tough hydrogels identified by repeatable and fully recoverable hysteresis loops in force-distance (F-D) curves, velocity dependence of the elastic modulus and indentation depth, as well as partly viscous stress relaxation. Fitting a power-law rheology (PLR) model directly to the (F-D) curves yielded a power-law relaxation exponent α of roughly < 0.2 for both films, suggesting 80% of elastic storage and 20% of viscous loss in force measurements, which was supported by stress relaxation measurements. Fitting a stretched exponential force decay model to stress relaxation measurements of hydrated IF films further revealed a lower stretched exponential factor β for coagulation films (β = 0.31) than for drop-cast films (β = 0.45), implying a broader distribution of relaxation times for the coagulation films. Also, coagulation films exhibited a higher relaxation time (τ = 0.75 s) than drop-cast films (τ = 0.4 s) at a given peak load of 90 nN, suggesting that the more heterogeneous and porous structure takes longer to relax. Increasing loads (strain) in stress relaxation resulted in higher relaxation times, suggesting that physical entanglements are more disrupted at larger strains and thus take longer to dissipate the stress. We propose that hagfish IF films possess β-sheet clusters from an α→β transformed central part of the IFs embedded in an amorphous matrix constituted by the physically entangled C-terminal tail-domains, which determines cohesion and viscoelasticity in hydrated films. Upon stress the matrix entanglements are disrupted whereby a larger stress causes more disruption and thus requires a longer time for the physical contact points to dissipate this stress. These physical contact points of the tail-domain matrix do not seem strong enough to stretch the IF β-sheets and thus induce strain hardening.

We further suggest that viscoelasticity and strong hydrogen bonding interactions of the coagulation film with the buffer surface are crucial for a successful fiber making process, in which a coagulation film is pulled from the buffer interface into a fiber. The combination of relaxing stresses within the film and strong hydrogen bonding of the film with the water interface allow for a continuous stretching yet prevent early removal of the film from the interface, thus creating long biomimetic fibers with high IF alignment similar to natural hagfish fibers. X-ray measurements revealed that this method yields reconstituted fibers that possess order parameters of $S \approx 0.3$ for the β-strands and $S \approx 0.5$ for the β-sheets, implying a nematic-like alignment as similarly observed in natural fibers. This study shows that functional IF materials that immediately swell and soften in water without dissolving can be produced from hagfish slime fibers, which could potentially be used in applications such as tissue implants, scaffolds for cell cultures, or contact lenses.

Chapter 8 - Concluding Remarks and Outlook

The aim of this thesis was to study hagfish slime in a vertically integrated 'from fish to fiber' approach. Our approach allowed us to preserve and thereupon to investigate the functionality of hagfish slime along the whole slime value chain - from exudate harvest in Norway to the reconstitution of biomimetic fibers in Switzerland.
In a first part, we studied the boundary conditions necessary for the stabilization of hagfish exudate for transport and subsequent slime regeneration in laboratory experiments. We highlighted the importance of rigorous cooling as well as the crucial effect of time and temperature on the degradation process and provided guidelines for the choice of appropriate stabilization methods. In a second part, the crucial role of ionic strength and seawater cations were investigated. Here, we showed that a functional defensive slime that entraps and retains water can only be formed in the presence of divalent seawater cations Ca^{2+} or Mg^{2+} at a high ionic strength. We found that calcium seems to have three distinct important roles in hagfish slime: mucin condensation within vesicles, mucin decondensation via Ca^{2+}-activated transporters in the vesicle membrane at high ionic strength, and mucin gelation in the deployed slime. In a third part, we then investigated the flow properties of hagfish slime and found that the flow behavior in shear and extension seem beneficial for the biological survival strategies of hagfish slime. Extensional flow - created through suction feeding of would-be predators - induces an increase in extensional viscosity of hagfish mucin. An increased viscosity reduces the water flow and thus could support gill clogging. Shear forces, in contrast lead to a collapse of the slime network, which is supported by mucin aggregation. This property was considered useful as hagfish are able to form a sliding knot with their body to release themselves from their slime if they get caught in their own weapon. Based on these results we proposed that hagfish slime flow properties, thickening in elongation and thinning in shear, may be beneficial for both, escape and defense. In a fourth and final part, intermediate filament (IF) protein was obtained from hagfish slime fibers and biomimetic films and fibers were produced. In this part we demonstrated that hagfish slime fibers constitute a valuable source of functional IF proteins that immediately swell, soften and become viscoelastic in water without dissolving. We suggested that viscoelasticity and strong hydrogen bonding interactions with the buffer surface are crucial for a successful fiber making process, in which a coagulation film is pulled from the buffer interface into a fiber. The combination of relaxing stresses within the film and strong hydrogen bonding of the film with the water interface allow for a continuous stretching yet prevent early removal of the film from the interface, thus creating long biomimetic fibers with high IF alignment similar to natural hagfish fibers.
We showed that we can successfully exploit slime value chain. Having functional samples at hand, *in vitro* studies were used to gain structure-property insights, which were then translated into the design of novel biomimetic materials. However, many open questions spanning many length scales accumulated over the course of this thesis and I want to share some of them with the reader.

On a microscale, these questions concern the absence of α-helices in hagfish intermediate filament (IF) films and the aggregation of mucin under shear. Hagfish IFs were used to produce films and fibers. Neither FTIR nor X-ray measurements unambiguously showed the presence of α-helices, as clearly reported by Fudge *et al*.[10] for slime fibers of the Pacific hagfish. As discussed in the respective chapter, it is possible that an α→β transition happens at the air water interface of the buffer or while drying at the formic acid-air interface. However, also when investigating dry

skeins - in the in absence of any strain history and before being transformed into films and fibers - no α-helices were observed. In the hydrated state, a small peak around 5.15 Å occurred in X-ray measurements, which could be linked to the presence of α-helices but the peak was small compared to the much larger β-sheet peak at 4.7 Å. These findings raise the question if slime fibers of the Atlantic hagfish (*M. glutinosa*) contain a much lower content of α-helices than the fibers of the Pacific hagfish (*E. stoutii*) or if they contain α-helices at all. The skeins of both species of hagfish are known to unravel differently - spontaneously for the Pacific hagfish and with the aid of attaching mucin strands for the Atlantic hagfish - and therefore this does not seem unlikely. However, as both fibers most certainly have IFs as the basic building block and IFs are known to have a central coiled-coil (α-helices) domain, these findings are currently difficult to explain. A second question on the microscale concerns the irreversible aggregation of hagfish mucin under shear, which is not a common feature of other long polymers. One hypothesis for this observation is that the mucins form extremely long polymer chains in the range of microns, which was also observed in AFM images. It is possible that such long molecules can also entangle and clump on a micron scale, similar to the slime fibers. Once collapsed, the mucin becomes insoluble and does not form viscoelastic solutions anymore. The only method we observed to re-solubilize freeze-dried mucin was in formic acid and then dropping it onto the $MgCl_2$ buffer bath as performed for the IFs. The mucins seemed to form an interfacial film on the buffer, which showed similar tacky features to the native mucin. However, whether the bulk viscosity can be reconstituted remains unknown.

On the mesoscale, the questions concerned the contribution of mucin to the global viscoelastic response of hagfish slime and why vesicle decondensation and skein unraveling seem intimately linked. Oscillatory shear measurements proved to be highly challenging for hagfish mucin at the natural concentration, as the torque response is weak, making a separation of sample response from surface tension effects of seawater difficult. This was not the case in extensional rheology measurements, which showed that depending on the flow type hagfish mucins exhibit viscoelasticity also at low concentrations. However, in recent measurements we found that dialyzed hagfish mucin indeed can form gelled systems that are measurable in oscillatory shear. The G'/G'' values were very similar to the moduli of whole hagfish slime. This raises the question whether the viscoelastic response of hagfish slime at small deformations is dominated by the fibres or by the mucin? It is also possible that the fiber network simply lowers the mucin overlap concentration and thus the slime reaches similar 'concentrations' as the higher concentrated mucin-only dialyzed sample. I think that the mechanic response of hagfish slime at small deformations may dominated by the mucin part and that the fibers start to contribute only at higher deformations. However, those large deformations are hard to achieve with a standard cup and bob geometries because the slime will just slip in the gap instead of being properly stretched as observed. A second question concerns the observation why vesicle decondensation and skein unraveling for the Atlantic hagfish are considered to be intimately linked? This does not seem to be the case for the Pacific hagfish, as reported in literature. We think that also for the Atlantic hagfish the skeins can unravel without the presence of vesicles. However, the major challenge we faced when examining this problem was that skeins cannot really be separated from vesicles. The majority of vesicles can be washed away, but some vesicles will always remain on the skein - unless it is harshly washed but then it loses its ability to spontaneously unravel. Based on many microscopy videos we think however, that also the skeins of the Atlantic hagfish can unravel spontaneously but they have less driving force that the ones from the Pacific hagfish, i.e. less stored strain energy that drives unraveling. This hypothesis is based on the observation that when skeins were exposed to Milli-Q they unraveled fast and on the spot, without mucin strands pulling them open. The deionized water caused the thread to presumably swell much more than seawater,

causing a spontaneous unraveling. However, finding conditions where only one of the two components open - skein or vesicles - was not achieved and thus the observation that their stability criteria are the same remains.
And eventually on a macroscale it would be interesting to know what flows exactly are the best for an optimum slime formation. Mixing is crucial in regenerating hagfish slime in the lab. Wrong mixing such as with a stirrer resulted in a failed slime network. Having a automatic gyroscopic mixer or alike, which has a defined and working mixing protocol could also strongly support slime science. Also, it would be interesting to test specific flows such as elongational for their ability to form slime, maybe even with aligned fibers.

It is to be hoped, that hagfish will not be exploited for their slime. A lively hagfish business established in South Korea, where hagfish are eaten as a delicacy. Before cooking, the hagfish are skinned and all the slime glands filled with exudate remain on that skin. These side-stream skins could potentially be used to recover hagfish slime and would constitute a rather sustainable source for hagfish slime. However, regardless all our endeavors some secrets will remain trapped in the fibrous network of hagfish slime. After all, who would easily give away a successful strategy that worked for the last 300 million years?

Bibliography

(1) Parker, T. J.; Haswell, W. A. *A Textbook of Zoology*; Macmillan, 1910.
(2) Zintzen, V.; Roberts, C. D.; Anderson, M. J.; Stewart, A. L.; Struthers, C. D.; Harvey, E. S. Hagfish Predatory Behaviour and Slime Defence Mechanism. *Sci. Rep.* **2011**, *1*, 131.
(3) Lim, J.; Fudge, D. S.; Levy, N.; Gosline, J. M. Hagfish Slime Ecomechanics: Testing the Gill-Clogging Hypothesis. *J. Exp. Biol.* **2006**, *209* (Pt 4), 702–710.
(4) Fernholm, B. Thread Cells from the Slime Glands of Hagfish (Myxinidae). *Acta Zool.* **1981**, *62* (3), 137–145.
(5) Downing, S. W.; Spitzer, R. H.; Salo, W. L.; Downing, J. S.; Saidel, L. J.; Koch, E. A. Threads in the Hagfish Slime Gland Thread Cells: Organization, Biochemical Features, and Length. *Science* **1981**, *212* (4492), 326–328.
(6) Herr, J. E.; Winegard, T. M.; O'Donnell, M. J.; Yancey, P. H.; Fudge, D. S. Stabilization and Swelling of Hagfish Slime Mucin Vesicles. *J. Exp. Biol.* **2010**, *213* (Pt 7), 1092–1099.
(7) Salo, W. L.; Downing, S. W.; Lidinsky, W. A.; Gallagher, W. H.; Spitzer, R. H.; Koch, E. A. Fractionation of Hagfish Slime Gland Secretions: Partial Characterization of the Mucous Vesicle Fraction. *Prep. Biochem.* **1983**, *13* (2), 103–135.
(8) Fudge, D. S.; Levy, N.; Chiu, S.; Gosline, J. M. Composition, Morphology and Mechanics of Hagfish Slime. *J. Exp. Biol.* **2005**, *208* (Pt 24), 4613–4625.
(9) Ewoldt, R. H.; Winegard, T. M.; Fudge, D. S. Non-Linear Viscoelasticity of Hagfish Slime. *Int. J. Non Linear Mech.* **2011**, *46* (4), 627–636.
(10) Fudge, D. S.; Gardner, K. H.; Forsyth, V. T.; Riekel, C.; Gosline, J. M. The Mechanical Properties of Hydrated Intermediate Filaments: Insights from Hagfish Slime Threads. *Biophys. J.* **2003**, *85* (3), 2015–2027.
(11) Martini, F. H. The Ecology of Hagfishes. In *The Biology of Hagfishes*; 1998; pp 57–77.
(12) Near, T. J. Conflict and Resolution between Phylogenies Inferred from Molecular and Phenotypic Data Sets for Hagfish, Lampreys, and Gnathostomes. *J. Exp. Zool. B Mol. Dev. Evol.* **2009**, *312B* (7), 749–761.
(13) McCauley, D. W.; Kuratani, S. Cyclostome Studies in the Context of Vertebrate Evolution. *Zoolog. Sci.* **2008**, *25* (10), 953–954.
(14) Edwards, S. L.; Goss, G. G. *Hagfish Biology*; CRC Press, 2015.
(15) Gorbman, A.; Kobayashi, H.; Honma, Y.; Matsuyama, M. The Hagfishery of Japan. *Fisheries* **1990**, *15* (4), 12–18.
(16) Bigelow, H. B.; Schroeder, W. *Fishes of the Gulf of Maine*; Washington, United States Government Printing Office, 1953.
(17) von Linné, C. *Systema Naturae per Regna Tria Naturae, Secundum Classes, Ordines, Genera, Species, Cum Characteribus, Differentiis, Synonimis Locis*; 1758.
(18) Leppi, T. J. Morphochemical Analysis of Mucous Cells in the Skin and Slime Glands of Hagfishes. *Histochemie* **1968**, *15* (1), 68–78.
(19) Schorno, S.; Gillis, T. E.; Fudge, D. S. Emptying and Refilling of Slime Glands in Atlantic () and Pacific () Hagfishes. *J. Exp. Biol.* **2018**, *221* (Pt 7).
(20) Spitzer, R. H.; Koch, E. A. Hagfish Skin and Slime Glands. In *The Biology of Hagfishes*; 1998; pp 109–132.
(21) Lane, E. B.; Whitear, M. Skein Cells in Lamprey Epidermis. *Can. J. Zool.* **1980**, *58* (3), 450–455.
(22) Fudge, D. S.; Schorno, S.; Ferraro, S. Physiology, Biomechanics, and Biomimetics of Hagfish Slime. *Annu. Rev. Biochem.* **2015**, *84*, 947–967.
(23) Winegard, T. M.; Fudge, D. S. Deployment of Hagfish Slime Thread Skeins Requires the Transmission of Mixing Forces via Mucin Strands. *J. Exp. Biol.* **2010**, *213* (Pt 8), 1235–1240.
(24) Herrmann, H.; Bär, H.; Kreplak, L.; Strelkov, S. V.; Aebi, U. Intermediate Filaments: From Cell Architecture to Nanomechanics. *Nat. Rev. Mol. Cell Biol.* **2007**, *8* (7), 562–573.
(25) Fuchs, E.; Cleveland, D. W. A Structural Scaffolding of Intermediate Filaments in Health and Disease. *Science* **1998**, *279* (5350), 514–519.
(26) Magin, T. M.; Hesse, M.; Schröder, R. Novel Insights into Intermediate-Filament Function from Studies of Transgenic and Knockout Mice. *Protoplasma* **2000**, *211* (3-4), 140–150.
(27) Qin, Z.; Buehler, M. J.; Kreplak, L. A Multi-Scale Approach to Understand the Mechanobiology of Intermediate Filaments. *J. Biomech.* **2010**, *43* (1), 15–22.

(28) Ramms, L.; Fabris, G.; Windoffer, R.; Schwarz, N.; Springer, R.; Zhou, C.; Lazar, J.; Stiefel, S.; Hersch, N.; Schnakenberg, U.; et al. Keratins as the Main Component for the Mechanical Integrity of Keratinocytes. *Proc. Natl. Acad. Sci. U. S. A.* **2013**, *110* (46), 18513–18518.
(29) Seltmann, K.; Fritsch, A. W.; Käs, J. A.; Magin, T. M. Keratins Significantly Contribute to Cell Stiffness and Impact Invasive Behavior. *Proc. Natl. Acad. Sci. U. S. A.* **2013**, *110* (46), 18507–18512.
(30) Strelkov, S. V.; Herrmann, H.; Aebi, U. Molecular Architecture of Intermediate Filaments. *Bioessays* **2003**, *25* (3), 243–251.
(31) Block, J.; Schroeder, V.; Pawelzyk, P.; Willenbacher, N.; Köster, S. Physical Properties of Cytoplasmic Intermediate Filaments. *Biochimica et Biophysica Acta (BBA) - Molecular Cell Research* **2015**, *1853* (11), 3053–3064.
(32) Kreplak, L.; Fudge, D. Biomechanical Properties of Intermediate Filaments: From Tissues to Single Filaments and Back. *Bioessays* **2007**, *29* (1), 26–35.
(33) Köster, S.; Weitz, D. A.; Goldman, R. D.; Aebi, U.; Herrmann, H. Intermediate Filament Mechanics in Vitro and in the Cell: From Coiled Coils to Filaments, Fibers and Networks. *Curr. Opin. Cell Biol.* **2015**, *32*, 82–91.
(34) Mücke, N.; Kreplak, L.; Kirmse, R.; Wedig, T.; Herrmann, H.; Aebi, U.; Langowski, J. Assessing the Flexibility of Intermediate Filaments by Atomic Force Microscopy. *J. Mol. Biol.* **2004**, *335* (5), 1241–1250.
(35) Kreplak, L.; Herrmann, H.; Aebi, U. Tensile Properties of Single Desmin Intermediate Filaments. *Biophys. J.* **2008**, *94* (7), 2790–2799.
(36) Guzmán, C.; Jeney, S.; Kreplak, L.; Kasas, S.; Kulik, A. J.; Aebi, U.; Forró, L. Exploring the Mechanical Properties of Single Vimentin Intermediate Filaments by Atomic Force Microscopy. *J. Mol. Biol.* **2006**, *360* (3), 623–630.
(37) Nöding, B.; Köster, S. Intermediate Filaments in Small Configuration Spaces. *Phys. Rev. Lett.* **2012**, *108* (8), 088101.
(38) Kreplak, L.; Bär, H.; Leterrier, J. F.; Herrmann, H.; Aebi, U. Exploring the Mechanical Behavior of Single Intermediate Filaments. *J. Mol. Biol.* **2005**, *354* (3), 569–577.
(39) Block, J.; Witt, H.; Candelli, A.; Peterman, E. J. G.; Wuite, G. J. L.; Janshoff, A.; Köster, S. Nonlinear Loading-Rate-Dependent Force Response of Individual Vimentin Intermediate Filaments to Applied Strain. *Phys. Rev. Lett.* **2017**, *118* (4), 048101.
(40) Downing, S. W.; Spitzer, R. H.; Koch, E. A.; Salo, W. L. The Hagfish Slime Gland Thread Cell. I. A Unique Cellular System for the Study of Intermediate Filaments and Intermediate Filament-Microtubule Interactions. *J. Cell Biol.* **1984**, *98* (2), 653–669.
(41) Spitzer, R. H.; Koch, E. A.; Downing, S. W. Maturation of Hagfish Gland Thread Cells: Composition and Characterization of Intermediate Filament Polypeptides. *Cell Motil. Cytoskeleton* **1988**, *11* (1), 31–45.
(42) Koch, E. A.; Spitzer, R. H.; Pithawalla, R. B.; Castillos, F. A., 3rd; Parry, D. A. Hagfish Biopolymer: A Type I/type II Homologue of Epidermal Keratin Intermediate Filaments. *Int. J. Biol. Macromol.* **1995**, *17* (5), 283–292.
(43) Spitzer, R. H.; Downing, S. W.; Koch, E. A.; Salo, W. L.; Saidel, L. J. Hagfish Slime Gland Thread Cells. II. Isolation and Characterization of Intermediate Filament Components Associated with the Thread. *J. Cell Biol.* **1984**, *98* (2), 670–677.
(44) Koch, E. A.; Spitzer, R. H.; Pithawalla, R. B.; Parry, D. A. An Unusual Intermediate Filament Subunit from the Cytoskeletal Biopolymer Released Extracellularly into Seawater by the Primitive Hagfish (Eptatretus Stouti). *J. Cell Sci.* **1994**, *107 (Pt 11)*, 3133–3144.
(45) Schaffeld, M.; Schultess, J. Genes Coding for Intermediate Filament Proteins Closely Related to the Hagfish “thread Keratins (TK)” α and γ Also Exist in Lamprey, Teleosts and Amphibians. *Exp. Cell Res.* **2006**, *312* (9), 1447–1462.
(46) Fu, J.; Guerette, P. A.; Pavesi, A.; Horbelt, N.; Lim, C. T.; Harrington, M. J.; Miserez, A. Artificial Hagfish Protein Fibers with Ultra-High and Tunable Stiffness. *Nanoscale* **2017**, *9* (35), 12908–12915.
(47) Fu, J.; Guerette, P. A.; Miserez, A. Self-Assembly of Recombinant Hagfish Thread Keratins Amenable to a Strain-Induced α-Helix to β-Sheet Transition. *Biomacromolecules* **2015**, *16* (8), 2327–2339.
(48) Downing, S. W.; Salo, W. L.; Spitzer, R. H.; Koch, E. A. The Hagfish Slime Gland: A Model System for Studying the Biology of Mucus. *Science* **1981**, *214* (4525), 1143–1145.
(49) Winegard, T.; Herr, J.; Mena, C.; Lee, B.; Dinov, I.; Bird, D.; Bernards, M., Jr; Hobel, S.; Van Valkenburgh, B.; Toga, A.; et al. Coiling and Maturation of a High-Performance Fibre in Hagfish Slime Gland Thread Cells. *Nat. Commun.* **2014**, *5*, 3534.
(50) Terakado, K.; Ogawa, M.; Hashimoto, Y.; Matsuzaki, H. Ultrastructure of the Thread Cells in the Slime Gland of Japanese Hagfishes, Paramyxine Atami and Eptatretus Burgeri. *Cell Tissue Res.* **1975**,

159 (3), 311–323.
(51) Helfand, B. T.; Loomis, P.; Yoon, M.; Goldman, R. D. Rapid Transport of Neural Intermediate Filament Protein. *J. Cell Sci.* **2003**, *116* (Pt 11), 2345–2359.
(52) Uchida, A.; Alami, N. H.; Brown, A. Tight Functional Coupling of Kinesin-1A and Dynein Motors in the Bidirectional Transport of Neurofilaments. *Mol. Biol. Cell* **2009**, *20* (23), 4997–5006.
(53) Bernards, M. A., Jr; Oke, I.; Heyland, A.; Fudge, D. S. Spontaneous Unraveling of Hagfish Slime Thread Skeins Is Mediated by a Seawater-Soluble Protein Adhesive. *J. Exp. Biol.* **2014**, *217* (Pt 8), 1263–1268.
(54) Greenberg, D. A.; Fudge, D. S. Regulation of Hard α-Keratin Mechanics via Control of Intermediate Filament Hydration: Matrix Squeeze Revisited. *Proc. Biol. Sci.* **2013**, *280* (1750), 20122158.
(55) Fudge, D. S.; Gosline, J. M. Molecular Design of the Alpha-Keratin Composite: Insights from a Matrix-Free Model, Hagfish Slime Threads. *Proc. Biol. Sci.* **2004**, *271* (1536), 291–299.
(56) Fudge, D. S.; Hillis, S.; Levy, N.; Gosline, J. M. Hagfish Slime Threads as a Biomimetic Model for High Performance Protein Fibres. *Bioinspir. Biomim.* **2010**, *5* (3), 035002.
(57) Gosline, J. M.; Guerette, P. A.; Ortlepp, C. S.; Savage, K. N. The Mechanical Design of Spider Silks: From Fibroin Sequence to Mechanical Function. *J. Exp. Biol.* **1999**, *202* (Pt 23), 3295–3303.
(58) Luchtel, D. L.; Martin, A. W.; Deyrup-Olsen, I. Ultrastructure and Permeability Characteristics of the Membranes of Mucous Granules of the Hagfish. *Tissue Cell* **1991**, *23* (6), 939–948.
(59) Deyrup-Olsen, I.; Luchtel, D. L. Secretion of Mucous Granules and Other Membrane-Bound Structures: A Look beyond Exocytosis. *Int. Rev. Cytol.* **1998**, *183*, 95–141.
(60) Herr, J. E.; Clifford, A. M.; Goss, G. G.; Fudge, D. S. Defensive Slime Formation in Pacific Hagfish Requires Ca2 - and Aquaporin-Mediated Swelling of Released Mucin Vesicles. *J. Exp. Biol.* **2014**, *217* (13), 2288–2296.
(61) Bansil, R.; Stanley, E.; Lamont, J. T. Mucin Biophysics. *Annu. Rev. Physiol.* **1995**, *57* (1), 635–657.
(62) Bansil, R.; Turner, B. S. Mucin Structure, Aggregation, Physiological Functions and Biomedical Applications. *Curr. Opin. Colloid Interface Sci.* **2006**, *11* (2-3), 164–170.
(63) Moniaux, N.; Escande, F.; Porchet, N.; Aubert, J. P.; Batra, S. K. Structural Organization and Classification of the Human Mucin Genes. *Front. Biosci.* **2001**, *6*, D1192–D1206.
(64) Coles, J. M.; Chang, D. P.; Zauscher, S. Molecular Mechanisms of Aqueous Boundary Lubrication by Mucinous Glycoproteins. *Curr. Opin. Colloid Interface Sci.* **2010**, *15* (6), 406–416.
(65) Bansil, R.; Celli, J. P.; Hardcastle, J. M.; Turner, B. S. The Influence of Mucus Microstructure and Rheology in Helicobacter Pylori Infection. *Front. Immunol.* **2013**, *4*, 310.
(66) Bell, S. L.; Xu, G.; Khatri, I. A.; Wang, R.; Rahman, S.; Forstner, J. F. N-Linked Oligosaccharides Play a Role in Disulphide-Dependent Dimerization of Intestinal Mucin Muc2. *Biochem. J* **2003**, *373* (3), 893–900.
(67) Sheehan, J. K.; Oates, K.; Carlstedt, I. Electron Microscopy of Cervical, Gastric and Bronchial Mucus Glycoproteins. *Biochem. J* **1986**, *239* (1), 147–153.
(68) Lai, S. K.; Wang, Y.-Y.; Wirtz, D.; Hanes, J. Micro- and Macrorheology of Mucus. *Adv. Drug Deliv. Rev.* **2009**, *61* (2), 86–100.
(69) Sheehan, J. K.; Kirkham, S.; Howard, M.; Woodman, P.; Kutay, S.; Brazeau, C.; Buckley, J.; Thornton, D. J. Identification of Molecular Intermediates in the Assembly Pathway of the MUC5AC Mucin. *J. Biol. Chem.* **2004**, *279* (15), 15698–15705.
(70) Znamenskaya, Y.; Sotres, J.; Engblom, J.; Arnebrant, T.; Kocherbitov, V. Effect of Hydration on Structural and Thermodynamic Properties of Pig Gastric and Bovine Submaxillary Gland Mucins. *J. Phys. Chem. B* **2012**, *116* (16), 5047–5055.
(71) Hong, Z.; Chasan, B.; Bansil, R.; Turner, B. S.; Bhaskar, K. R.; Afdhal, N. H. Atomic Force Microscopy Reveals Aggregation of Gastric Mucin at Low pH. *Biomacromolecules* **2005**, *6* (6), 3458–3466.
(72) Girod, S.; Zahm, J. M.; Plotkowski, C.; Beck, G.; Puchelle, E. Role of the Physiochemical Properties of Mucus in the Protection of the Respiratory Epithelium. *Eur. Respir. J.* **1992**, *5* (4), 477–487.
(73) Randell, S. H.; Boucher, R. C.; University of North Carolina Virtual Lung Group. Effective Mucus Clearance Is Essential for Respiratory Health. *Am. J. Respir. Cell Mol. Biol.* **2006**, *35* (1), 20–28.
(74) Dulfano, M. J.; Adler, K.; Philippoff, W. Sputum Viscoelasticity in Chronic Bronchitis. *Am. Rev. Respir. Dis.* **1971**, *104* (1), 88–98.
(75) Dawson, M.; Wirtz, D.; Hanes, J. Enhanced Viscoelasticity of Human Cystic Fibrotic Sputum Correlates with Increasing Microheterogeneity in Particle Transport. *J. Biol. Chem.* **2003**, *278* (50), 50393–50401.
(76) Slomiany, B. L.; Slomiany, A. Role of Mucus in Gastric Mucosal Protection. *J. Physiol. Pharmacol.* **1991**, *42* (2), 147–161.
(77) Sharpe, W. N. *Springer Handbook of Experimental Solid Mechanics*; Springer Science & Business

Media, 2008.
(78) Morrison, F. A. *Understanding Rheology*; Oxford University Press, USA, 2001.
(79) Malkin, A. Y.; Ya. Malkin, A.; Arinstein, A.; Kulichikhin, V. G. Polymer Extension Flows and Instabilities. *Prog. Polym. Sci.* **2014**, *39* (5), 959–978.
(80) Springer, T. A. Von Willebrand Factor, Jedi Knight of the Bloodstream. *Blood* **2014**, *124* (9), 1412–1425.
(81) Rammensee, S.; Slotta, U.; Scheibel, T.; Bausch, A. R. Assembly Mechanism of Recombinant Spider Silk Proteins. *Proc. Natl. Acad. Sci. U. S. A.* **2008**, *105* (18), 6590–6595.
(82) Barnes, H. A. *A Handbook of Elementary Rheology*; University of Wales, Institute of Non-Newtonian Fluid Mechanics, 2000.
(83) Macosko, C. W. *Rheology: Principles, Measurements, and Applications*; Wiley, 1994.
(84) Haward, S. J.; Oliveira, M. S. N.; Alves, M. A.; McKinley, G. H. Optimized Cross-Slot Flow Geometry for Microfluidic Extensional Rheometry. *Phys. Rev. Lett.* **2012**, *109* (12), 128301.
(85) Meissner, J. Development of a Universal Extensional Rheometer for the Uniaxial Extension of Polymer Melts. *Transactions of the Society of Rheology* **1972**, *16* (3), 405–420.
(86) Taylor, G. I. The Viscosity of a Fluid Containing Small Drops of Another Fluid. *Proceedings of the Royal Society A: Mathematical, Physical and Engineering Sciences* **1932**, *138* (834), 41–48.
(87) Winter, H. H.; Macosko, C. W.; Bennett, K. E. Orthogonal Stagnation Flow, a Framework for Steady Extensional Flow Experiments. *Rheol. Acta* **1979**, *18* (3), 323–334.
(88) Tirtaatmadja, V.; Sridhar, T. A Filament Stretching Device for Measurement of Extensional Viscosity. *J. Rheol.* **1993**, *37* (6), 1081–1102.
(89) Bazilevsky, A. V.; Entov, V. M.; Rozhkov, A. N. Liquid Filament Microrheometer and Some of Its Applications. In *Third European Rheology Conference and Golden Jubilee Meeting of the British Society of Rheology*; 1990; pp 41–43.
(90) McKinley, G. H.; Tripathi, A. How to Extract the Newtonian Viscosity from Capillary Breakup Measurements in a Filament Rheometer. *J. Rheol.* **2000**, *44* (3), 653–670.
(91) Kolte, M. I.; Szabo, P. Capillary Thinning of Polymeric Filaments. *J. Rheol.* **1999**, *43* (3), 609–625.
(92) Anna, S. L.; McKinley, G. H. Elasto-Capillary Thinning and Breakup of Model Elastic Liquids. *J. Rheol.* **2001**, *45* (1), 115–138.
(93) Haward, S. J.; Sharma, V.; Odell, J. A. Extensional Opto-Rheometry with Biofluids and Ultra-Dilute Polymer Solutions. *Soft Matter* **2011**, *7* (21), 9908.
(94) Rodd, L. E.; Scott, T. P.; Cooper-White, J. J.; McKinley, G. H. Capillary Break-up Rheometry of Low-Viscosity Elastic Fluids. *Appl. Rheol.* **2005**, *15* (12), 12–27.
(95) Miller, E.; Clasen, C.; Rothstein, J. P. The Effect of Step-Stretch Parameters on Capillary Breakup Extensional Rheology (CaBER) Measurements. *Rheol. Acta* **2009**, *48* (6), 625–639.
(96) Ardekani, A. M.; Sharma, V.; McKINLEY, G. H. Dynamics of Bead Formation, Filament Thinning and Breakup in Weakly Viscoelastic Jets. *J. Fluid Mech.* **2010**, *665*, 46–56.
(97) Fischer-Cripps, A. C. *Nanoindentation*; Springer New York, 2011.
(98) Efremov, Y. M.; Wang, W.-H.; Hardy, S. D.; Geahlen, R. L.; Raman, A. Measuring Nanoscale Viscoelastic Parameters of Cells Directly from AFM Force-Displacement Curves. *Sci. Rep.* **2017**, *7* (1), 1541.
(99) Hertz, H. On the Contact of Elastic Solids. *J. Reine Angew. Math.* **1881**, *92*, 156–171.
(100) Rebelo, L. M.; de Sousa, J. S.; Mendes Filho, J.; Radmacher, M. Comparison of the Viscoelastic Properties of Cells from Different Kidney Cancer Phenotypes Measured with Atomic Force Microscopy. *Nanotechnology* **2013**, *24* (5), 055102.
(101) Nawaz, S.; Sánchez, P.; Bodensiek, K.; Li, S.; Simons, M.; Schaap, I. A. T. Cell Visco-Elasticity Measured with AFM and Optical Trapping at Sub-Micrometer Deformations. *PLoS One* **2012**, *7* (9), e45297.
(102) Moreno-Flores, S.; Benitez, R.; Vivanco, M. dM; Toca-Herrera, J. L. Stress Relaxation and Creep on Living Cells with the Atomic Force Microscope: A Means to Calculate Elastic Moduli and Viscosities of Cell Components. *Nanotechnology* **2010**, *21* (44), 445101.
(103) Alcaraz, J.; Buscemi, L.; Grabulosa, M.; Trepat, X.; Fabry, B.; Farré, R.; Navajas, D. Microrheology of Human Lung Epithelial Cells Measured by Atomic Force Microscopy. *Biophys. J.* **2003**, *84* (3), 2071–2079.
(104) Huang, G.; Wang, B.; Lu, H. Measurements of Viscoelastic Functions of Polymers in the Frequency-Domain Using Nanoindentation. *Mech. Time Depend. Mater.* **2004**, *8* (4), 345–364.
(105) Lucas, B. N.; Oliver, W. C.; Swindeman, J. E. The Dynamics of Frequency-Specific, Depth-Sensing Indentation Testing. *MRS Proceedings* **1998**, *522*.
(106) Darling, E. M.; Zauscher, S.; Guilak, F. Viscoelastic Properties of Zonal Articular Chondrocytes Measured by Atomic Force Microscopy. *Osteoarthritis Cartilage* **2006**, *14* (6), 571–579.

(107) Moeendarbary, E.; Valon, L.; Fritzsche, M.; Harris, A. R.; Moulding, D. A.; Thrasher, A. J.; Stride, E.; Mahadevan, L.; Charras, G. T. The Cytoplasm of Living Cells Behaves as a Poroelastic Material. *Nat. Mater.* **2013**, *12* (3), 253–261.
(108) Lu, H.; Wang, B.; Ma, J.; Huang, G.; Viswanathan, H. Measurement of Creep Compliance of Solid Polymers by Nanoindentation. *Mech. Time Depend. Mater.* **2003**, *7* (3/4), 189–207.
(109) Mathur, A. B.; Collinsworth, A. M.; Reichert, W. M.; Kraus, W. E.; Truskey, G. A. Endothelial, Cardiac Muscle and Skeletal Muscle Exhibit Different Viscous and Elastic Properties as Determined by Atomic Force Microscopy. *J. Biomech.* **2001**, *34* (12), 1545–1553.
(110) Lee, E. H.; Radok, J. R. M. The Contact Problem for Viscoelastic Bodies. *J. Appl. Mech.* **1960**, *27* (3), 438.
(111) Ting, T. C. T. The Contact Stresses Between a Rigid Indenter and a Viscoelastic Half-Space. *J. Appl. Mech.* **1966**, *33* (4), 845.
(112) Kester, D. R.; Duedall, I. W.; Connors, D. N.; Pytkowicz, R. M. Preparation Of Artificial Seawater. *Limnol. Oceanogr.* **1967**, *12* (1), 176–179.
(113) Bligh, E. G.; Dyer, W. J. A Rapid Method of Total Lipid Extraction and Purification. *Can. J. Biochem. Physiol.* **1959**, *37* (8), 911–917.
(114) Olsson, P.; Holmbäck, J.; Herslöf, B. Separation of Lipid Classes by HPLC on a Cyanopropyl Column. *Lipids* **2012**, *47* (1), 93–99.
(115) Haward, S. J.; McKinley, G. H. Stagnation Point Flow of Wormlike Micellar Solutions in a Microfluidic Cross-Slot Device: Effects of Surfactant Concentration and Ionic Environment. *Physical Review E* **2012**, *85* (3).
(116) Negishi, A.; Armstrong, C. L.; Kreplak, L.; Rheinstadter, M. C.; Lim, L.-T.; Gillis, T. E.; Fudge, D. S. The Production of Fibers and Films from Solubilized Hagfish Slime Thread Proteins. *Biomacromolecules* **2012**, *13* (11), 3475–3482.
(117) Hu, X.; Kaplan, D.; Cebe, P. Determining Beta-Sheet Crystallinity in Fibrous Proteins by Thermal Analysis and Infrared Spectroscopy. *Macromolecules* **2006**, *39* (18), 6161–6170.
(118) Zou, Y.; Li, Y.; Hao, W.; Hu, X.; Ma, G. Parallel β-Sheet Fibril and Antiparallel β-Sheet Oligomer: New Insights into Amyloid Formation of Hen Egg White Lysozyme under Heat and Acidic Condition from FTIR Spectroscopy. *J. Phys. Chem. B* **2013**, *117* (15), 4003–4013.
(119) Dimitriadis, E. K.; Horkay, F.; Maresca, J.; Kachar, B.; Chadwick, R. S. Determination of Elastic Moduli of Thin Layers of Soft Material Using the Atomic Force Microscope. *Biophys. J.* **2002**, *82* (5), 2798–2810.
(120) Niu, T.; Cao, G. Finite Size Effect Does Not Depend on the Loading History in Soft Matter Indentation. *J. Phys. D Appl. Phys.* **2014**, *47* (38), 385303.
(121) Bagley, R. L. Power Law and Fractional Calculus Model of Viscoelasticity. *AIAA Journal* **1989**, *27* (10), 1412–1417.
(122) Johnston, D. C. Stretched Exponential Relaxation Arising from a Continuous Sum of Exponential Decays. *Phys. Rev. B: Condens. Matter Mater. Phys.* **2006**, *74* (18).
(123) Mauro, J. C.; Mauro, Y. Z. On the Prony Series Representation of Stretched Exponential Relaxation. *Physica A: Statistical Mechanics and its Applications* **2018**, *506*, 75–87.
(124) Berry, G. C.; Plazek, D. J. On the Use of Stretched-Exponential Functions for Both Linear Viscoelastic Creep and Stress Relaxation. *Rheol. Acta* **1997**, *36* (3), 320–329.
(125) Zanzotto, L.; Stastna, J. Dynamic Master Curves from the Stretched Exponential Relaxation Modulus. *J. Polym. Sci. B Polym. Phys.* **1997**, *35* (8), 1225–1232.
(126) Uzüm, C.; Hellwig, J.; Madaboosi, N.; Volodkin, D.; von Klitzing, R. Growth Behaviour and Mechanical Properties of PLL/HA Multilayer Films Studied by AFM. *Beilstein J. Nanotechnol.* **2012**, *3*, 778–788.
(127) Böcker, L.; Rühs, P. A.; Böni, L.; Fischer, P.; Kuster, S. Fiber-Enforced Hydrogels: Hagfish Slime Stabilized with Biopolymers Including κ-Carrageenan. *ACS Biomaterials Science & Engineering* **2016**, *2* (1), 90–95.
(128) Böni, L.; Fischer, P.; Böcker, L.; Kuster, S.; Rühs, P. A. Hagfish Slime and Mucin Flow Properties and Their Implications for Defense. *Sci. Rep.* **2016**, *6*, 30371.
(129) Koch, E. A.; Spitzer, R. H.; Pithawalla, R. B.; Downing, S. W. Keratin-like Components of Gland Thread Cells Modulate the Properties of Mucus from Hagfish (Eptatretus Stoutii). *Cell Tissue Res.* **1991**, *264* (1), 79–86.
(130) Ewoldt, R. H.; Johnston, M. T.; Caretta, L. M. Experimental Challenges of Shear Rheology: How to Avoid Bad Data. In *Biological and Medical Physics, Biomedical Engineering*; 2014; pp 207–241.
(131) Böni, L.; Rühs, P. A.; Windhab, E. J.; Fischer, P.; Kuster, S. Gelation of Soy Milk with Hagfish Exudate Creates a Flocculated and Fibrous Emulsion- and Particle Gel. *PLoS One* **2016**, *11* (1), e0147022.

(132) Hardy, G. J.; Nayak, R.; Zauscher, S. Model Cell Membranes: Techniques to Form Complex Biomimetic Supported Lipid Bilayers via Vesicle Fusion. *Curr. Opin. Colloid Interface Sci.* **2013**, *18* (5), 448–458.
(133) Seantier, B.; Breffa, C.; Félix, O.; Decher, G. Dissipation-Enhanced Quartz Crystal Microbalance Studies on the Experimental Parameters Controlling the Formation of Supported Lipid Bilayers. *J. Phys. Chem. B* **2005**, *109* (46), 21755–21765.
(134) Garcia-Manyes, S.; Oncins, G.; Sanz, F. Effect of Temperature on the Nanomechanics of Lipid Bilayers Studied by Force Spectroscopy. *Biophys. J.* **2005**, *89* (6), 4261–4274.
(135) Gong, D. H.; Turner, B.; Bhaskar, K. R.; Lamont, J. T. Lipid Binding to Gastric Mucin: Protective Effect against Oxygen Radicals. *Am. J. Physiol.* **1990**, *259* (4 Pt 1), G681–G686.
(136) Zhang, J.; Lv, Y.; Wang, B.; Zhao, S.; Tan, M.; Lv, G.; Ma, X. Influence of Microemulsion-Mucin Interaction on the Fate of Microemulsions Diffusing through Pig Gastric Mucin Solutions. *Mol. Pharm.* **2015**, *12* (3), 695–705.
(137) Rogunova, M.; Blackwell, J.; Jamieson, A.; Pasumarthy, M.; Gerken, T. Effect of Lipids on the Structure and Rheology of Gels Formed by Canine Submaxillary Mucin. *Biorheology* **1997**, *34* (4-5), 295–308.
(138) Verdugo, P. Supramolecular Dynamics of Mucus. *Cold Spring Harb. Perspect. Med.* **2012**, *2* (11).
(139) Khare, A. R.; Peppas, N. A. Swelling/deswelling of Anionic Copolymer Gels. *Biomaterials* **1995**, *16* (7), 559–567.
(140) Vasheghani-Farahani, E.; Vera, J. H.; Cooper, D. G.; Weber, M. E. Swelling of Ionic Gels in Electrolyte Solutions. *Ind. Eng. Chem. Res.* **1990**, *29* (4), 554–560.
(141) Wells, R. M.; Forster, M. E.; Davison, W.; Taylor, H. H.; Davie, P. S.; Satchell, G. H. Blood Oxygen Transport in the Free-Swimming Hagfish, Eptatretus Cirrhatus. *J. Exp. Biol.* **1986**, *123*, 43–53.
(142) Perez-Vilar, J.; Olsen, J. C.; Chua, M.; Boucher, R. C. pH-Dependent Intraluminal Organization of Mucin Granules in Live Human Mucous/goblet Cells. *J. Biol. Chem.* **2005**, *280* (17), 16868–16881.
(143) Kesimer, M.; Makhov, A. M.; Griffith, J. D.; Verdugo, P.; Sheehan, J. K. Unpacking a Gel-Forming Mucin: A View of MUC5B Organization after Granular Release. *Am. J. Physiol. Lung Cell. Mol. Physiol.* **2010**, *298* (1), L15–L22.
(144) Ambort, D.; Johansson, M. E. V.; Gustafsson, J. K.; Nilsson, H. E.; Ermund, A.; Johansson, B. R.; Koeck, P. J. B.; Hebert, H.; Hansson, G. C. Calcium and pH-Dependent Packing and Release of the Gel-Forming MUC2 Mucin. *Proc. Natl. Acad. Sci. U. S. A.* **2012**, *109* (15), 5645–5650.
(145) Flory, P. J. *Principles of Polymer Chemistry*; Cornell University Press, 1953.
(146) Espinosa, M.; Noé, G.; Troncoso, C.; Ho, S. B.; Villalón, M. Acidic pH and Increasing [Ca(2+)] Reduce the Swelling of Mucins in Primary Cultures of Human Cervical Cells. *Hum. Reprod.* **2002**, *17* (8), 1964–1972.
(147) Perez-Vilar, J. Mucin Granule Intraluminal Organization. *Am. J. Respir. Cell Mol. Biol.* **2007**, *36* (2), 183–190.
(148) Rodriguez, J.; Gupta, N.; Smith, R. D.; Pevzner, P. A. Does Trypsin Cut before Proline? *J. Proteome Res.* **2008**, *7* (1), 300–305.
(149) Pilson, M. E. Q. *An Introduction to the Chemistry of the Sea*; Cambridge University Press, 2012.
(150) Katchalsky, A.; Michaeli, I. Polyelectrolyte Gels in Salt Solutions. *J. Polym. Sci.* **1955**, *15* (79), 69–86.
(151) Skouri, R.; Schosseler, F.; Munch, J. P.; Candau, S. J. Swelling and Elastic Properties of Polyelectrolyte Gels. *Macromolecules* **1995**, *28* (1), 197–210.
(152) Katchalsky, A.; Lifson, S.; Exsenberg, H. Equation of Swelling for Polyelectrolyte Gels. *J. Polym. Sci.* **1951**, *7* (5), 571–574.
(153) Rud, O.; Richter, T.; Borisov, O.; Holm, C.; Košovan, P. A Self-Consistent Mean-Field Model for Polyelectrolyte Gels. *Soft Matter* **2017**, *13* (18), 3264–3274.
(154) Košovan, P.; Richter, T.; Holm, C. Modeling of Polyelectrolyte Gels in Equilibrium with Salt Solutions. *Macromolecules* **2015**, *48* (20), 7698–7708.
(155) Fudge, D. S. The Biomechanics of Intermediate Filament-Based Materials: Insights From Hagfish Slime Threads, The University of British Columbia, 2002.
(156) Höpfner, J.; Klein, C.; Wilhelm, M. A Novel Approach for the Desalination of Seawater by Means of Reusable Poly(acrylic Acid) Hydrogels and Mechanical Force. *Macromol. Rapid Commun.* **2010**, *31* (15), 1337–1342.
(157) Böni, L. J.; Zurflüh, R.; Widmer, M.; Fischer, P.; Windhab, E. J.; Rühs, P. A.; Kuster, S. Hagfish Slime Exudate Stabilization and Its Effect on Slime Formation and Functionality. *Biol. Open* **2017**, *6* (7), 1115–1122.
(158) Feughelman, M. A Two-Phase Structure for Keratin Fibers. *Text. Res. J.* **1959**, *29* (3), 223–228.
(159) Deacon, M. P.; McGurk, S.; Roberts, C. J.; Williams, P. M.; Tendler, S. J.; Davies, M. C.; Davis, S. S.;

Harding, S. E. Atomic Force Microscopy of Gastric Mucin and Chitosan Mucoadhesive Systems. *Biochem. J* **2000**, *348 Pt 3*, 557–563.
(160) Bhaskar, K. R.; Gong, D. H.; Bansil, R.; Pajevic, S.; Hamilton, J. A.; Turner, B. S.; LaMont, J. T. Profound Increase in Viscosity and Aggregation of Pig Gastric Mucin at Low pH. *Am. J. Physiol.* **1991**, *261* (5 Pt 1), G827–G832.
(161) Donaldson, S. H.; Bennett, W. D.; Zeman, K. L.; Knowles, M. R.; Tarran, R.; Boucher, R. C. Mucus Clearance and Lung Function in Cystic Fibrosis with Hypertonic Saline. *N. Engl. J. Med.* **2006**, *354* (3), 241–250.
(162) Wills, P. J.; Hall, R. L.; Chan, W.; Cole, P. J. Sodium Chloride Increases the Ciliary Transportability of Cystic Fibrosis and Bronchiectasis Sputum on the Mucus-Depleted Bovine Trachea. *J. Clin. Invest.* **1997**, *99* (1), 9–13.
(163) Elkins, M. R.; Bye, P. T. P. Mechanisms and Applications of Hypertonic Saline. *J. R. Soc. Med.* **2011**, *104 Suppl 1*, S2–S5.
(164) Liron, N.; Ostfeld, E.; Priel, Z.; Roth, Y. *Cilia, Mucus, and Mucociliary Interactions*; CRC Press, 1998.
(165) Morozova, S.; Muthukumar, M. Elasticity at Swelling Equilibrium of Ultrasoft Polyelectrolyte Gels: Comparisons of Theory and Experiments. *Macromolecules* **2017**, *50* (6), 2456–2466.
(166) Ferry, J. D. A Fibrous Protein From The Slime Of The Hagfish. *J. Biol. Chem.* **1941**, *138* (1), 263–268.
(167) Verdugo, P.; Deyrup-Olsen, I.; Aitken, M.; Villalon, M.; Johnson, D. Molecular Mechanism of Mucin Secretion: I. The Role of Intragranular Charge Shielding. *J. Dent. Res.* **1987**, *66* (2), 506–508.
(168) Verdugo, P. Mucin Exocytosis. *Am. Rev. Respir. Dis.* **1991**, *144* (3 Pt 2), S33–S37.
(169) Nguyen, T.; Chin, W. C.; Verdugo, P. Role of Ca2+/K+ Ion Exchange in Intracellular Storage and Release of Ca2+. *Nature* **1998**, *395* (6705), 908–912.
(170) Schlichter, L. C. Unstirred Mucus Layers: Ion Exchange Properties and Effect On Ion Regulation in Lymnaea Stagnalis. *J. Exp. Biol.* **1982**, *98* (1), 363–372.
(171) Ridley, C.; Kouvatsos, N.; Raynal, B. D.; Howard, M.; Collins, R. F.; Desseyn, J.-L.; Jowitt, T. A.; Baldock, C.; Davis, C. W.; Hardingham, T. E.; et al. Assembly of the Respiratory Mucin MUC5B: A New Model for a Gel-Forming Mucin. *J. Biol. Chem.* **2014**, *289* (23), 16409–16420.
(172) Forstner, J. F.; Forstner, G. G. Calcium Binding to Intestinal Goblet Cell Mucin. *Biochim. Biophys. Acta* **1975**, *386* (1), 283–292.
(173) Raynal, B. D. E.; Hardingham, T. E.; Sheehan, J. K.; Thornton, D. J. Calcium-Dependent Protein Interactions in MUC5B Provide Reversible Cross-Links in Salivary Mucus. *J. Biol. Chem.* **2003**, *278* (31), 28703–28710.
(174) Mattai, J.; Kwak, J. C. T. Divalent Metal Ion Binding to Polyelectrolytes with Different Polyion Structure and Functional Groups. *Macromolecules* **1986**, *19* (6), 1663–1667.
(175) Mattai, J.; Kwak, J. C. T. Influence of Univalent Counterions on the Binding of Divalent Metal Ions by the Biopolyelectrolyte Dextran Sulfate. *J. Phys. Chem.* **1982**, *86* (6), 1026–1030.
(176) Satoh, M.; Kawashima, T.; Komiyama, J. Competitive Counterion Binding and Dehydration of Polyelectrolytes in Aqueous Solutions. *Polymer* **1991**, *32* (5), 892–896.
(177) Manning, G. S. Limiting Laws and Counterion Condensation in Polyelectrolyte Solutions I. Colligative Properties. *J. Chem. Phys.* **1969**, *51* (3), 924–933.
(178) Manning, G. S. Counterion Binding in Polyelectrolyte Theory. *Acc. Chem. Res.* **1979**, *12* (12), 443–449.
(179) Dobrynin, A. V.; Rubinstein, M. Counterion Condensation and Phase Separation in Solutions of Hydrophobic Polyelectrolytes. *Macromolecules* **2001**, *34* (6), 1964–1972.
(180) Wainwright, P.; Carroll, A. M.; Collar, D. C.; Day, S. W.; Higham, T. E.; Holzman, R. A. Suction Feeding Mechanics, Performance, and Diversity in Fishes. *Integr. Comp. Biol.* **2007**, *47* (1), 96–106.
(181) Day, S. W.; Higham, T. E.; Wainwright, P. C. Time Resolved Measurements of the Flow Generated by Suction Feeding Fish. *Exp. Fluids* **2007**, *43* (5), 713–724.
(182) Strahan, R. The Behaviour of Myxinoids. *Acta Zool.* **1963**, *44* (1-2), 73–102.
(183) Adam, H. Different Types of Body Movement in the Hagfish, Myxine Glutinosa L. *Nature* **1960**, *188* (4750), 595–596.
(184) Phillips, G. O.; Williams, P. A. *Handbook of Hydrocolloids*; Elsevier, 2009.
(185) Bromberg, L. E.; Barr, D. P. Self-Association of Mucin. *Biomacromolecules* **2000**, *1* (3), 325–334.
(186) Jørgensen, J. M.; Lomholt, J. P.; Weber, R. E.; Malte, H. *The Biology of Hagfishes*; Springer Science & Business Media, 2012.
(187) Higham, T. E. Multidimensional Analysis of Suction Feeding Performance in Fishes: Fluid Speed, Acceleration, Strike Accuracy and the Ingested Volume of Water. *J. Exp. Biol.* **2006**, *209* (14), 2713–2725.
(188) Muller, M.; Osse, J. W. M. Hydrodynamics of Suction Feeding in Fish. *The Transactions of the*

Zoological Society of London **1984**, *37* (2), 51–135.
(189) Muller, M.; Osse, J. W. M.; Verhagen, J. H. G. A Quantitative Hydrodynamical Model of Suction Feeding in Fish. *J. Theor. Biol.* **1982**, *95* (1), 49–79.
(190) Brick Peres, M.; Haimovici, E. Alimentação Do Cherne-Poveiro Polyprion Americanus (Polyprionidae, Teleostei) No Sul Do Brasil. *Atlântica, Rio Gd* **2003**, *25*, 201–208.
(191) De Schepper, N.; De Kegel, B.; Adriaens, D. Morphological Specializations in Heterocongrinae (Anguilliformes: Congridae) Related to Burrowing and Feeding. *J. Morphol.* **2007**, *268* (4), 343–356.
(192) Wilga, C.; Motta, P. Conservation and Variation in the Feeding Mechanism of the Spiny Dogfish Squalus Acanthias. *J. Exp. Biol.* **1998**, *201 (Pt 9)*, 1345–1358.
(193) Berta, A.; Sumich, J. L.; Kovacs, K. M. *Marine Mammals: Evolutionary Biology*; Elsevier, 2015.
(194) Marshall, C. D.; Wieskotten, S.; Hanke, W.; Hanke, F. D.; Marsh, A.; Kot, B.; Dehnhardt, G. Feeding Kinematics, Suction, and Hydraulic Jetting Performance of Harbor Seals (Phoca Vitulina). *PLoS One* **2014**, *9* (1), e86710.
(195) Fudge, D. S.; Winegard, T.; Ewoldt, R. H.; Beriault, D.; Szewciw, L.; McKinley, G. H. From Ultra-Soft Slime to Hard {alpha}-Keratins: The Many Lives of Intermediate Filaments. *Integr. Comp. Biol.* **2009**, *49* (1), 32–39.
(196) Christanti, Y.; Walker, L. M. Surface Tension Driven Jet Break up of Strain-Hardening Polymer Solutions. *J. Non-Newtonian Fluid Mech.* **2001**, *100* (1-3), 9–26.
(197) Haward, S. J.; Odell, J. A.; Berry, M.; Hall, T. Extensional Rheology of Human Saliva. *Rheol. Acta* **2010**, *50* (11-12), 869–879.
(198) Wagner, C.; Bourouiba, L.; McKinley, G. H. An Analytic Solution for Capillary Thinning and Breakup of FENE-P Fluids. *J. Non-Newtonian Fluid Mech.* **2015**, *218*, 53–61.
(199) Tabatabaei, S.; Jahromi, H. T.; Webster, M. F.; Williams, P. R.; Holder, A. J.; Lewis, K. E.; Davies, G. A.; Griffin, L.; Ebden, P.; Askill, C. A CaBER Computational–experimental Rheological Study on Human Sputum. *J. Non-Newtonian Fluid Mech.* **2015**, *222*, 272–287.
(200) Wagner, C. An Experimental and Theoretical Investigation of the Rheological Properties and Degradation of Mucin Solutions: (or Why Saliva Becomes Watery When Removed from Your Mouth), Massachusetts Institute of Technology, 2015.
(201) Charrier, E. E.; Janmey, P. A. Mechanical Properties of Intermediate Filament Proteins. *Methods Enzymol.* **2016**, *568*, 35–57.
(202) Fraser, R. D.; Macrae, T. P. Molecular Structure and Mechanical Properties of Keratins. *Symp. Soc. Exp. Biol.* **1980**, *34*, 211–246.
(203) Fey, E. G. Epithelial Cytoskeletal Framework and Nuclear Matrix-Intermediate Filament Scaffold: Three-Dimensional Organization and Protein Composition. *J. Cell Biol.* **1984**, *98* (6), 1973–1984.
(204) Desai, A.; Mitchison, T. J. Microtubule Polymerization Dynamics. *Annu. Rev. Cell Dev. Biol.* **1997**, *13* (1), 83–117.
(205) Lehtonen, A.; Kärkkäinen, J.; Haahti, E. Carbohydrate Components in the Epithelial Mucin of Hagfish, Myxine Glutinosa. *Acta Chem. Scand.* **1966**, *20* (6), 1456–1462.
(206) Powell, D. A.; Turula, V.; Dehaseth, J. A.; Vanhalbeek, H.; Meyer, B. Sulfate Detection in Glycoprotein-Derived Oligosaccharides by Artificial Neural Network Analysis Fourier-Transform Infrared Spectra. *Anal. Biochem.* **1994**, *220* (1), 20–27.
(207) Lewis, A. T.; Jones, K.; Lewis, K. E.; Jones, S.; Lewis, P. D. Detection of Lewis Antigen Structural Change by FTIR Spectroscopy. *Carbohydr. Polym.* **2013**, *92* (2), 1294–1301.
(208) Nikonenko, N. A.; Bushnak, I. A.; Keddie, J. L. Spectroscopic Ellipsometry of Mucin Layers on an Amphiphilic Diblock Copolymer Surface. *Appl. Spectrosc.* **2009**, *63* (8), 889–898.
(209) Lewis, S. P.; Lewis, A. T.; Lewis, P. D. Prediction of Glycoprotein Secondary Structure Using ATR-FTIR. *Vib. Spectrosc.* **2013**, *69*, 21–29.
(210) Ahn, J.; Crouzier, T.; Ribbeck, K.; Rubner, M. F.; Cohen, R. E. Tuning the Properties of Mucin via Layer-by-Layer Assembly. *Biomacromolecules* **2015**, *16* (1), 228–235.
(211) Bavington, C. D.; Lever, R.; Mulloy, B.; Grundy, M. M.; Page, C. P.; Richardson, N. V.; McKenzie, J. D. Anti-Adhesive Glycoproteins in Echinoderm Mucus Secretions. *Comp. Biochem. Physiol. B Biochem. Mol. Biol.* **2004**, *139* (4), 607–617.
(212) Lalonde, S. V.; Dafoe, L. T.; Pemberton, S. G.; Gingras, M. K.; Konhauser, K. O. Investigating the Geochemical Impact of Burrowing Animals: Proton and Cadmium Adsorption onto the Mucus Lining of Terebellid Polychaete Worms. *Chem. Geol.* **2010**, *271* (1-2), 44–51.
(213) Mezzenga, R.; Fischer, P. The Self-Assembly, Aggregation and Phase Transitions of Food Protein Systems in One, Two and Three Dimensions. *Rep. Prog. Phys.* **2013**, *76* (4), 046601.
(214) Schwegman, J. J.; Carpenter, J. F.; Nail, S. L. Infrared Microscopy for in Situ Measurement of Protein Secondary Structure during Freezing and Freeze-Drying. *J. Pharm. Sci.* **2007**, *96* (1), 179–195.
(215) Herrmann, H.; Aebi, U. Intermediate Filaments: Molecular Structure, Assembly Mechanism, and

Integration into Functionally Distinct Intracellular Scaffolds. *Annu. Rev. Biochem.* **2004**, *73*, 749–789.
(216) Fraser, R. D. B.; MacRae, T. P.; Parry, D. A. D.; Suzuki, E. The Structure of β-Keratin. *Polymer* **1969**, *10*, 810–826.
(217) Kornreich, M.; Avinery, R.; Malka-Gibor, E.; Laser-Azogui, A.; Beck, R. Order and Disorder in Intermediate Filament Proteins. *FEBS Lett.* **2015**, *589* (19 Pt A), 2464–2476.
(218) Beck, R.; Deek, J.; Jones, J. B.; Safinya, C. R. Gel-Expanded to Gel-Condensed Transition in Neurofilament Networks Revealed by Direct Force Measurements. *Nat. Mater.* **2010**, *9* (1), 40–46.
(219) Beck, R.; Deek, J.; Choi, M. C.; Ikawa, T.; Watanabe, O.; Frey, E.; Pincus, P.; Safinya, C. R. Unconventional Salt Trend from Soft to Stiff in Single Neurofilament Biopolymers. *Langmuir* **2010**, *26* (24), 18595–18599.
(220) Wen, Q.; Janmey, P. A. Polymer Physics of the Cytoskeleton. *Curr. Opin. Solid State Mater. Sci.* **2011**, *15* (5), 177–182.
(221) Janmey, P. A.; Slochower, D. R.; Wang, Y.-H.; Wen, Q.; Cēbers, A. Polyelectrolyte Properties of Filamentous Biopolymers and Their Consequences in Biological Fluids. *Soft Matter* **2014**, *10* (10), 1439–1449.
(222) Kumar, S.; Yin, X.; Trapp, B. D.; Hoh, J. H.; Paulaitis, M. E. Relating Interactions between Neurofilaments to the Structure of Axonal Neurofilament Distributions through Polymer Brush Models. *Biophys. J.* **2002**, *82* (5), 2360–2372.
(223) Zhulina, E. B.; Leermakers, F. A. M. The Polymer Brush Model of Neurofilament Projections: Effect of Protein Composition. *Biophys. J.* **2010**, *98* (3), 462–469.
(224) Koch, E. Structural Forms and Possible Roles of Aligned Cytoskeletal Biopolymers in Hagfish (slime Eel) mucus*1. *J. Struct. Biol.* **1991**, *106* (3), 205–210.
(225) Böni, L. J.; Zurflüh, R.; Baumgartner, M. E.; Windhab, E. J.; Fischer, P.; Kuster, S.; Rühs, P. A. Effect of Ionic Strength and Seawater Cations on Hagfish Slime Formation. *Sci. Rep.* **2018**, *8* (1), 9867.
(226) Brown, H. G.; Hoh, J. H. Entropic Exclusion by Neurofilament Sidearms: A Mechanism for Maintaining Interfilament Spacing. *Biochemistry* **1997**, *36* (49), 15035–15040.
(227) Parbhu, A. N.; Bryson, W. G.; Lal, R. Disulfide Bonds in the Outer Layer of Keratin Fibers Confer Higher Mechanical Rigidity: Correlative Nano-Indentation and Elasticity Measurement with an AFM. *Biochemistry* **1999**, *38* (36), 11755–11761.
(228) Bhushan, B.; Chen, N. AFM Studies of Environmental Effects on Nanomechanical Properties and Cellular Structure of Human Hair. *Ultramicroscopy* **2006**, *106* (8-9), 755–764.
(229) Farran, L.; Roland Ennos, A.; Eichhorn, S. J. Microindentation and Nanoindentation of Human Fingernails at Varying Relative Humidity. *J. Mater. Res.* **2009**, *24* (03), 980–984.
(230) Lin, Y.-C.; Yao, N. Y.; Broedersz, C. P.; Herrmann, H.; Mackintosh, F. C.; Weitz, D. A. Origins of Elasticity in Intermediate Filament Networks. *Phys. Rev. Lett.* **2010**, *104* (5), 058101.
(231) Zhao, X. Multi-Scale Multi-Mechanism Design of Tough Hydrogels: Building Dissipation into Stretchy Networks. *Soft Matter* **2014**, *10* (5), 672–687.
(232) Cappella, B. *Mechanical Properties of Polymers Measured through AFM Force-Distance Curves*; Springer Laboratory; Springer International Publishing: Cham, 2016.
(233) Schopferer, M.; Bär, H.; Hochstein, B.; Sharma, S.; Mücke, N.; Herrmann, H.; Willenbacher, N. Desmin and Vimentin Intermediate Filament Networks: Their Viscoelastic Properties Investigated by Mechanical Rheometry. *J. Mol. Biol.* **2009**, *388* (1), 133–143.
(234) Uhlig, M. R.; Magerle, R. Unraveling Capillary Interaction and Viscoelastic Response in Atomic Force Microscopy of Hydrated Collagen Fibrils. *Nanoscale* **2017**, *9* (3), 1244–1256.
(235) Yuan, Y.; Verma, R. Measuring Microelastic Properties of Stratum Corneum. *Colloids Surf. B Biointerfaces* **2006**, *48* (1), 6–12.
(236) Efremov, Y. M.; Bagrov, D. V.; Kirpichnikov, M. P.; Shaitan, K. V. Application of the Johnson-Kendall-Roberts Model in AFM-Based Mechanical Measurements on Cells and Gel. *Colloids Surf. B Biointerfaces* **2015**, *134*, 131–139.
(237) Chen, J. F.; Xu, K. J.; Tang, L. Q.; Liu, Z. J.; Zhou, L. C. Study on the Optimal Loading Rates in the Measurement of Viscoelastic Properties of Hydrogels by Conical Indentation. *Mech. Mater.* **2018**, *119*, 42–48.
(238) Attard, P. Measurement and Interpretation of Elastic and Viscoelastic Properties with the Atomic Force Microscope. *J. Phys. Condens. Matter* **2007**, *19* (47), 473201.
(239) Gillies, G.; Prestidge, C. A.; Attard, P. An AFM Study of the Deformation and Nanorheology of Cross-Linked PDMS Droplets. *Langmuir* **2002**, *18* (5), 1674–1679.
(240) Meng, F.; Pritchard, R. H.; Terentjev, E. M. Stress Relaxation, Dynamics, and Plasticity of Transient Polymer Networks. *Macromolecules* **2016**, *49* (7), 2843–2852.
(241) Pawelzyk, P.; Mücke, N.; Herrmann, H.; Willenbacher, N. Attractive Interactions among Intermediate Filaments Determine Network Mechanics in Vitro. *PLoS One* **2014**, *9* (4), e93194.

(242) Kroy, K.; Glaser, J. The Glassy Wormlike Chain. *New J. Phys.* **2007**, *9* (11), 416–416.
(243) Perticaroli, S.; Nickels, J. D.; Ehlers, G.; O'Neill, H.; Zhang, Q.; Sokolov, A. P. Secondary Structure and Rigidity in Model Proteins. *Soft Matter* **2013**, *9* (40), 9548.
(244) Perticaroli, S.; Nickels, J. D.; Ehlers, G.; Sokolov, A. P. Rigidity, Secondary Structure, and the Universality of the Boson Peak in Proteins. *Biophys. J.* **2014**, *106* (12), 2667–2674.
(245) De Rosa, C.; Auriemma, F. *Crystals and Crystallinity in Polymers: Diffraction Analysis of Ordered and Disordered Crystals*; John Wiley & Sons, 2013.
(246) Zugenmaier, P. X-Ray Analysis of Partial Crystalline Fibre Structure. In *Handbook of Textile Fibre Structure*; 2009; pp 46–120.
(247) Hermans, P. H.; Platzek, P. Beiträge Zur Kenntnis Des Deformationsmechanismus Und Der Feinstruktur Der Hydratzellulose. *Kolloid-Zeitschrift* **1939**, *88* (1), 68–72.

Curriculum Vitae

Personal Details:

Surname:	Böni
Name:	Lukas
Address:	Forchstrasse 126, 8032 Zürich, CH
Nationality:	Switzerland
Date of birth:	14.06.1989
Phone:	079 511 21 53
E-Mail:	Private: lukas.boeni@bluewin.ch Work: lukas.boeni@hest.ethz.ch

Education:

Doctorate 02/2015 - 11/2018	**PhD Student in the Food Process Engineering Group** ETH Zurich PhD Topic: "Biophysics and Biomimetics of Hagfish Slime". PhD Defense on 02.11.2018
Studies: 09/2012 - 10/2014	**Master Program in Food Science** ETH Zürich Major in Food Process Engineering Minor in Food Biotechnology Master Thesis: "Rheology of Hagfish Slime"
02/2013 - 07/2013	**Semester abroad at the University of Melbourne** Melbourne, Australia
09/2009 - 09/2012	**Bachelor in Food Science** ETH Zürich Bachelor Thesis: “Interfacial Rheology of Bacterial Biofilms”

Languages:

German:	Mother tongue
English:	Very good, oral and written

French :	Good, oral and written
Spanish:	Basic knowledge

Professional experience:

11/2013 - 02/2014	**ETH Juniors** Hired by ETH Juniors for an industrial project that included market- and need analyses as well as leading an innovation workshop
09/2012 - 01/2013	**Coop Quality Center, Pratteln** Internship in quality management with focus on risk analysis in points of sale and project work for business partner auditing
08/2009 - 02/2013	**City One Fitness Club GmbH, Rheinfelden** Fitness trainer

Awards:

Willi Studer Award 2016	Best Master's Degree Food Science ETH (grade point average)

Publications:

(1) Rühs, P. A.; Böni, L.; Fuller, G. G.; Inglis, R. F.; Fischer, P. In-Situ Quantification of the Interfacial Rheological Response of Bacterial Biofilms to Environmental Stimuli. *PLoS One* **2013**, *8*, e78524.
(2) Böni, L.; Fischer, P.; Böcker, L.; Kuster, S.; Rühs, P. A. Hagfish Slime and Mucin Flow Properties and Their Implications for Defense. *Sci. Rep.* **2016**, *6*, 30371.
(3) Böni, L.; Rühs, P. A.; Windhab, E. J.; Fischer, P.; Kuster, S. Gelation of Soy Milk with Hagfish Exudate Creates a Flocculated and Fibrous Emulsion- and Particle Gel. *PLoS One* **2016**, *11*, e0147022.
(4) Böcker, L.; Rühs, P. A.; Böni, L.; Fischer, P.; Kuster, S. Fiber-Enforced Hydrogels: Hagfish Slime Stabilized with Biopolymers Including κ-Carrageenan. *ACS Biomaterials Science & Engineering* **2015**, *2*, 90–95.
(5) Böni, L. J.; Zurflüh, R.; Widmer, M.; Fischer, P.; Windhab, E. J.; Rühs, P. A.; Kuster, S. Hagfish Slime Exudate Stabilization and Its Effect on Slime Formation and Functionality. *Biol. Open* **2017**, *6*, 1115–1122.
(6) Radtke, T.; Böni, L.; Bohnacker, P.; Maggi-Beba, M.; Fischer, P.; Kriemler, S.; Benden, C.; Dressel, H. Acute Effects of Combined Exercise and Oscillatory Positive Expiratory Pressure Therapy on Sputum Properties and Lung Diffusing Capacity in Cystic Fibrosis: A Randomized, Controlled, Crossover Trial. *BMC Pulm. Med.* **2018**, *18*, 99.
(7) Desmond, P.; Böni, L.; Fischer, P.; Morgenroth, E.; Derlon, N. Stratification in the Physical Structure and Cohesion of Membrane Biofilms — Implications for Hydraulic Resistance. *J. Memb. Sci.* **2018**, *564*, 897–904.
(8) Radtke, T.; Böni, L.; Bohnacker, P.; Fischer, P.; Benden, C.; Dressel, H. The Many Ways Sputum Flows – Dealing with High within-Subject Variability in Cystic Fibrosis Sputum Rheology. *Respir. Physiol. Neurobiol.* **2018**, *254*, 36–39.
(9) Böni, L. J.; Zurflüh, R.; Baumgartner, M. E.; Windhab, E. J.; Fischer, P.; Kuster, S.; Rühs, P. A. Effect of Ionic Strength and Seawater Cations on Hagfish Slime Formation. *Sci. Rep.* **2018**, *8*, 9867.